Lire
le début de la thèse

4 Satellite Selection

4.1 Motivations and Objectives

The use of two or more GNSS constellations and two frequencies in GAST-F produces several benefits, in terms of accuracy, integrity monitoring and system continuity. Despite the advantages in obtaining a larger number of measurements, there is at least one possible problem to cope with: the limited number of channels present in a GNSS receiver. The use of single frequency single constellation GBAS implies the tracking of up to 10-12 satellites. Considering the presence of a second constellation, this number can be doubled. It can be seen in the remainder of the chapter that 22 satellites may be visible at the same time, under defined circumstances, and this number must be also doubled if a second frequency is used. It is clear that any receiver, to work in dual constellation and dual frequency, need more than 44 channels to be sure that all satellites in view are tracked.

The problem of the number of visible satellites is, however, not only related to the number of channels in a receiver. In GBAS, another issue is represented by the maximum number of corrections that could be broadcasted through the VDB link. The correction message, as currently structured in GBAS GAST D, limits the number of corrections to 18. Considering the optimization of the message occupation, this number may increase to 27 (SESAR 15.3.7; WP3), which is considered as sufficient for GAST D. Considering the development of GAST F that uses a processing mode different from GAST D, and in order to maintain interoperability between the two GBAS services, the ground station must broadcast corrections for both GAST-D and F. Under these circumstances, the limit stated before must be split almost by two, even if, considering the redundancy of certain information present in the correction message, some space could be saved. Considering a possible limit of 15 corrections, there is a need to have a satellite selection algorithm in order to avoid accuracy problem when all satellites in view cannot be used.

Over the years, many methods were proposed to select a satellite subset instead of using all satellites in view in order to solve problems cited before. The choice of a satellite subset was focused on the search of the best subset in order to preserve the accuracy. The main parameter on which the search was focused on, was the DOP, also VDOP and HDOP, because it is the only index relating the accuracy to the constellation geometry.

4.2 Satellite Selection Methods

The algorithms presented in the next section were developed for the case of a subset having no more than four or five satellites. Their use to search a subset composed by a bigger number leads to an increase of the computational load in some cases, or to a non-optimal subset choice.

4.2.1 Optimal Solution

One of the main selection algorithms proposed in the past, is the optimal solution (Liu, et al., 2009). This algorithm computes the best value of GDOP trying all the possible satellite subset at the cost of a great computational load with the growth of the number of satellites in view. For example with 18 visible satellites and the search for a 12-satellite subset, the algorithm has to compute 18564 different GDOP values, the total amount being given by the following formula:

$$C_{12}^{18} = \frac{18!}{12!\,(18-12)!} = 18564$$

Using a 20-satellite subset out of 40 visible, the number increases to $1.38 \cdot 10^{11}$. It can thus be understood that this method works properly only for single constellation, when a low number of satellites is in view and a small satellite subset is searched for. Note that it is possible to use the same type of algorithm to optimize other DOP values, such as PDOP, HDOP or VDOP; also the protection level can be used as the optimization criterion.

4.2.2 Modified Minimum GDOP

An alternative method is the Modified Minimum GDOP. In this algorithm the first chosen satellite of the subset is the one with the highest elevation angle and the other satellites are searched as in the "optimal solution" case (Cryan, et al., 1992). This method reduces the computational burden in comparison with the "optimal solution" but the number of all possible combinations to be analysed can be still prohibitively large. Using the same example used for the optimal solution, 18 satellites available and a 12 satellites subset, and choosing the first as the one with the higher elevation angle the total amount of possible combination to be considered is 12376 and is given by:

$$C_{11}^{17} = \frac{17!}{11!(17-11)!} = 12376$$

It can be seen that the number of combinations to be analyzed is still very large.

4.2.3 Lear's Simple Satellite Selection

This technique, shown in (Cryan, et al., 1992), follows a defined procedure to choose the first three satellites and the last one is chosen minimizing the DOP value. The procedure works in the following manner:

- The first satellite is chosen finding the one with the highest elevation angle.
- The second is the one having an angle between the LOS (Line Of Sight) of the selected satellite and the LOS of the first satellite as close as possible to 90°.
- The third satellite chosen is the one that has the LOS perpendicular to the plane formed by the two previous satellites chosen.

- The last satellite is chosen to minimize the GDOP (Cryan, et al., 1992).

This technique has almost no computational load compared to the two previous methodologies. The main drawback of this method is that it was developed only for a four satellites subset and this is not enough for GBAS, even for single constellation and single frequency GBAS.

4.2.4 Fast Satellite Selection Algorithm

The main problem of the previous techniques is that they were developed to work better, in some cases to work only, with a 4 satellite subset and a limited number of satellites in view. When a larger number of satellites in the subset is searched, and there are a lot of satellites in view, the computational burden increases rapidly. Considering the scope of this analysis and the development of dual constellation dual frequency GBAS service, the number of satellites for the subset can be larger than ten. In order to overcome the problem of finding a subset with more than ten satellites without increasing too much the computational load, new algorithms were developed and are presented in the following.

The algorithm proposed in (Zhang, et al., 2008) is a good solution to the problem related with a subset bigger than 4 satellites. In this technique, a preliminary study with a simulated constellation was used to find the subset geometry with the best GDOP value starting from 4 and up to 15 satellites. From the result analysis, it is possible to see how the best GDOP varies according to the number of satellites selected at the zenith or near ($> 80°$) it and selecting the remaining according to their azimuth in order to have a homogenous distribution.

Table 14 – GDOP values for different number of satellite at high elevation for a simulated study *(Zhang, et al., 2008)*

		NUMBER OF SV AT THE ZENITH						
		1	2	3	4	5	6	7
SATELLITE SUBSET	4	3.3528						
	5	2.8169	2.7482					
	6	2.4953	2.2123	2.5466				
	7	2.281	1.8907	2.0108	2.4459			
	8	2.1279	1.6764	1.6892	1.91	2.3854		
	9	2.013	1.5233	1.4749	1.5884	1.8495	2.3451	
	10	1.9237	1.4084	1.3217	1.3741	1.528	1.8092	2.3163
	11	1.8523	1.3191	1.2069	1.221	1.3136	1.4877	1.7804
	12	1.7938	1.2477	1.1176	1.1061	1.1605	1.2733	1.4589
	13	1.7451	1.1892	1.0461	1.0168	1.0457	1.1202	1.2445
	14	1.7039	1.1405	0.9877	0.9454	0.9564	1.0054	1.0914
	15	1.6685	1.0993	0.939	0.8869	0.8849	0.9161	0.9766
	16	1.6379	1.0639	0.8977	0.8382	0.8265	0.8446	0.8873

The values of the GDOP shown in Table 14 are computed for a simulated constellation placing satellites at high elevation angle and the remaining equally spaced at low elevation angle. This study permits to establish how many satellites must be selected between the ones with the higher elevation angle before selecting the remaining ones following a defined algorithm.

The algorithm works in 4 steps:

1. Computation of the elevation and azimuth angle of all visible satellites.
2. According to the number of satellites of the subset, n, the number of satellites with the highest elevation angle is selected. Defined *p=number of satellite at zenith*; to find the *p* satellites with the highest elevation.
3. To divide the sky in $K = n - p$ equally-spaced in azimuth portions and group the satellites in each portions. It is possible to start the sky division from one particular direction or to select one satellite as reference and start from its azimuth. The satellite with the lowest elevation angle must be found and noted as S_{p+1}, it can be removed or used as reference for the group subdivision.
4. The fourth step is to combine one satellite from each k^{th} group with the others chosen in the second step. If there are more satellites in one or more groups, a GDOP computation for each

possible subset has to be done, the satellites that belong to the subset with minimum GDOP are selected for the solution computation. The total number of subset is:

$$T = C_1 \times C_2 \times \ldots \times C_{n-p} \qquad \text{Eq. 4.1}$$

Where:

- C_k is the number of satellites in the k^{th} group.

In Figure 51 an example of sky plot subdivision with high elevation angle satellites noted in green and the remaining satellites sort in groups. The satellite with the lowest elevation angle is coloured in red, it can be removed from the subsets or used as starting point of the groups subdivision.

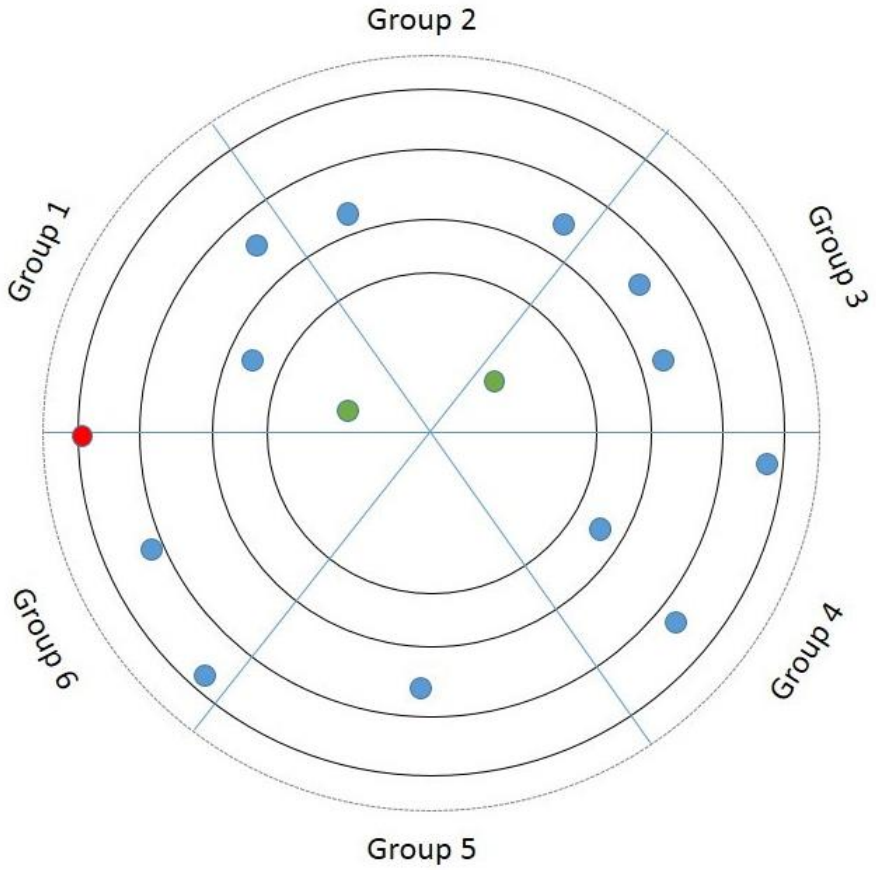

Figure 51 – Fast satellite selection sky subdivision example (Zhang, et al., 2008)

4.3 Selected Methods for Simulation

Considering the methods found in literature and the conditions of DF/DC GBAS, all methods developed to work properly for searching four or five satellites presented in section 4.2.1, 4.2.2 and 4.2.3 are not considered due to the high computational burden. However, the Optimal Solution method will be used to find the real best DOP value or protection level and to compare it with the other selection methods. The computational load of the optimal solution will be considered as well to compare it with the ones

of other analyzed methods. The selection algorithm proposed in 4.2.4 is used to find the best subset due to its ability to find it without increasing too much the computational load. A last methods, even if is not a satellite selection algorithm is the selection of the n satellites with the highest elevation angle.

To summarize the selection algorithms or methods used for simulation are:

- Fast Satellite Selection; In order to make the algorithm faster, instead of computing the DOP for each combination, the satellite with the lower elevation angle will be systematically selected in each bin along with the satellites with high elevation angle.
- Maximum Elevation Angle; even if this is not an algorithm and it has not been presented before it will be used for its simplicity. The advantage of this method is to completely cancel the computational load. In this case, only the n highest elevation satellites are kept. The choice of the higher elevation satellites is determined by the analysis of the GAD and AAD model and as well as by the impact of the ionospheric delay and multipath on low elevation satellites. Analysing the GAD and AAD model, it is possible to see that the standard deviation of the residual errors is smaller for the satellite with higher elevation angle. The residual uncertainty of the tropospheric and ionospheric delay also shows a relationship between elevation angle and standard deviation values: the higher the elevation, the lower the standard deviation.
- Brute Force VPL (Optimal Solution); this is a modification of the optimal solution, where the optimization criteria is the VPL instead of the DOPs value. In the algorithm, a control also of the S_{vert} and S_{vert2} is done to be sure to find the lowest and valid protection level.

All the algorithms will be compared with the all-in-view condition to analyse also the accuracy loss or the protection level loss.

4.4 Simulations Baseline

In order to evaluate the impact in using a satellites subset instead of the whole set of satellites in view, a series of parameters have been computed across 18 airports for a simulated period of 10 days with 60 seconds resolution.

4.4.1 Airports Coordinates

The airports location used for the simulations are:

Table 15 – Airports coordinates used in simulation

Airport	Latitude (°)	Longitude (°)
Memphis	35.0424	-89.9767
Denver	39.8584	-104.667
Dallas	32.8964	-97.0376
Newark	40.6925	-74.1687
Washington	38.9445	-77.4558
Los Angeles	33.9425	-118.4081
Orlando	28.4289	-81.3160
Minneapolis	44.8805	-93.2169
Chicago	41.9796	-87.9045
Tacoma	47.1377	-122.4765
Anchorage	61.2167	-149.90
Bremen	53.0429	8.7808
Malaga	36.68	4.5124
Sydney	-33.9636	151.1859
Amsterdam	52.30907	4.763385
Rio	-22.8088	-43.2436
Peking	40.080109	116.584503
Johannesburg	-26.139099	28.246000

4.4.2 DOP Analysis and Computational Load

The concept of DOP has been already presented in 0. For this analysis the VDOP and HDOP of the satellite subsets and of the all-in-view situation will be analyzed.

$$H = (G^T \cdot G)^{-1} \quad \text{Eq. 4.2}$$

$$VDOP = H_{3,3};\ \ HDOP = \sqrt{H_{1,1}^2 + H_{2,2}^2} \quad \text{Eq. 4.3}$$

A second type of parameter that helps to understand the computational load of each selection algorithm is the time spent to find the selected subset. The aim in analysing this parameters is just to have an index

of the computational load of each method, it is however not representative of a real time implementation in an aircraft embedded subsystem.

4.4.3 Protection Level Computation

The previous parameters are not dependent on the simulated processing mode but only on the subset's satellite number. To take into account the possibility to use different processing modes, two subsections are present: GAST D and the I-Free processing mode. The parameters analyzed for each one are the Vertical Protection Level (VPL) and the Lateral Protection Level (LPL) computed as in (RTCA Inc.; DO253-C, 2008):

$$VPL = \max\{VPL_{H0}; VPL_{H1}\} \quad \text{Eq. 4.4}$$

$$LPL = \max\{HPL_{H0}; LPL_{H1}\} \quad \text{Eq. 4.5}$$

Details about the VPL and LPL are given in 2.3.3.2

Values of $\sigma_{pr\ gnd}$ are used according to results obtained in section 3.4

4.4.4 Geometry Screening Availability

The values of S_{vert} and S_{vert2} are also analyzed in order to simulate the impact of the subset on the geometry screening monitor 5.1.2. Details about S_{vert} are given in 2.3.3.2.

$$\max\{S_{vert}\} = \max_{i}\{S_{3,i} + S_{1,i}\ tg(GPA)\} \quad \text{Eq. 4.6}$$

S_{vert2} is the sum of the two biggest S_{vert}. The two parameters have to not exceed a limit dependent on the number of constellations used. The limit for a single constellation GBAS service is respectively 4 and 6. Considering the use of dual constellation in the simulations, they can be adapted to 2 and 3.

4.5 Simulation Results

4.5.1 Dual Constellation 12 Satellite subset

In this simulation, a dual constellation composed by the optimal 24 GPS and the optimal 24 Galileo constellations is simulated because these two constellations represent the baseline for the GAST-F service. The next figure shows the number of visible satellites across all the epochs and airports.

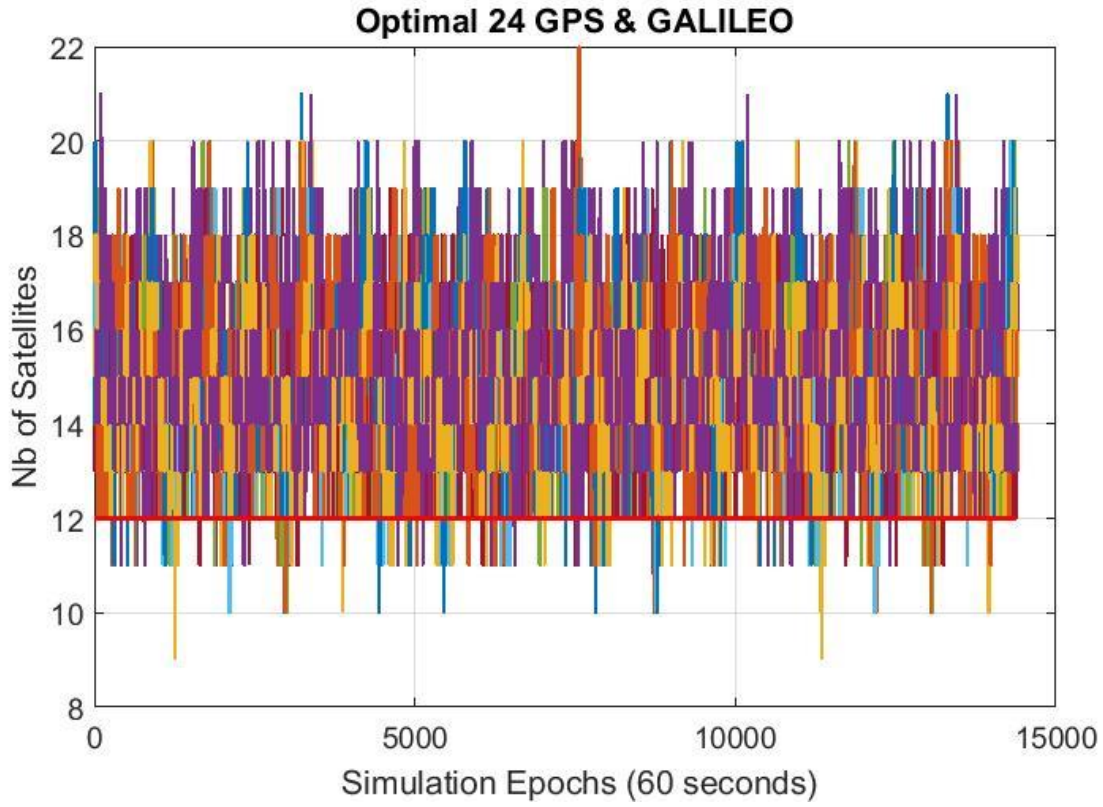

Figure 52 – Number of Satellites for all the simulated epochs and airports and 12 satellites subset in red

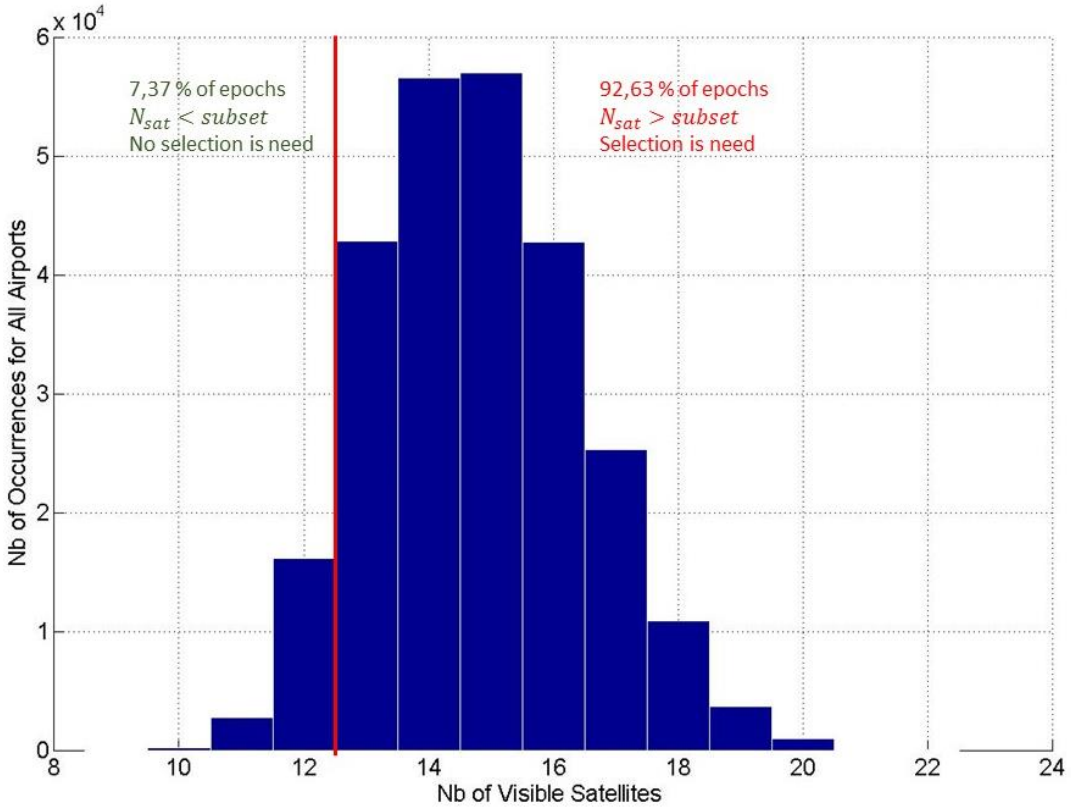

Figure 53 – Histogram of satellites number across all airports and epochs with percentage of use of satellite selection for subset 12

It is possible to see in the previous figures that for more than 92% of epochs, there are more satellites than the subset limit across all airport. Under this condition, the parameters computed for the all-in-view case and the ones computed using only a subset may be quite different. The computational load, due to a difference of 10 satellites in rare case between satellites in view and subset, is expected to be very high.

4.5.1.1 Impact of the Selection Method on the DOP Value

The values of the DOP, in the vertical and horizontal domain, provide a feedback about the accuracy that the all-in-view and the three selection algorithms are able to provide according to the number of satellite and their geometry in the sky. In Figure 54 and Figure 55 the values of VDOP and HDOP are shown.

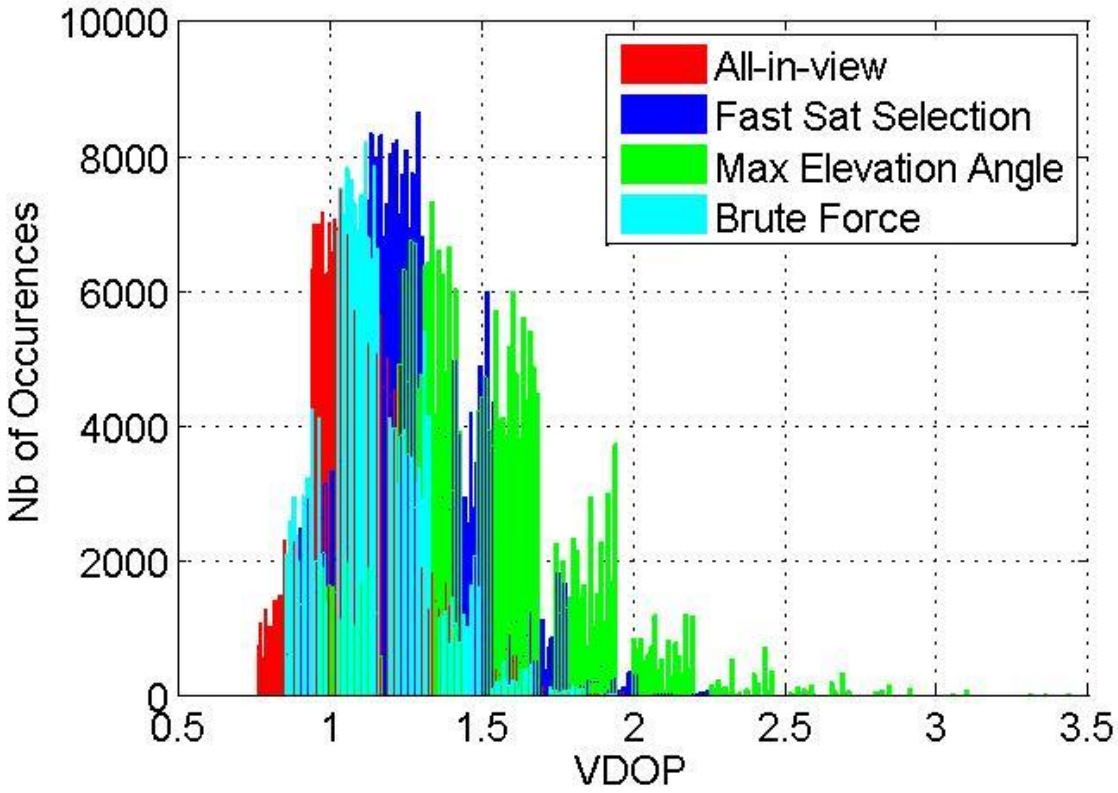

Figure 54 – VDOP values across all epochs and airports for all the methods and for all-in-view satellites

Table 16 – VDOP percentile at 95, 99 and 99.9 % for 12 satellites subset

	95 % VDOP	99 % VDOP	99.9% VDOP
All-in-view	1.4115	1.6099	1.9041
Fast Satellite Selection	1.6208	1.8551	2.1710
Maximum Elevation Angle	2.0411	2.4575	3.0718
Brute Force	1.4236	1.6180	1.9103

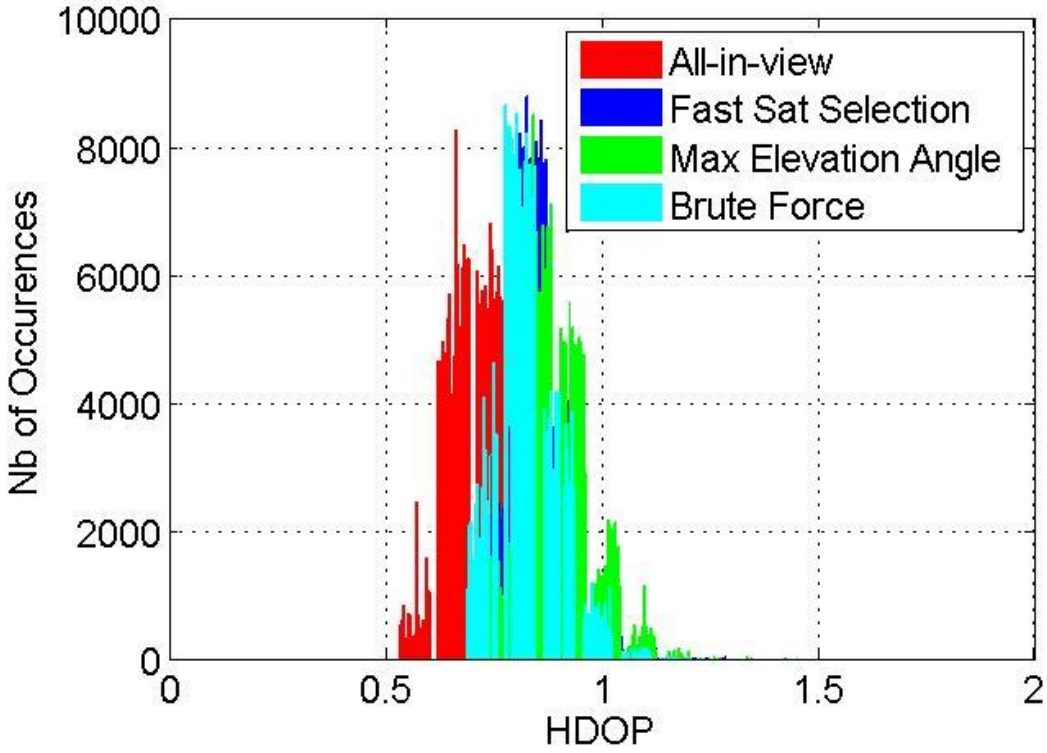

Figure 55 – HDOP values across all epochs and airports for all the methods and for all-in-view satellites

Table 17 – HDOP percentile at 95, 99 and 99.9 % for 12 satellites subset

	95 % HDOP	99 % HDOP	99.9% HDOP
All-in-view	**0.8758**	**0.9770**	**1.1125**
Fast Satellite Selection	**0.9760**	**1.0675**	**1.2383**
Maximum Elevation Angle	**1.0274**	**1.1182**	**1.3037**
Brute Force	**0.9547**	**1.0415**	**1.1935**

It is possible to see from the analysis of Figure 54, Figure 55, Table 16and Table 17 that, using a satellite subset, the DOP values are higher than for the all-in-view case. In particular, for the maximum elevation angle selection method, the VDOP values are clearly bigger than the other methods. The fast satellite selection and the brute force are able to provide values similar in magnitude to the all-in-view solution, the brute force methods seems in any case to provide slightly better results than the fast selection criteria.

In the next table, the average time to compute the previous parameters for one airport will be listed for all the three methods. The maximum time for each method will be listed as well in Table 18. This analysis aims to provide an insight of the computational load of each method.

Table 18 – Computational time, in seconds, for all methods with 12 satellites subset

	All-in-View	**Fast Satellite Selection**	**Max Elevation Angle**	**Brute Force**
Maximum Time	0.0604	0.1668	0.0537	119.14
Average Time	$6.3702 * 10^{-4}$	$1.5 * 10^{-3}$	$3.2416 * 10^{-4}$	0.8096

The brute force selection criteria is, as expected, the one with the highest computational load due to the number of combinations that has to be analyzed in order to find the best VPL. The other selection criteria require a computation time similar to the all-in-view case where no selection is done.

4.5.1.2 GAST D Protection Level

The simulated processing mode is the one used in GAST D, the sigma values for this service type are computed considering the model proposed in (RTCA Inc. DO245-A) and in (RTCA Inc.; DO253-C, 2008).

- the non-aircraft RMS error is computed considering results obtained in Table 10 and divided by $\sqrt{4}$ to consider the presence of four reference receivers at ground
- the airborne pseudorange performance are computed using the AAD model considering a B level (2.3.3), then it is multiplied by a factor of 1.3 in order to take into account the increased noise level related to the use of 30 seconds as smoothing constant instead of 100 seconds (Murphy, et al., 2010).
- the RMS of the aircraft multipath is computed as in the model given in Eq. 2.69
- the ionospheric and the tropospheric Residual Error are computed as in Eq. 2.70 and Eq. 2.52

D_V and D_L , represent the difference in the vertical and lateral domain between the 30 seconds and the 100 seconds smoothed solution. They are computed using a model proposed in (Wang, et al., 2014).

$$Th(D_V) = K_{fdD}\sqrt{\sum_{i=1}^{N} S_{Apr\ vert,i}^2\ \sigma_{D_R}^2} \qquad \text{Eq. 4.7}$$

$$Th(D_L) = K_{fdD}\sqrt{\sum_{i=1}^{N} S_{Apr\ lat,i}^2\ \sigma_{D_R}^2} \qquad \text{Eq. 4.8}$$

- $KfdD$, is the multiplier taking into account for the probability of false alarm. It is set at 5.5 considering a continuity risk of 4×10^{-8}
- $\sigma_{D_R} = F_{PP} \times \sigma_{vig} \times 140 \times V\_air$; Considering a value of $\sigma_{vig} = 4\ mm/km$ and a landing speed of the aircraft of $72\ m/s$, the previous model can be approximated to $\sigma_{D_R} = F_{PP} \times 0.04\ m$

The next figures show the VPL and LPL as in Eq. 4.4 and Eq. 4.5 and the values of S_{vert} and S_{vert2}. The aim of these two plots is to verify that at any epoch, the limit value of 10 meters is not exceeded by VPL or LPL, or the 2 and 3 limits are not overcome by S_{vert} and S_{vert2}.

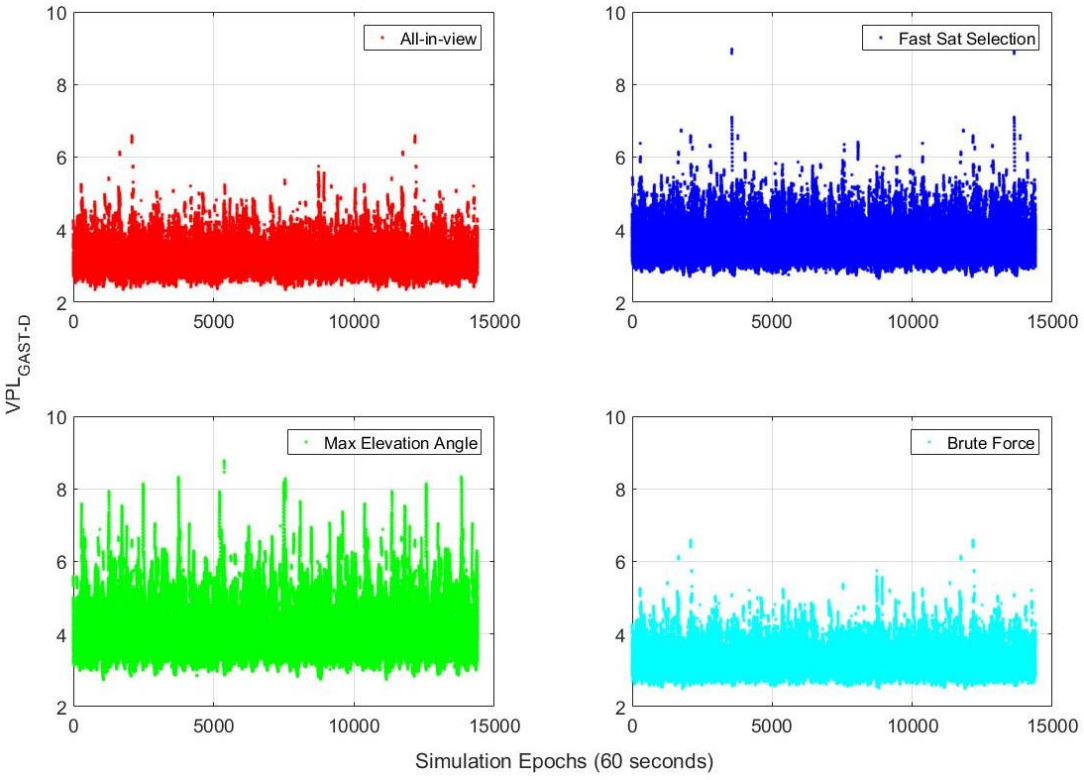

Figure 56 – GAST-D VPL computed across all the epochs and airports for three selection methods and all-in-view satellites

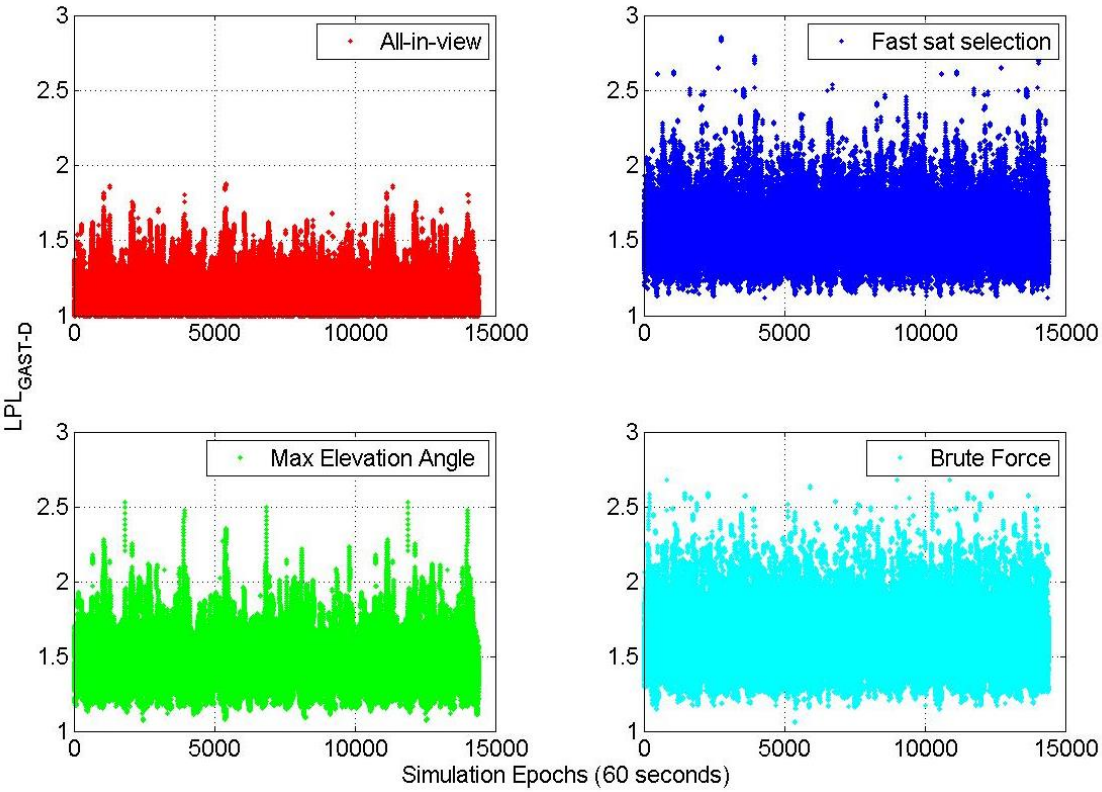

Figure 57 – GAST-D LPL computed across all the epochs and airports for three selection methods and all-in-view satellites

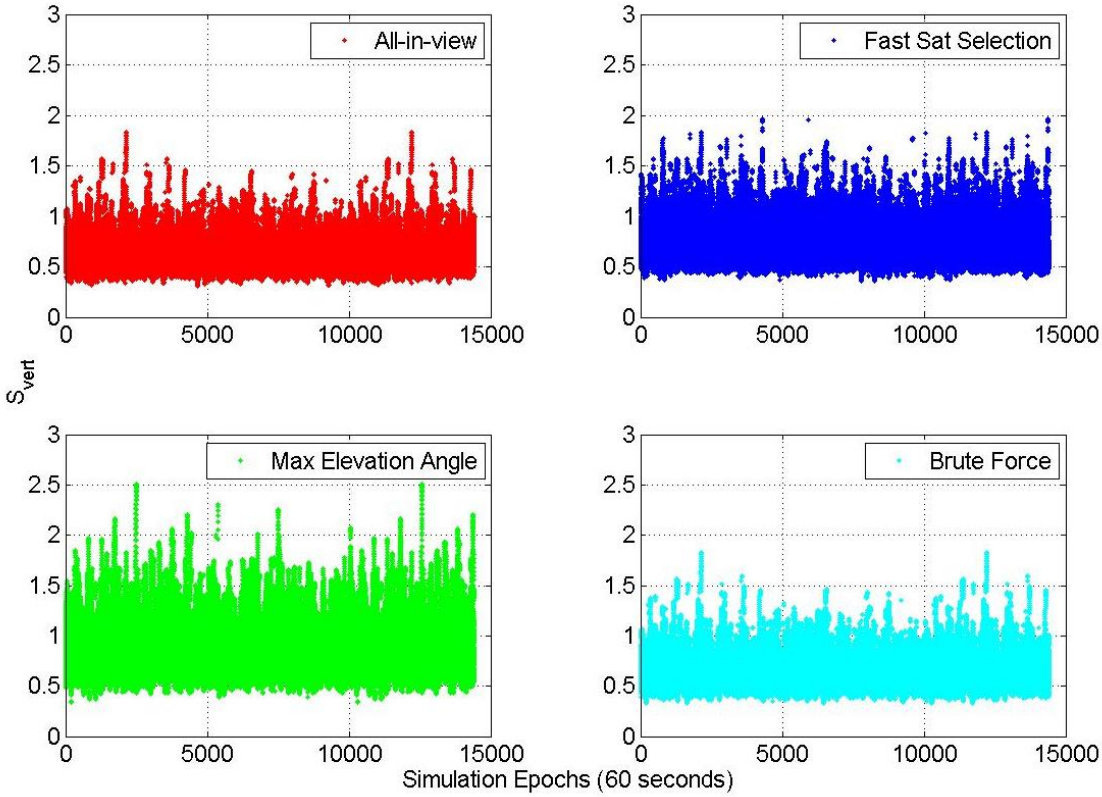

Figure 58 – GAST D S_{vert} values across all epochs and airports for three methods and all-in-view satellites

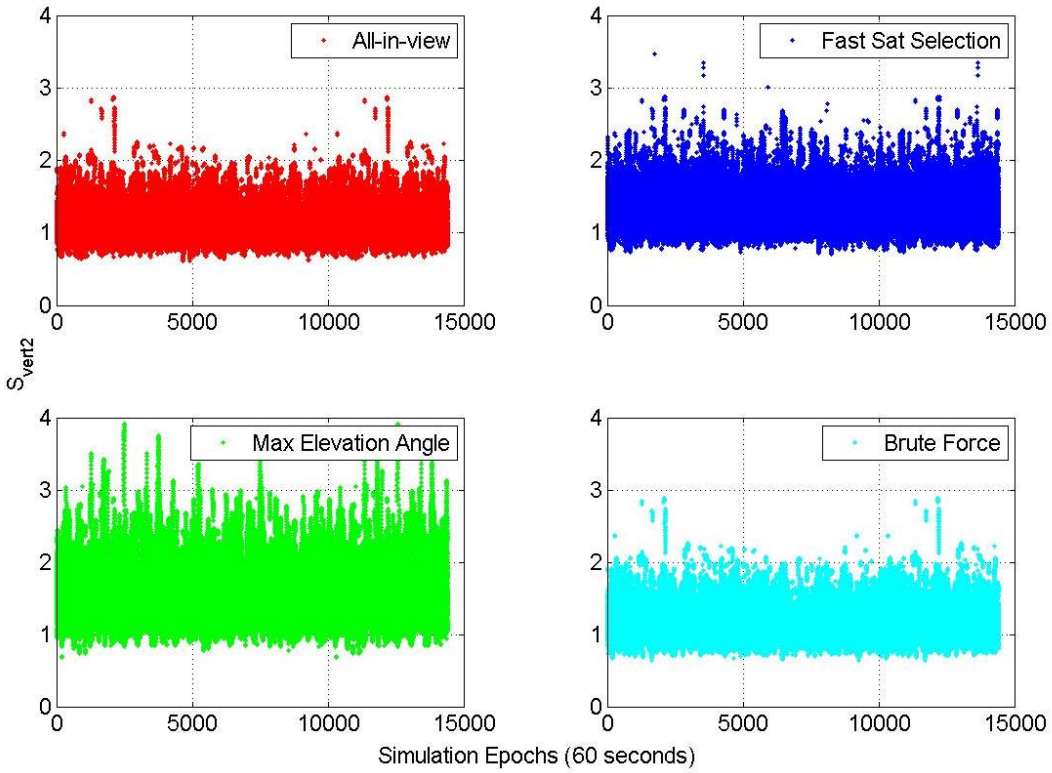

Figure 59 – GAST D S_{vert2} values across all epochs and airports for three methods and all-in-view satellites

As expected, the VPL provides larger values than the LPL. In both figures, the protection levels do not overcome the 10 meters limit, making the GAST D service available at all airports and at all epochs. The brute force algorithm is optimized to find the lowest VPL. This explains why at several epochs, the LPLs found by the brute force algorithm is higher than the ones found by the other two methodologies.

Table 19 – Geometry screening availability for all the selection methods with 12 satellites and all in view case

	VPL Availability	**LPL Availability**	**S_{vert} Availability**	**S_{vert2} Availability**
All-in-view	100 %	100 %	100 %	100 %
Fast Sat Selection	100 %	100 %	100 %	>99.999 %
Max Elevation Angle	100 %	100 %	99.92 %	99.79 %
Brute Force	100 %	100 %	100 %	100 %

The comparison between the three selection methods shows that the brute force algorithm is able to find the lowest VPL, the fast satellite selection finds geometries providing VPL values slightly larger than the brute force. This last provides, indeed, some geometry screening unavailability due to the overcoming of the S_{vert2} limit of 3. The use of geometries based on the selection of the satellites with the maximum elevation angle is the one providing the largest VPL values, moreover in several epochs the S_{vert} and S_{vert2} limits are overcome, making these epochs unavailable. In the horizontal domain the use of the maximum elevation angle criteria provide better result than the other two methodologies, the results are however good for all the three selection criteria.

4.5.1.3 I-Free Protection Level

In the frame of dual constellation and dual frequency GBAS research, a possible candidate for the processing mode is the I-Free (2.2.2.2.3). This mode permits to remove entirely the ionospheric delay from the code measurement at the cost of increased noise level, at the ground for the computation of the pseudorange correction and at the airborne level for the final position computation. To compute the protection level considering the use of this technique, there are no official formula as for the GAST D service, so the computation of these parameters will be done considering the results obtained in the analysis of the performance for noise and multipath at ground station level for L1 and L5. It has to be reminded that a calibration issue has been found n L5 band measurements and that it impacts also the I-free results. All the components taking into account the ionospheric delay for the computation of the protection level in GAST D will be removed for the I-Free protection level. The divergence terms, D_V and D_L, are set at zero because the double smoothing constant is not used in this case. The sigma ground will be inflated considering the use of the two frequencies, as well as the sigma airborne. The total sigma is:

$$\sigma_{tot\ I-Free}(i) = \sqrt{\sigma^2_{pr\ gnd\ I-Free,i} + \sigma_{tropo,i} + \sigma^2_{pr\ air\ I-Free,i}} \qquad \text{Eq. 4.9}$$

Where:

- $\sigma_{pr\ gnd\ I-Free}$ is defined using the bound defined in 3.4
- $\sigma_{pr\ air\ I-Free} = \sqrt{\sigma^2{}_{pr\ air\ L1}\left(1-\frac{1}{\alpha}\right)^2 + \sigma^2{}_{pr\ air\ L5}\ \frac{1}{\alpha^2}}$

Because lack of information about accuracy of L5 measurement at airborne side, $\sigma_{pr\ air\ L5}$ is assumed to have the same values as $\sigma_{pr\ air\ L1}$ computed relying on the AAD model (Table 12)

- $\sigma_{pr\ air\ I-Free} = \sigma_{pr\ air}\sqrt{\left(1-\frac{1}{\alpha}\right)^2 + \frac{1}{\alpha^2}}$

As for the previous case the protection level, the S_{vert} and S_{vert2} will be analyzed.

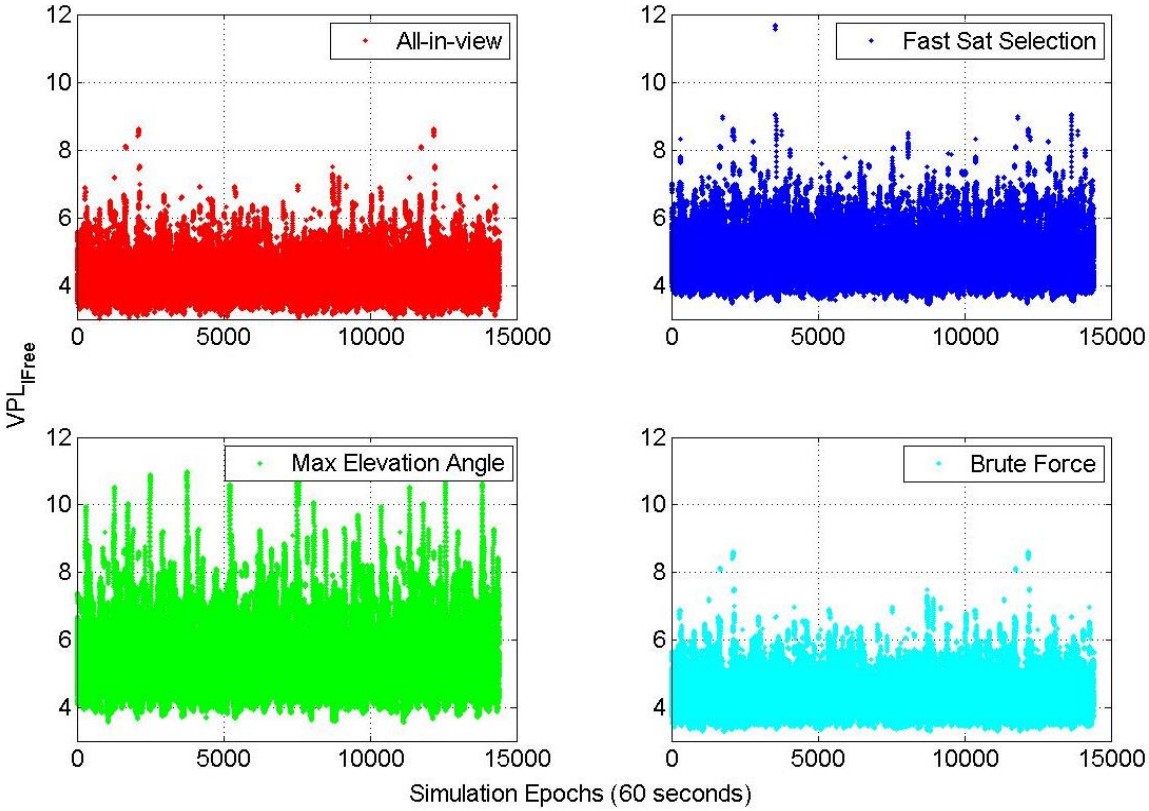

Figure 60 – I-Free VPL across all epochs and airports for three methods and all-in-view satellites

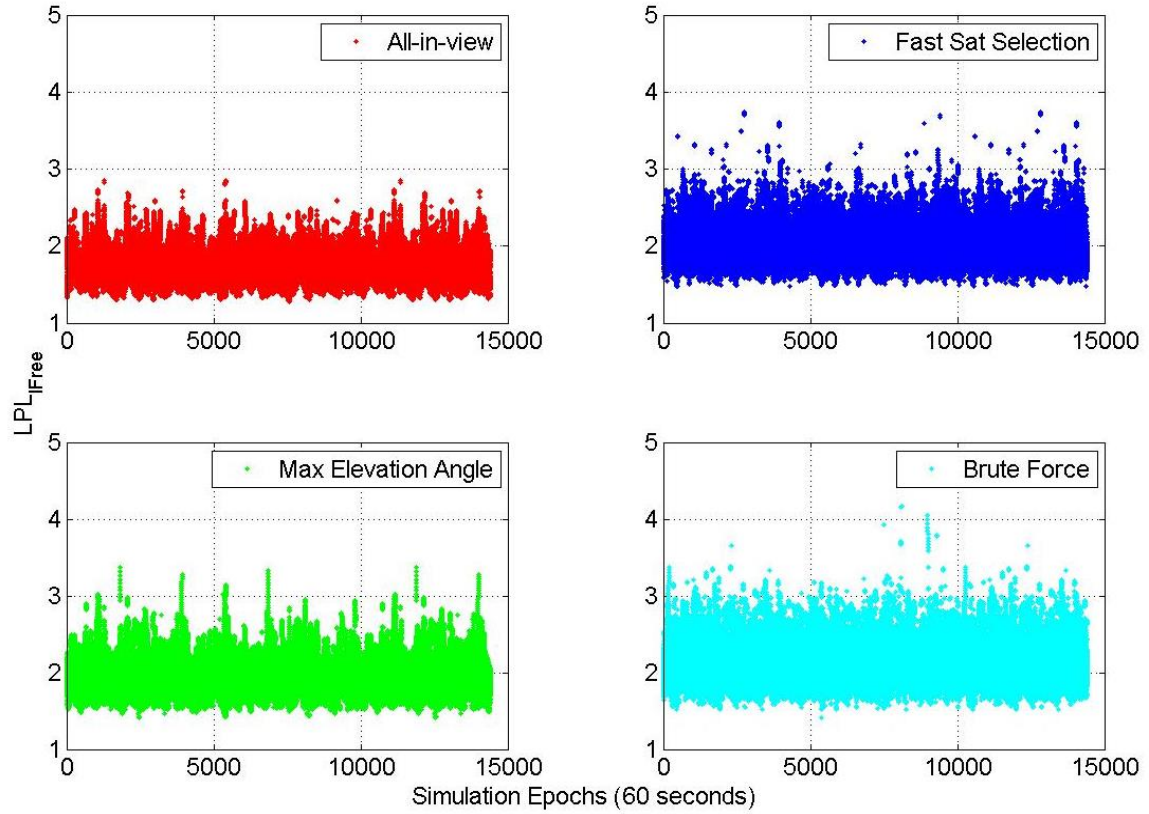

Figure 61 – I-Free LPL across all epochs and airports for three methods and all-in-view satellites

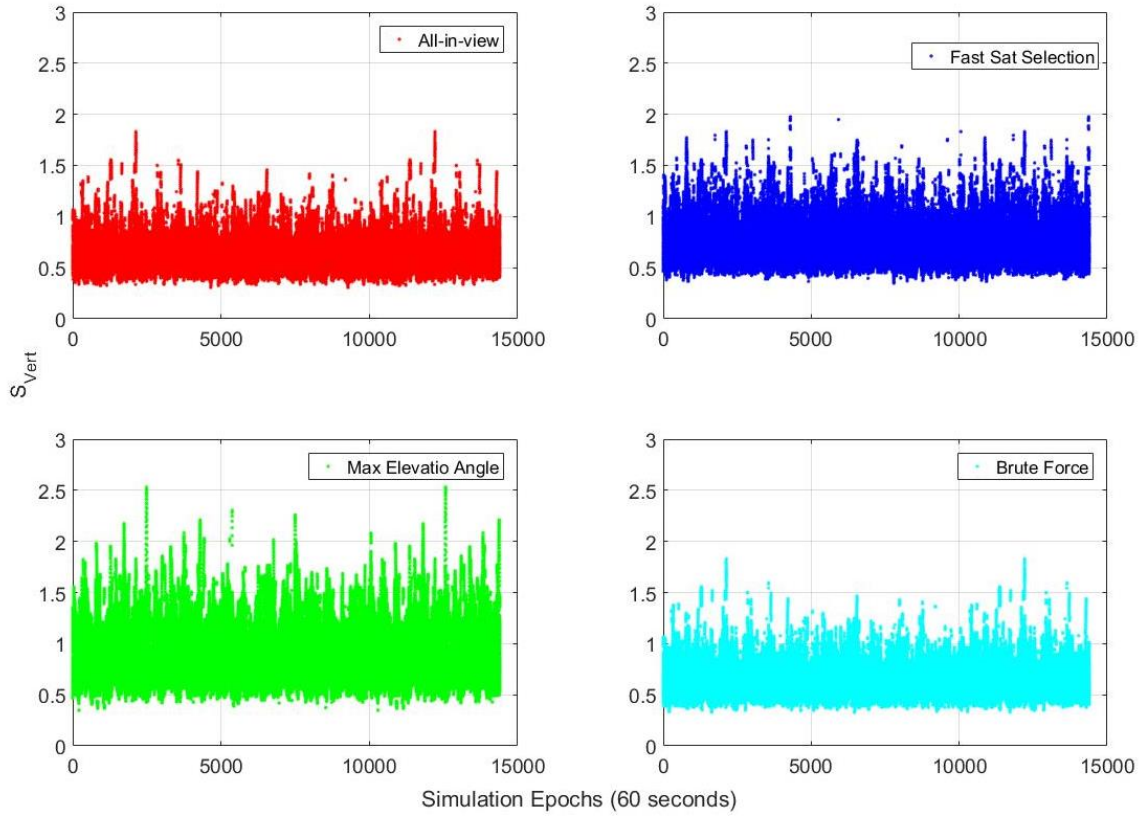

Figure 62 – I-Free S_{vert} values across all epochs and airports for three methods and all-in-view satellites

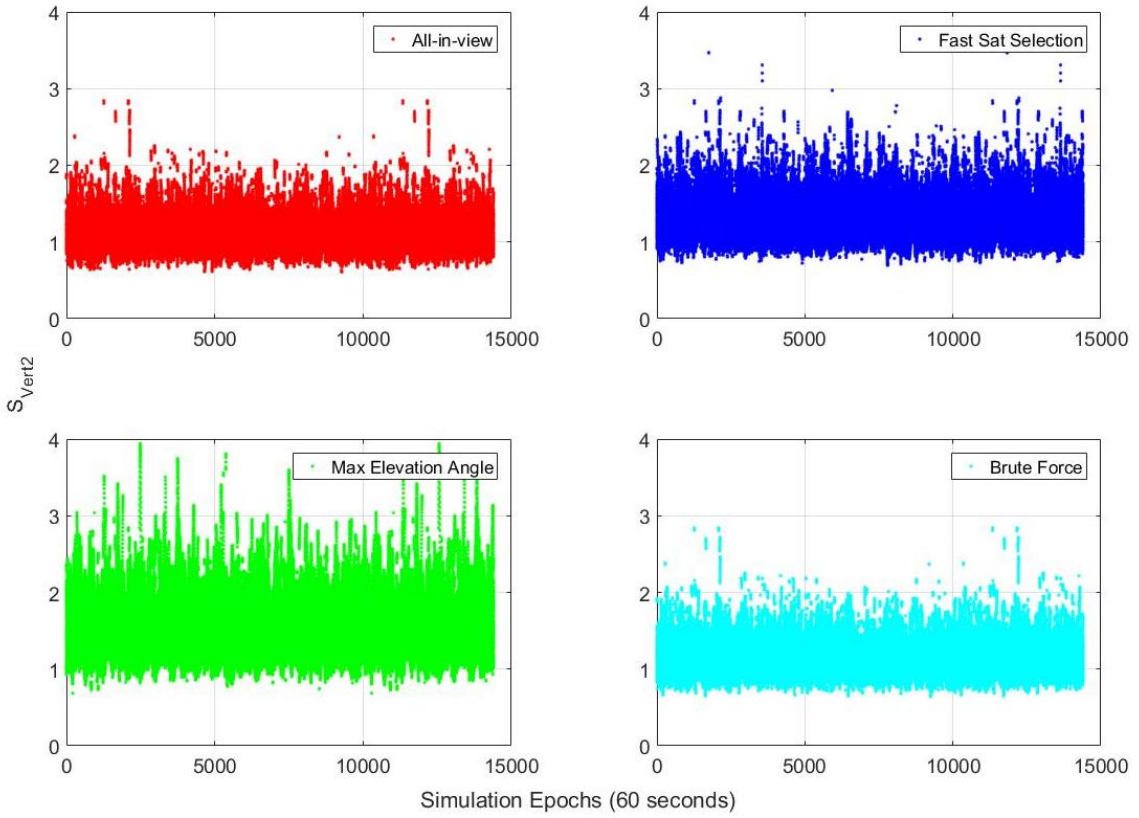

Figure 63 – I-Free S_{vert2} values across all epochs and airports for three methods and all-in-view satellites

Table 20 – Geometry screening availability for all selection methods and all in view case

	VPL Availability	**LPL Availability**	**S_{vert} Availability**	**S_{vert2} Availability**
All-in-view	100 %	100 %	100 %	100 %
Fast Sat Selection	> 99.999 %	100 %	100 %	99.91 %
Max Elevation Angle	99.92 %	100 %	99.91 %	99.78 %
Brute Force	100 %	100 %	100 %	100 %

The use of I-Free techniques, despite the absence of the sigma ionosphere value and the absence of the D_V or D_L in the protection level formula, generates values of VPL bigger than the GAST D case. This is because the value of standard deviation at ground and at airborne side are bigger than for GAST D. The fast satellite selection and the maximum elevation angle have values of VPL overcoming the alert limit of 10, leading to a system unavailability. The S values are as well as high fort the two methods, leading to unavailability in some epochs.

In particular the most critical conditions appear when the maximum elevation angle algorithm is used as selection method providing the lowest percentage of availability. The fast satellite selection method provides good performances and only in a few epochs the VPL exceeds the limit, as well as for the S_{vert} and S_{vert2} . The brute force algorithm is able to provide values of VPL almost similar to the all-in-view condition and does not exceed the 10 meters limit in any epoch, the percentage of availability for this method is 100 %.

4.5.2 Dual Constellation 15 Satellites Subset

In this simulation the same two constellations used in 4.5 are used, the only difference is the number of satellites used for the subset.

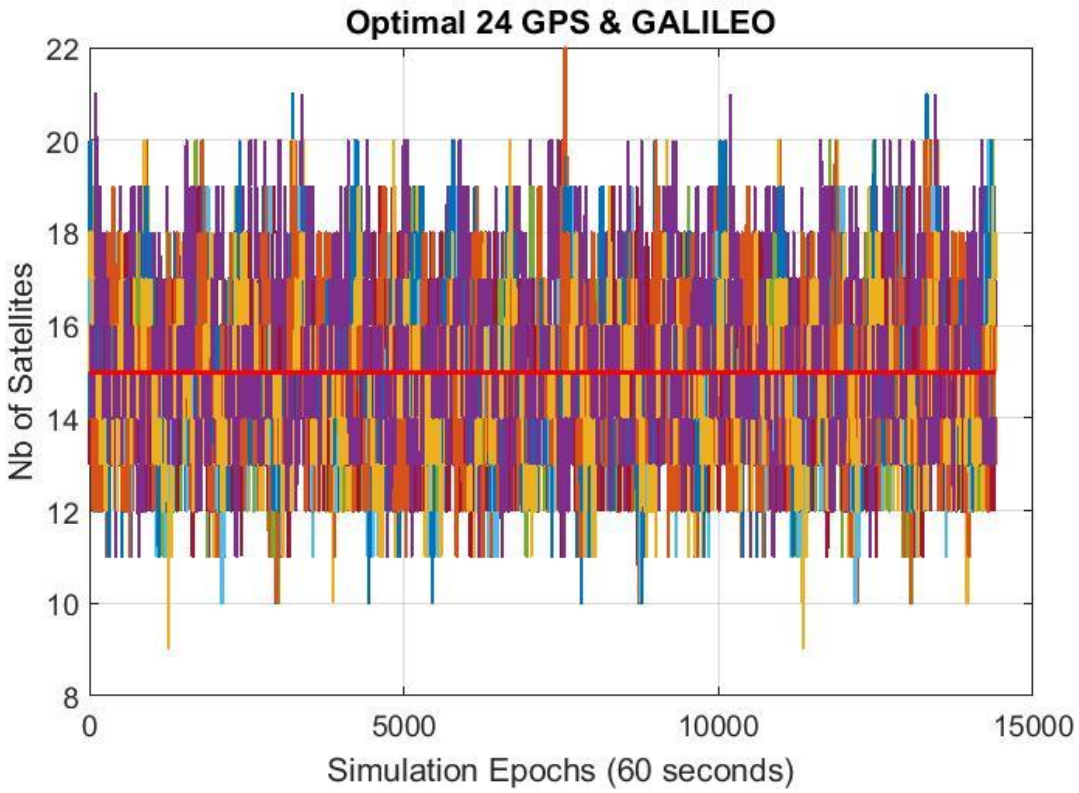

Figure 64 – Number of satellites for all the epochs and airports and 15 satellites subset in red

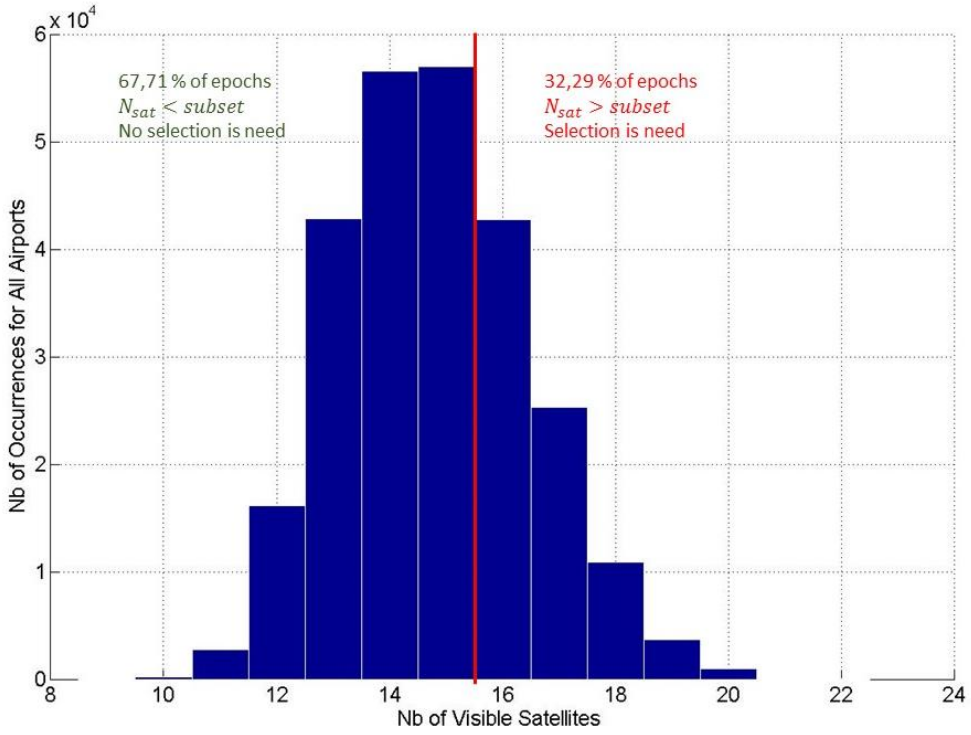

Figure 65 – Histogram of satellites number across all airports and epochs with percentage of use of satellite selection for subset 15

From the previous figures, it is possible to see that in 67.71 % of the epochs, for all the airports, there are less satellites in view than the subset limit. This will provide more similar results between the all-in-view and the subset parameters, reducing also the computational load due to the limited time of use of the algorithm and limiting the number of combinations to analyze per epoch thanks to the limited difference between satellites in view and subset dimension.

4.5.2.1 Impact of the Selection Method on the DOP Value

In the next figures the values of the DOP for the vertical and horizontal will be analyzed.

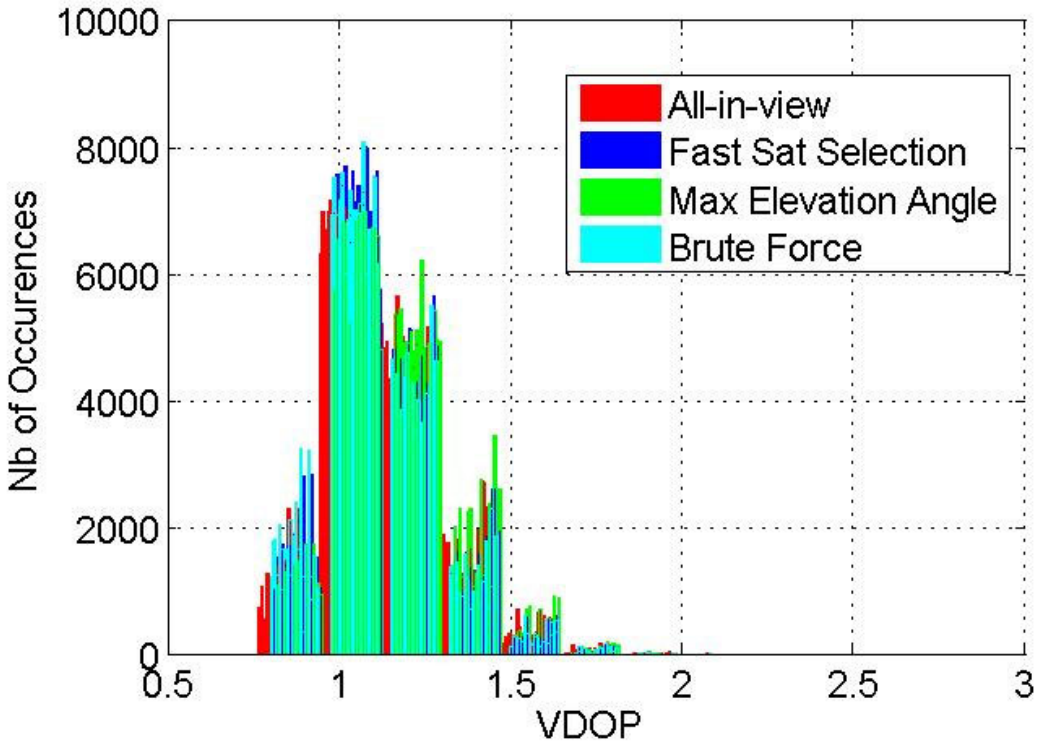

Figure 66 – VDOP values across all epochs and airports for all the selection criteria and for all-in-view satellites

Table 21 – VDOP percentile at 95, 99 and 99.9 % for 15 satellites subset

	95 % VDOP	99 % VDOP	99.9% VDOP
All-in-view	**1.4115**	**1.6099**	**1.9041**
Fast Satellite Selection	**1.4177**	**1.6121**	**1.9041**
Maximum Elevation Angle	**1.4668**	**1.6480**	**1.9129**
Brute Force	**1.4120**	**1.6099**	**1.9103**

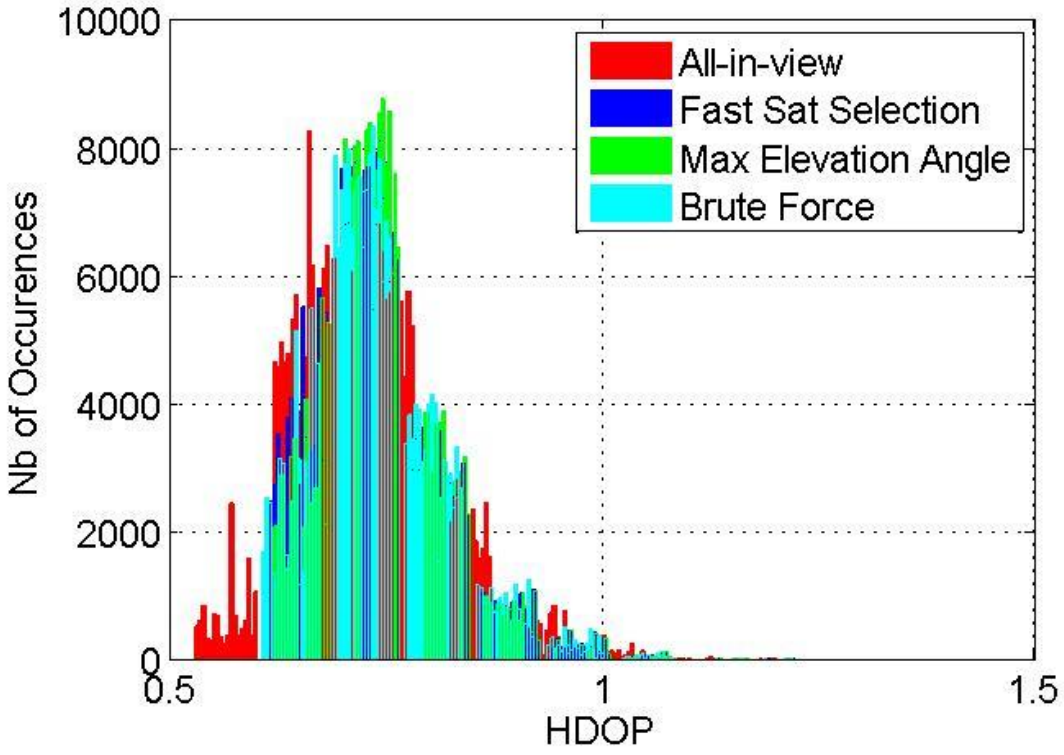

Figure 67 – HDOP values across all epochs and airports for all the selection criteria and for all-in-view satellites

Table 22 – HDOP percentile at 95, 99 and 99.9 % for 15 satellites subset

	95 % HDOP	**99 % HDOP**	**99.9% HDOP**
All-in-view	0.8758	0.9770	1.1125
Fast Satellite Selection	0.8760	0.9770	1.1125
Maximum Elevation Angle	0.8780	0.9773	1.1125
Brute Force	0.8760	0.9770	1.1125

Analyzing the DOP values, Figure 66, Figure 67, Table 21 – VDOP percentile at 95, 99 and 99.9 % for 15 satellites subset Table 21 and Table 22, it is possible to assess that the maximum elevation angle provides slightly degraded results compared to the other two methods. The other selection criteria provide results similar to the all-in view case.

The last analysis regards the computational time for each methods and for the all-in-view case.

Table 23 – Computational time, in seconds, for all methods with 15 satellites subset

	All-in-View	Fast Satellite Selection	Max Elevation Angle	Brute Force
Maximum Time	0.0243	0.2059	0.0591	4.125
Average Time	$5.2735 * 10^{-4}$	$8.2895 * 10^{-4}$	$7.4479 * 10^{-4}$	$7.8 * 10^{-3}$

The brute force selection criteria is, also when 15 satellites are selected as subset, the one with the highest computational load. Compared to the computation time for a subset with a size of 12 satellites, the maximum time for the brute force is very small. The other selection criteria have almost the same computational load as for the all-in-view case.

4.5.2.2 GAST-D Protection Level

In the next figures the VPL, LPL, S_{vert} and S_{vert2}, computed using the GAST D requirement, will be shown.

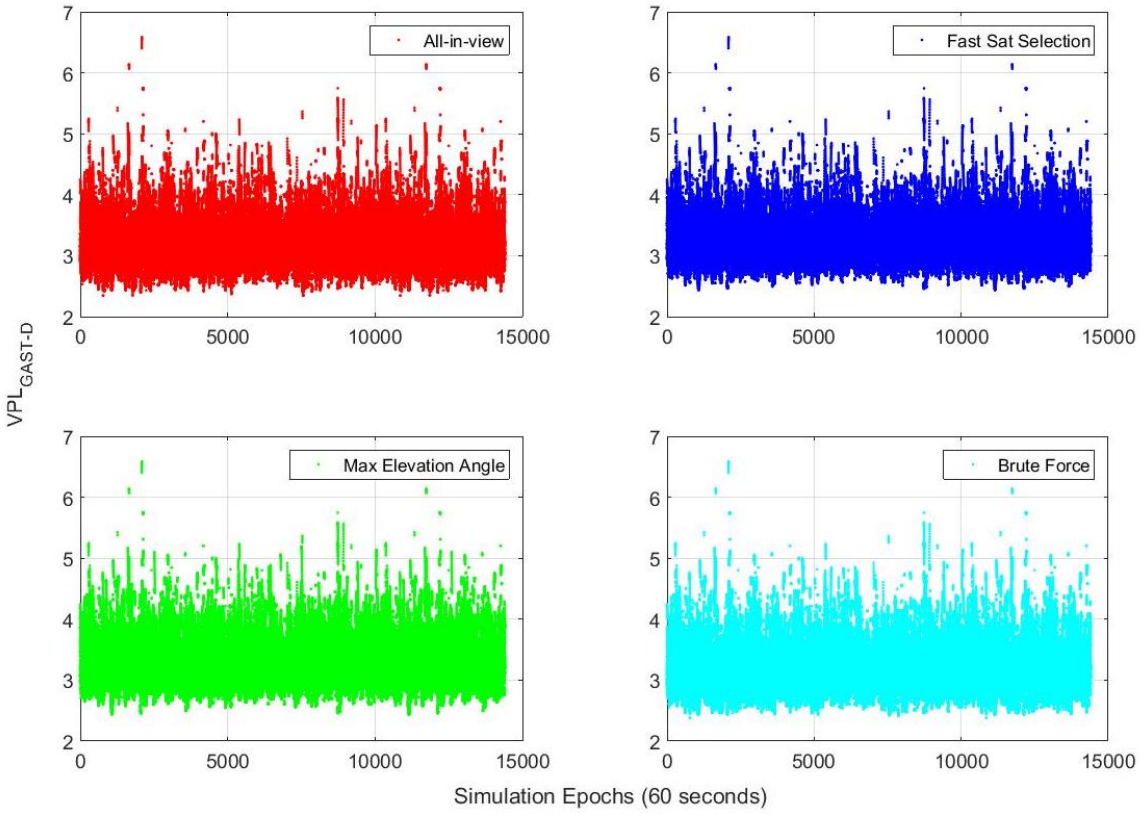

Figure 68 – GAST D VPL for all the epochs and airports for all the analyzed methods and all-in-view satellites

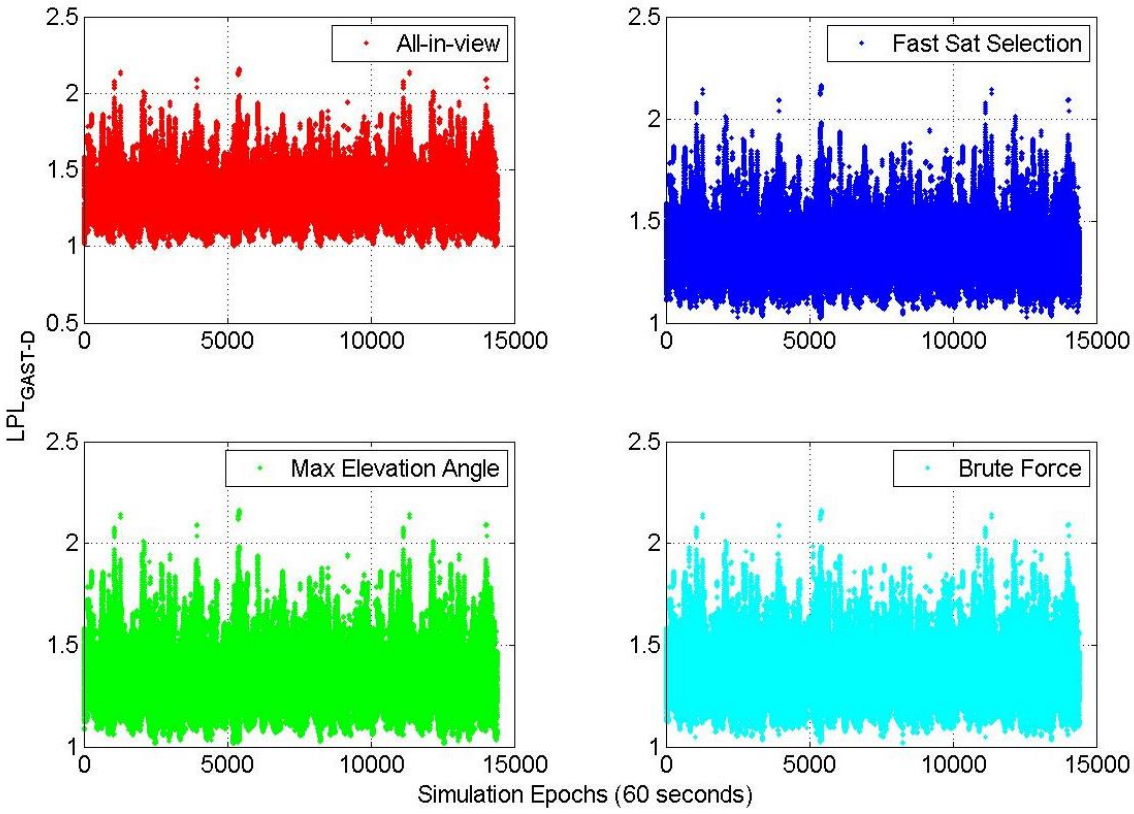

Figure 69 – GAST D LPL for all the epochs and airports for all the analyzed methods and all-in-view satellites

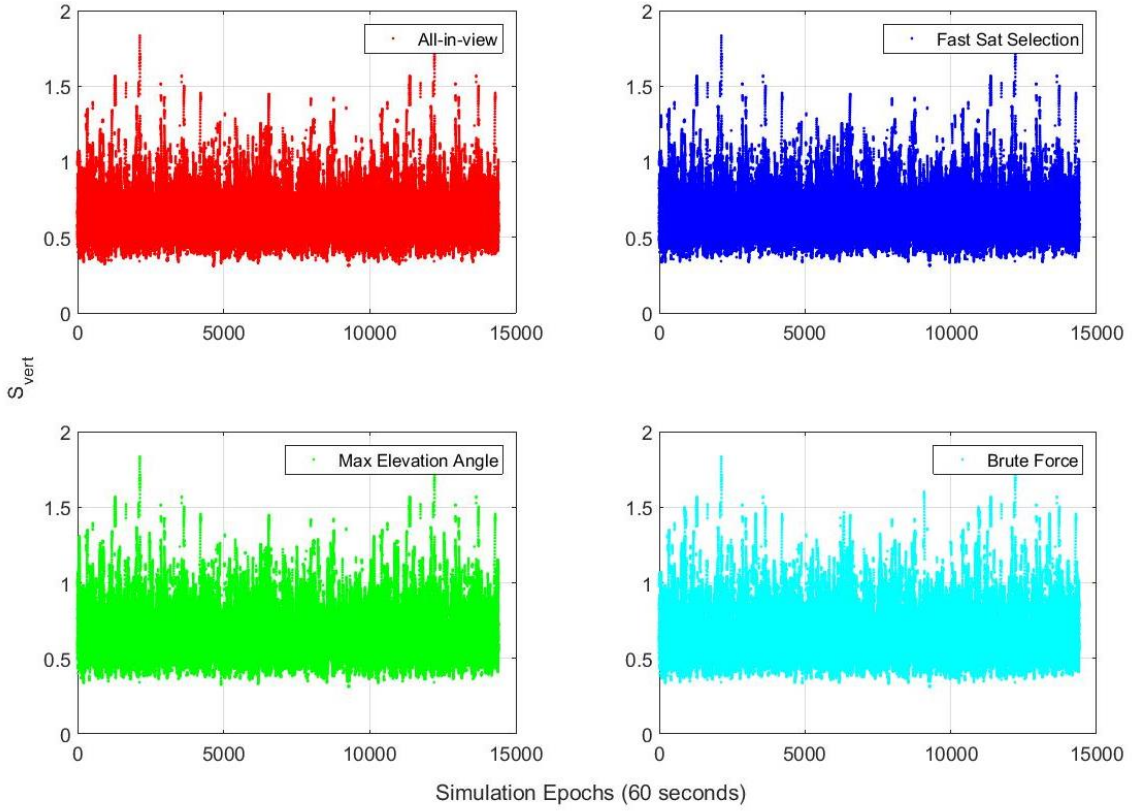

Figure 70 – GAST D S_{vert} computed for all the epochs and airports for all the analyzed methods and all-in-view satellite

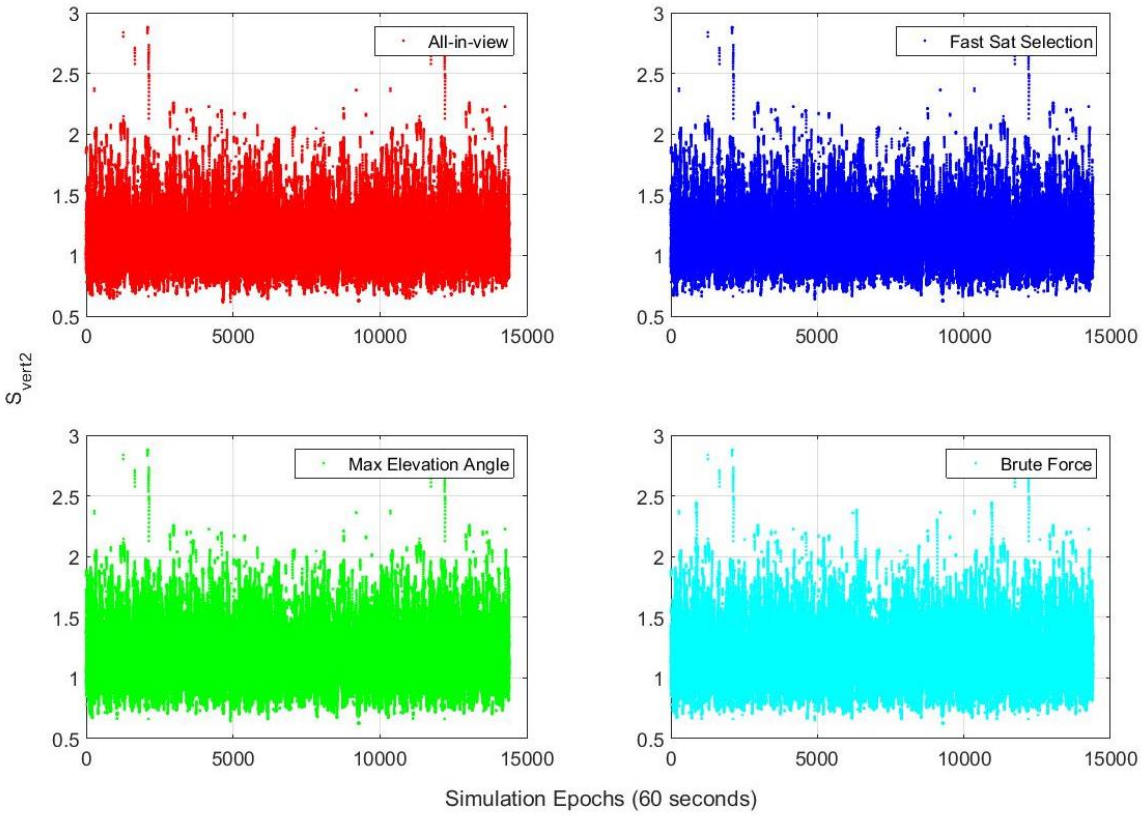

Figure 71 – GAST D S_{vert2} computed for all the epochs and airports for all the analyzed methods and all-in-view satellites

As expected, in more than the half of the epochs, the results between the all-in-view case and the ones computed using a subset are the same. There are no cases of system unavailability due to bad geometry condition. It is possible to note, for the VPL analysis in Figure 68, that the maximum elevation angle algorithm provides values of VPL slightly bigger than the other two selection methods.

4.5.2.3 I-Free Protection Level

In this simulation the parameters used are the same as in 4.5.2.3, the only difference is the dimension of the subset. The next two figures shows the VPL and the LPL for computed for this processing mode.

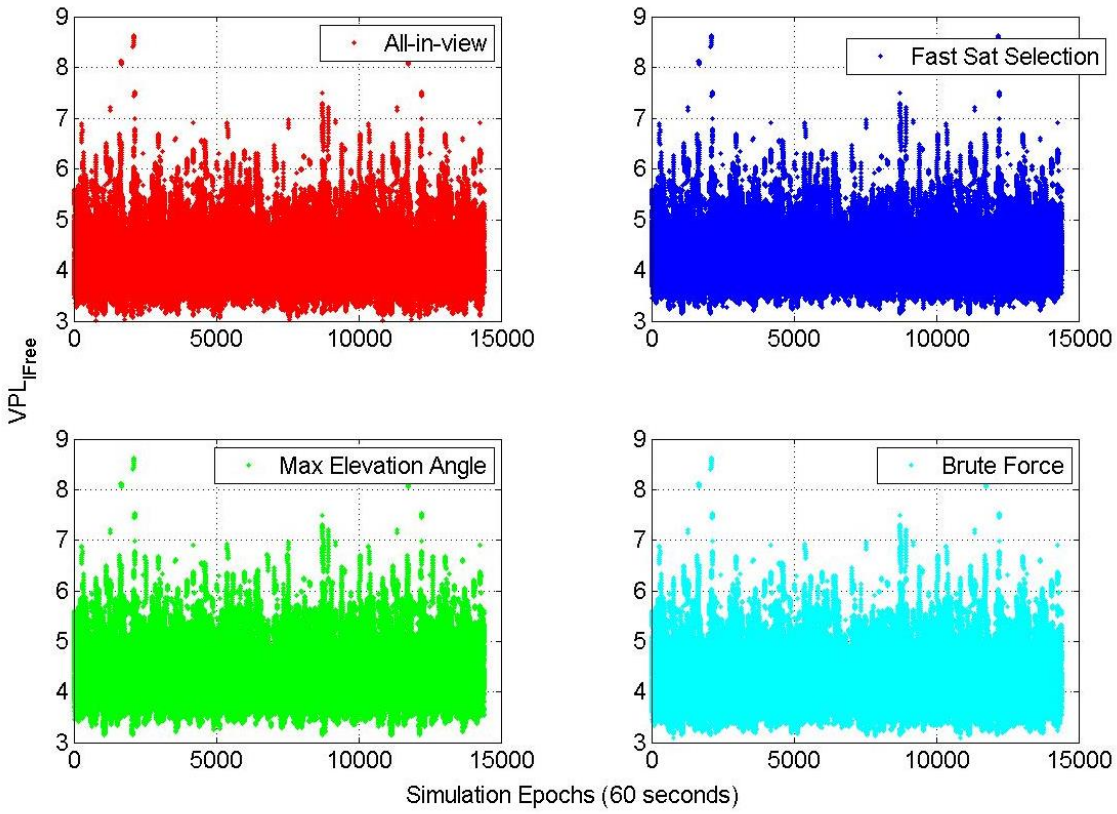

Figure 72 – I-Free VPL for all the epochs and airports for all the analyzed methods and all-in-view satellite

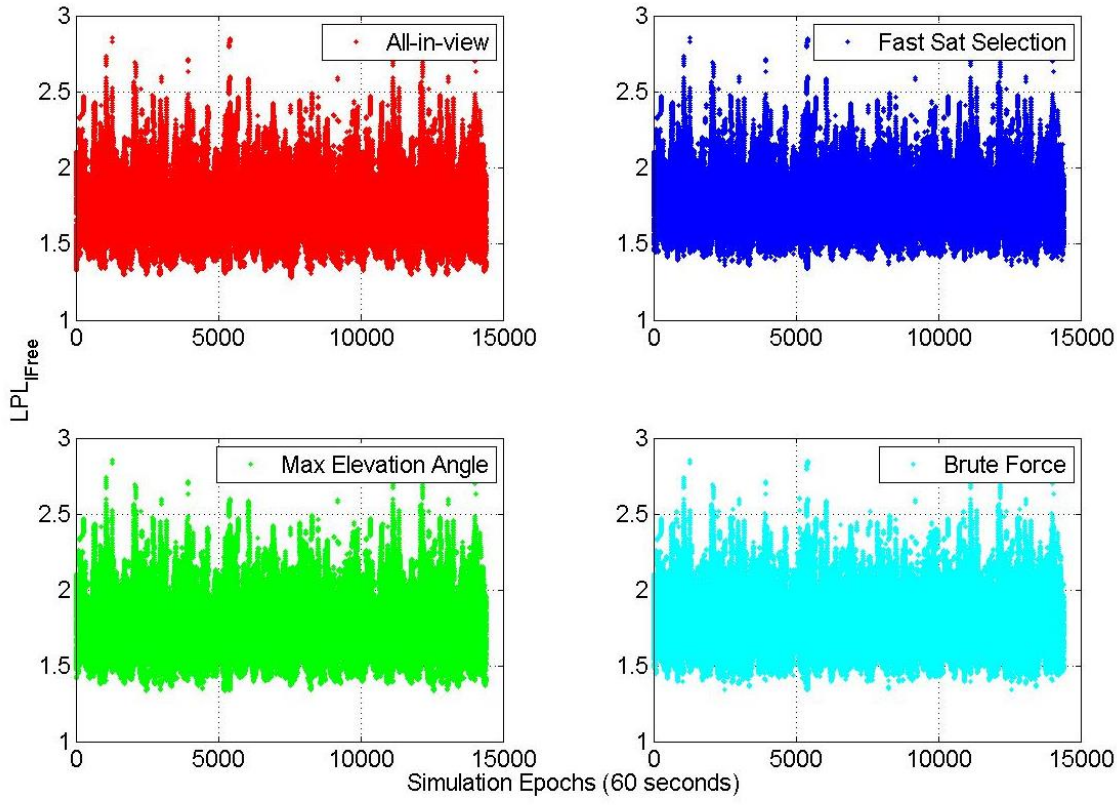

Figure 73 – I-Free LPL for all the epochs and airports for all the analyzed methods and all-in-view satellites

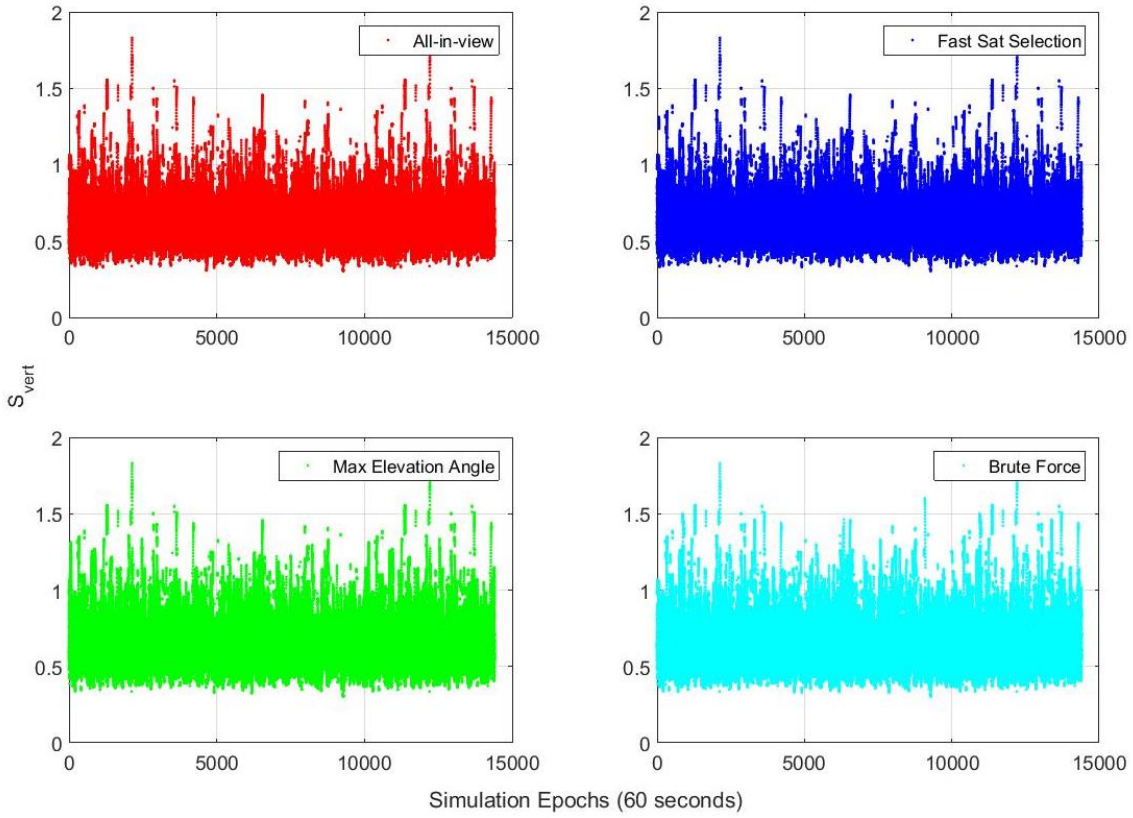

Figure 74 – I-Free S_{vert} computed for all the epochs and airports for all the analyzed methods and all-in-view satellites

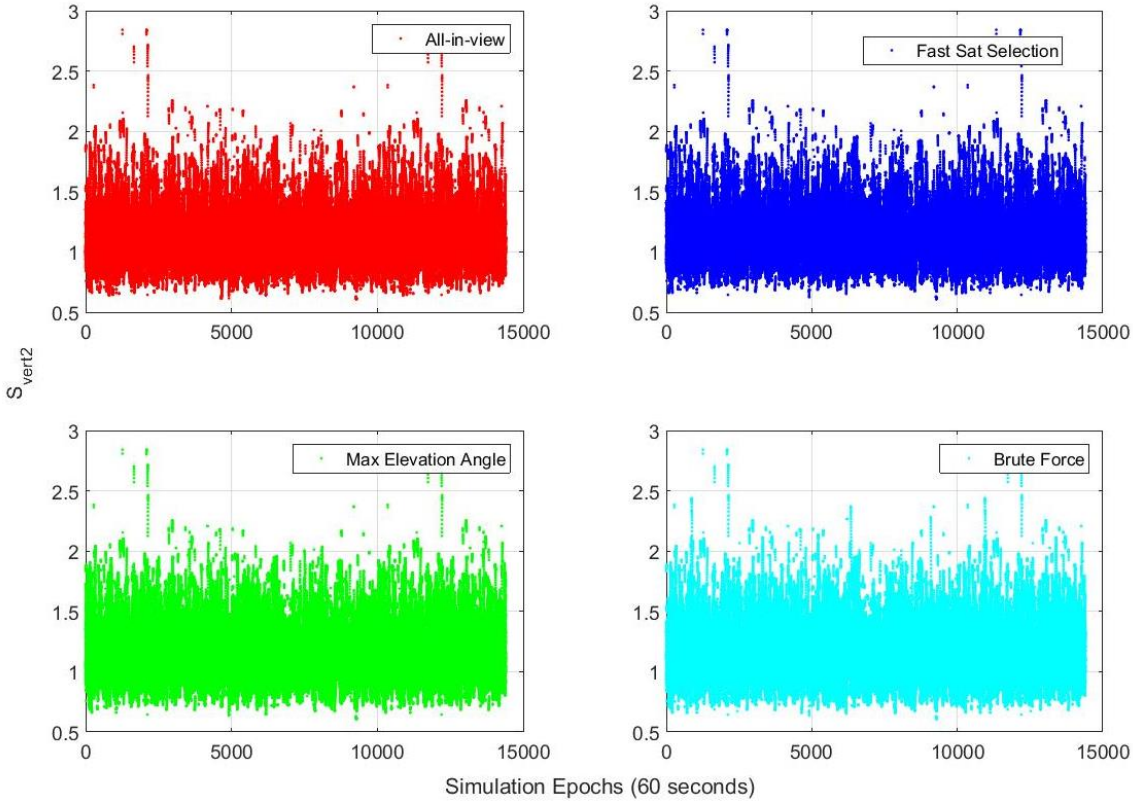

Figure 75 – I-Free S_{vert2} computed for all the epochs and airports for all the analyzed methods and all-in-view satellites

In this I-Free case, due to the increased number of satellites for the subset dimension, there are no epochs flagged as unavailable for exceeding the 10 meters limit or overcoming the S_{vert} limit. As for the GAST D case the maximum elevation angle seems to provide values of the protection level slightly bigger than the other selection criteria.

4.6 Conclusions

In this chapter, the possibility of using a satellite subset instead of using all the satellites in view has been investigated. The reason for this analysis stemmed from:

- The high number of signals coming from visible satellites to track with two constellations and two frequencies.
- The limitation of the number of corrections that is possible to broadcast in the current GBAS messages structure. The current limit for GAST D is 18 satellites, but with the development of GAST F, and the requirement to maintain interoperability between services, the limit could drop to lower values.

Considering these conditions, together with the number of visible satellites, has been chosen to analyse subsets composed of 12 and 15 satellites.

The first conclusion regards the minimum number of satellites to use as subset. For the dual constellation case, two subset sizes have been tested. The use of 12 satellites, as it is possible to see from the results in section 4.5, seems to not be sufficient from a geometrical point of view. The loss of accuracy analyzed by plotting the DOPs indicates that the vertical domain experiences an important degradation of the accuracy (VDOP increased by 2 in the worst cases). The only methods that seems able to work under this condition is the brute force solution, able to find subsets providing values of DOP similar to the all-in-view solution. The analysis of the computational load, however, clearly show that this method is not adapted to be used for a real time application due to the high number of combinations to be analyzed in some epochs. Analysing the protection level for the two processing modes, it is possible to see that the VPL, being the most critical protection level, overcomes in some epochs the limit of 10 meters in the I-Free case making these epochs unavailable. The analysis of the S_{vert} and S_{vert2} values confirms what has been seen in the VPL analysis. The use of a subset with 15 satellites provides better results, the values of the DOP are similar and the accuracy degradation is less important than the previous case. Analysing also the different processing modes, the it is possible to find out that no epochs can be flagged as unavailable due to a bad geometry, the VPL, the S_{vert} and the S_{vert2} do not overcome the alarm limit in any epoch.

The second conclusion regards the comparison between the three selected methods. The optimal solution is the best methods to find the lowest VPL in all the simulations done. If, on one side, this method works

better than the other, on the other hand, its computational burden results to be much higher than any other. Therefore, this methodology could be inappropriate for a real time application.

The maximum elevation angle provides the opposite result than the optimal solution: it has almost no computational load but it does not take into account the geometrical aspect of the accuracy derivation. It can be observed, especially in the vertical domain, that the loss of accuracy is very important, because the selection of the highest elevation satellites reduces the spread in the elevation angle. Considering the analysis of the protection level and the S values, this method provides the highest values and in several epochs the GBAS service may result as unavailable if a subset is used.

The fast satellite selection seems to be a compromise methodology between the two other methods, it has almost the same computational load as the maximum elevation angle criteria but it is able to find subset with good geometry. This method, in fact, takes into account the geometry as an important factor but is more efficient than the optimal solution in term of computational load. It takes into account also the elevation angle because in the slice of sky with more than one satellite, the one with the highest elevation angle can be selected.

Considering the joint analysis, the use of a subset with 15 satellites seems to be a better choice in order to guarantee the availability of the GBAS service, the fast satellite selection method is the one providing the best joint results: accuracy and low computational burden. Moreover with this subset size is possible to rely on the use of the I-free combination. Considering that GAST-D is still under validation due to a lack of integrity performance in detecting ionosphere anomalies and knowing that the I-free combination is the only one able to totally remove the ionospheric delay from the code measurement this condition has a relevant importance in the choice of the optimal subset size.

This analysis does not take into account other kinds of problems that may rise in GBAS, such as the impact of satellite selection on the smoothing process or monitors. It is well known that the smoothing steady state performances are reached when the time elapsed from the start of the filter is at least equivalent the smoothing constant used. This condition can represent a problem if the used selection methodology has a rate of change of subset that is too high. To be suitable for GBAS, the rate of change of subset for any methods has to be checked and the results must be taken into account with the previous analysis. A useful algorithm to avoid losing a setting satellite during the approach phase is the "Constellation Freezing" proposed in (Neri, 2011). It may help not to take into account in the subset search satellites that are present at the beginning of the approach and are going to set before the landing. Thanks to the use of this algorithm, the rate of change of subsets could be further reduced.

Another problem not considered in this study may be represented by the difference of satellites in view between the ground and the airborne subsystem, if the ground station selects a certain subset but for any reason one of them is not tracked by the aircraft, this would lead to an extra-degradation. A possible

solution to this kind of problem is the application of the satellite selection only at airborne level, in this way the probability to have a difference between the satellites in view is reduced.

5 GBAS Integrity

Integrity has been for all GBAS services one of the most critical parameter to meet. According to the level of service that each GAST service is expected to provide, the integrity concepts have been developed following different methodologies which are now summarised.

In GAST-C, the ground station is responsible for monitoring the entire system. In order to bound errors present at the aircraft side, where no monitors are present, the ground station computes a series of protection levels based on conservative assumptions such as accounting for a number of measurement outages. This complements the fault-free protection level determined within the aircraft whose role is to protect against positioning failures due to nominal errors. The ground based bounding is designed to ensure that undetected faults cannot cause a positioning failure for a 'worst' aircraft geometry under certain conditions. This service has been validated to provide CAT I precision approach operations. In case of anomalous ionospheric conditions the availability of the service is strongly impacted due to the absence of monitors at aircraft level and due to the conservative assumption done to cope with this absence.

The demonstrations of GAST-D airworthiness relying on the same concept used in GAST-C, linearization of the ILS performances, is not possible due to the higher level of performances expected for this kind of operations Figure 110. In order to better reproduce GBAS properties another concept has been used for GAST-D, the auto-land model. This consider the ability of the aircraft to land in a defined "box" (figure in appendix A) based on two main error sources.

- The Navigation System Error (NSE).
- The Flight Technical Error (FTE)

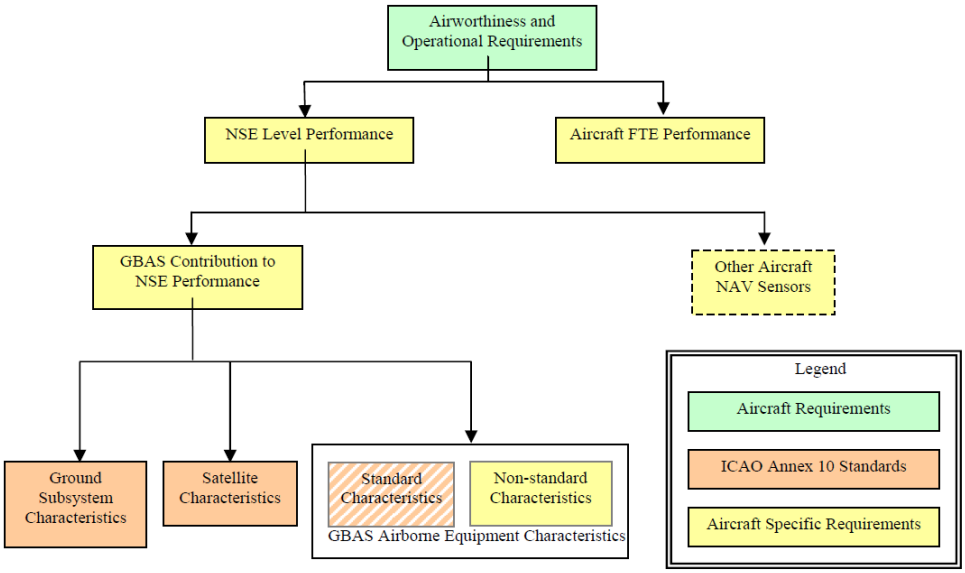

Figure 76 GBAS standards to support CAT III operations (ICAO NSP, 2010)

GBAS, under GAST-D, contributes only for the NSE. Considering the touchdown performances as dependent from the Total System Error (TSE), and this last being the sum of NSE and FTE. The derivation of the "expected GBAS contribution to NSE" may be derived. The challenge has been to derive GBAS performances that permit to demonstrate airworthiness to a large number of aircraft.

So in this service the aircraft is now responsible for determining its own airworthiness which partly relies on additional responsibilities regarding the monitoring of ionosphere anomalies. The ground station, on the other side, is only responsible for monitoring all ranging sources failures. In spite of the development of a new concept, and new monitors, this service remains to be fully validated and standardised since the proof of integrity relating to ionosphere monitoring has yet to be achieved.

Initial developments into a GAST F service, also with the goal of supporting Cat II/III operations, have begun within SESAR 15.3.7. A common requirements framework to GAST D has been assumed which will require the aircraft to assess its total system performance assuming a standardised ground monitoring capability for ranging source faults. New integrity challenges have been identified which are related to the use of new signals, DF combinations and possible new processing modes (different update rate for the PRC and RRC). Moreover the impact of the threats on new signals (frequency, constellation) must be assessed, for example the ionospheric delay differs according to the frequency used. For this new service, fallback modes has to be defined in case of loss of a frequency or loss of a constellation. In Figure 77 an example of fallback modes for GAST-F is shown.

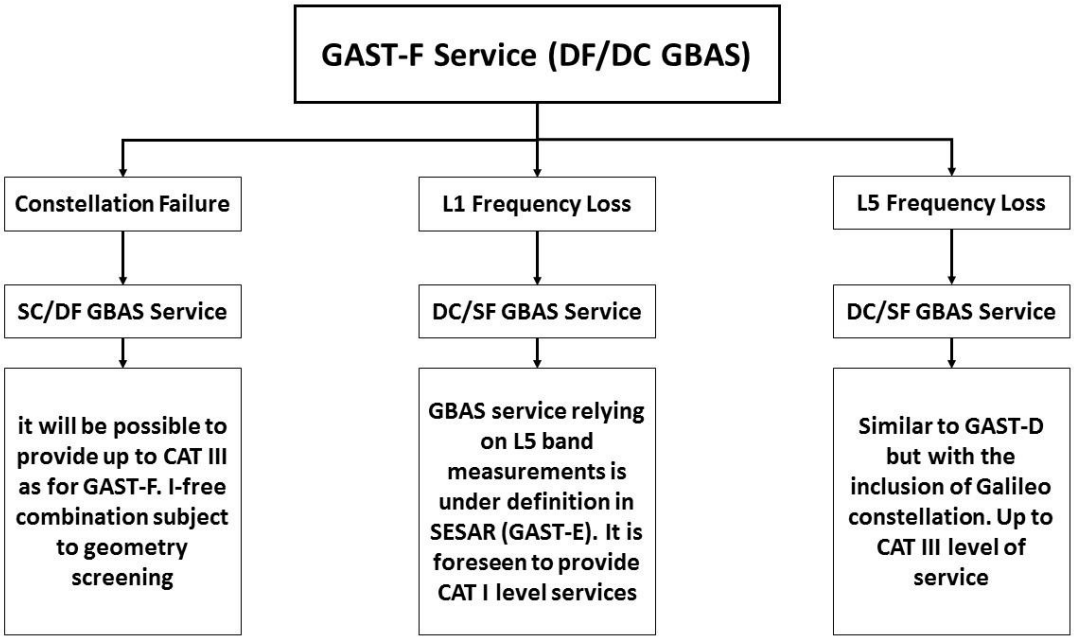

Figure 77 – GAST-F fallback modes example

5.1 The GAST D Concept

For GAST-C, international standardization bodies (ICAO, RTCA and EUROCAE) have worked jointly to define a standard that reuses the known performance of ILS Category I, which is defined angularly, to derive GBAS Landing System (GLS) Cat I performance. For GAST C, responsibility of the performance is ensured by the ground subsystem in the position domain for all aircraft operating in the GBAS Service volume and for all associated constellation geometries.

When the concept for GAST-D has been developed the fact that associated requirements, TSE and consequentially the FTE and NSE, are much more challenging to achieve for CAT II/III operation level has led to important new considerations. To derive GAST-D airworthiness a different approach was chosen, touchdown performance-based, instead of using the ILS-like method. Furthermore, performance allocation was split between air and ground taking advantage of the fact that the airborne subsystem knows best, which navigation data (e.g. which satellite set) it actually uses. This allows to not use conservative values of the FTE and NSE to derive the TSE and to use less conservative integrity requirements.

According to the GAST-D concept, the ground station protects the aircraft in the range domain instead of protecting it in the position domain (as GAST-C) by monitoring each GPS (or GLONASS) measurement against an acceptable error limit. Then, it is the airborne receiver which has now the responsibility to select satellite geometry because considering that the aircraft knows its own geometry is less conservative than assuming a degraded geometry at the ground as it was made in GAST C.

Finally, the mitigation of errors induced by anomalous ionospheric condition has been allocated to both the airborne system (RTCA Inc.; DO253-C, 2008) by adding a Dual Solution Ionospheric Monitoring Architecture (DSIGMA) monitor algorithm and the ground subsystem by implementing the Ionospheric Gradient Monitoring (IGM).

GAST-F is expected to follow the same concept adopted for GAST-D as outlined above yet with potentially different range error requirements.

5.1.1 Low Level Performance Requirements for Ground Monitors

Under GAST-D the ground station is responsible for the monitoring only of the ranging errors. At this scope a new requirement, considering the probability of an unsafe landing for a varying vertical error, has been developed in the range domain. It considers that under GAST-D the FTE is no longer estimated by the GS, using conservative values, the requirement is considered to have a low level of performances thanks to the possibility to relax the NSE.

The process followed in (ICAO NSP, 2010) is based at first on the probability to have an unsafe landing (P_{UL}), this means to land outside of a pre-defined box, computed considering standard NSE and FTE values and varying the vertical error. Then the values of P_{md},knowing that any unsafe landing condition has to be monitored with a $P_{md} < 10^{-5}$, is determined as:

$$P_{md}(E_v) = \frac{P_{UL}(E_v)}{10^{-5}}$$

Where:

- $P_{md}(E_v)$ is the probability of missed detection of a vertical error E_v
- $P_{UL}(E_v)$ is the probability of an unsafe landing for a given vertical error

Then the P_{md} curve is converted in the range domain dividing the vertical error by a worst-case S_{vert} value of 4. This process establishes the P_{md} requirement for the limit case (Figure 78)

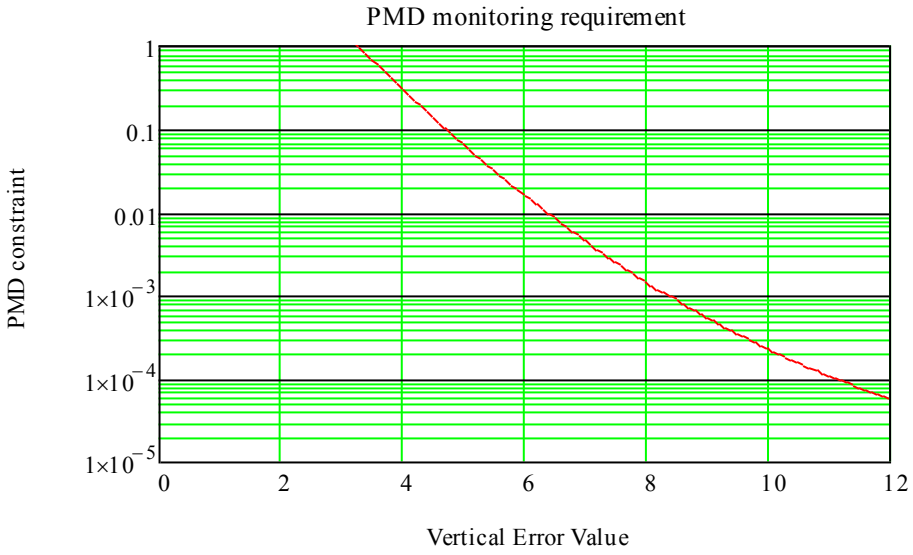

Figure 78 – Derived limit case P_{md} requirement for ranging source monitor (ICAO NSP, 2010)

The same analysis has been done for the malfunction case where an undetected error affects one range measurement. In this case the maximum vertical error that leads to a safe landing, always considering fixed values of NSE and FTE, has been computed. Once that the value, 6.44 meters, has been found, it has been converted in the range domain dividing it by 4, the worst S_{vert} possible, obtaining a value of 1.61 meters. This error must be monitored with a probability of missed detection of $1.3 \cdot 10^{-4}$, considering an a priori probability of fault $P_{fault} = 7.5 \cdot 10^{-6}$, in order to have a safe landing.

From the union of the two requirement, for limit and malfunction case, has been derived the general P_{md} requirement curve shown in Figure 79 for the range domain.

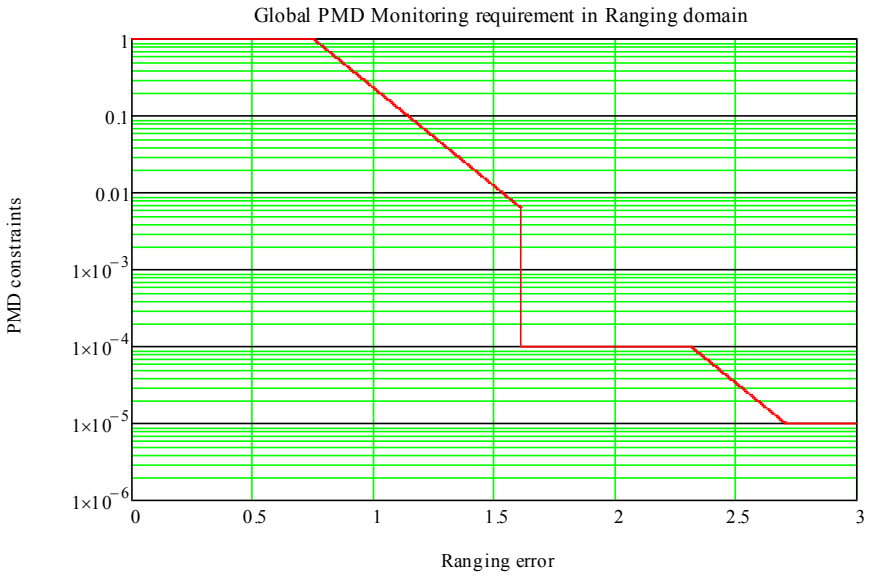

Figure 79 – General P_{md} requirement for ranging source monitors in range domain

For each monitor the performances have to be computed considering the test metric used, its distribution, its standard deviation and the P_{fa}. In Figure 80 an example of a compliant and a non- compliant monitor is shown.

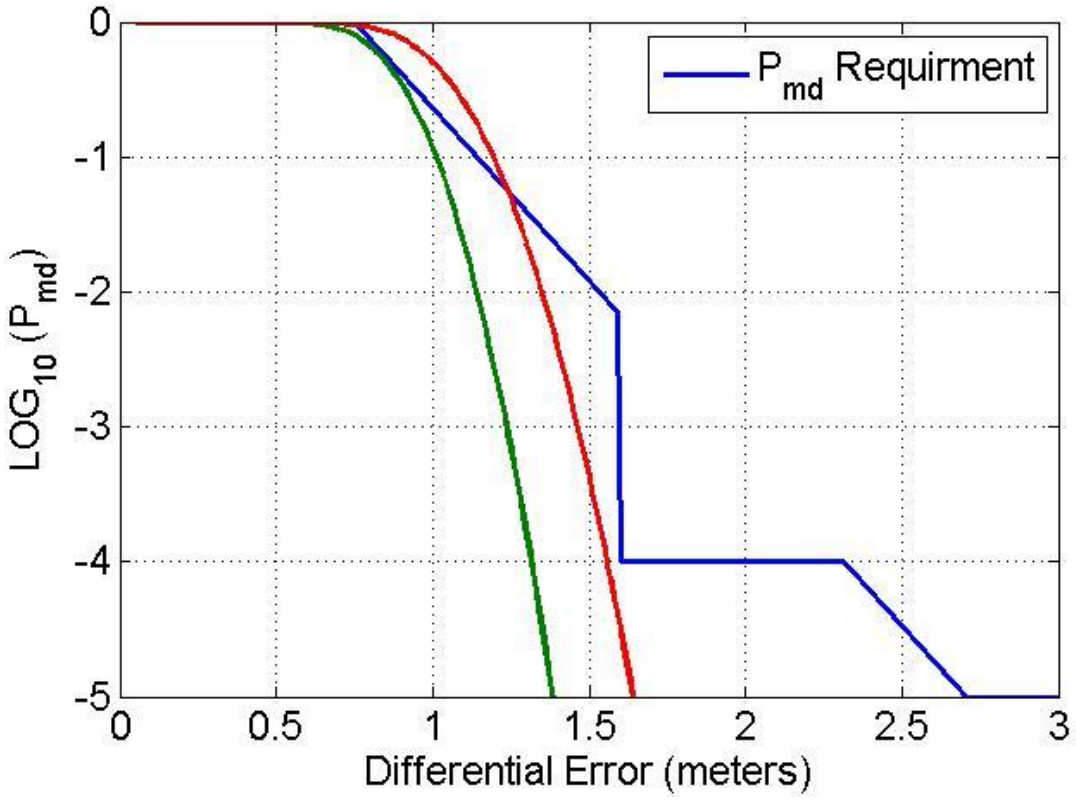

Figure 80 – Example of monitor performances Vs. P_{md} requirements

The red curve is related to the performances of a monitor with a test metric following a Gaussian distribution with $\sigma_{test} = 0.15$ meters and threshold set at 1 meter. This kind of monitor is compliant with the "malfunction case" requirement but it exceeds the "limit case" one in some case. The green curve is instead relative to a similar monitor where the $\sigma_{tets} = 0.123$ meters and the threshold is set to 0.85 meters. In this case the monitor is able to meet the requirement for all differential errors.

5.1.2 Geometry Screening

In GAST-D the aircraft is responsible for the selection of a satellite geometry, the subset that is adapted to its performance (CAT III for GAST-D). This process is done at aircraft level by geometry screening. Considering that relationship between errors on measurements and errors on the estimated position coordinates and receiver clock offset:

$$E_{sol} = E_{range}\, S \qquad \text{Eq. 5.1}$$

Where:

- E_{sol} is a vector of four terms expressing the estimation errors on X, Y, Z axis and the receiver clock bias
- E_{range} is the vector, with a length equal to the number of satellites used to compute the solution, indicating the differential errors on each corrected measurement
- S is the projection matrix presented in 2.3.3.2

Eq. 5.1 can be rewritten considering only the vertical and lateral components of the position error as

$$E_{vert,i} = E_i \, S_{vert,i} \quad \text{Eq. 5.2}$$

$$E_{lat,i} = E_i \, S_{lat,i} \quad \text{Eq. 5.3}$$

Where:

- $E_{vert,i}$ is the vertical position error caused by satellite i
- $E_{lat,i}$ is the lateral position error caused by satellite i
- E_i is the range error on the i^{th} satellite, is a vector with a length equal to the number of satellites, with zero values everywhere except at the i^{th} line, where the value is E_i
- $S_{vert,i}$ is defined in 2.3.3.2
- $S_{lat,i}$ is defined in 2.3.3.2

Knowing that the magnitude of the differential error is limited thanks to the presence of monitors, both at the grounds and aircraft side, by limiting the magnitude of S_{vert} and S_{lat}, it is possible to limit the error in the position domain.

For GAST-D considering the requirement in (ICAO NSP, 2010), any range error bigger than 1.6 meters must be detected with a P_{md} of 10^{-9}, the following limits are adopted: $S_{vert,i}$ and $S_{lat,i} < 4$ for any satellite. In order to protect the user, especially in the vertical position domain, against the presence of a fault on a second satellite at the same epoch, another value has to be monitored as well: $S_{vert2,i}$. This last value represents the sum of all possible pairs of satellites (ICAO NSP, 2010) and it shall not exceed 6.

5.1.3 SiS TTA

An important parameter to derive the integrity performances of the monitors is the SiS TTA. Although it has been already presented in 2.3.3, it is helpful to clarify the time-to-alert scheme as proposed in Figure 15. In (ICAO, 2006) the value, in seconds, of the TTA is set at 2.5 seconds. This time is the maximum interval that has to pass from the first faulty measurement received by the ground segment, to the reception at the airborne side of a message containing integrity information about the fault. This

time takes into account for 1.5 seconds as the maximum time to process and broadcast the information and two missed messages for the airborne equipment.

In Figure 81 a detailed scheme of the SiS TTA and the TTDAB (Time-To-Detect And Broadcast) is shown.

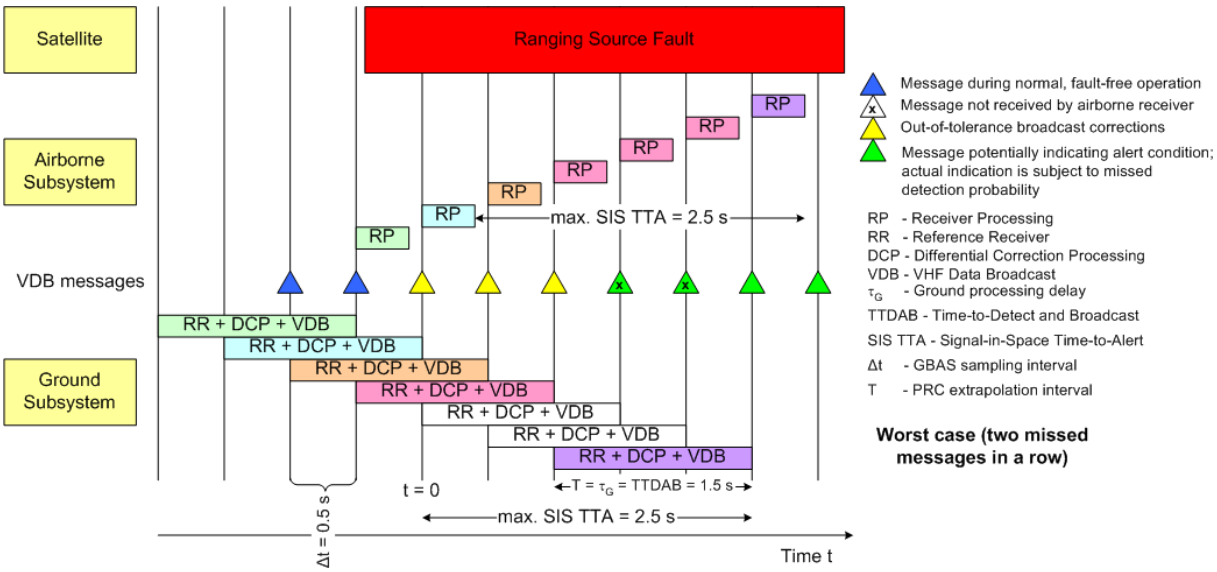

Figure 81 – Timing diagram derivation for below 200 ft. processing derived from (SESAR JU, 2011)

Figure 81 also helps to understand how an error impacts a differential system like GBAS. Considering an error onset just after $t = -0.5\ s$, it could be detected in measurement done at time $t = 0$ s by the ground station for which the measurement rate is 2 Hz. Corrections are received with a time delay of 1.5 seconds due to the time needed to process and broadcast the PRC and RRC. Considering the possibility to have two missed messages, the maximum time that can pass before receiving an integrity message after detection by the ground segment of the first faulty measurement is 2.5 seconds. Knowing that the SiS TTA is 2.5 seconds, and according to Figure 81, the biggest differential error is reached at $t = 2$ generated by an undetected fault lasting 2.5 seconds. It has to be considered that the aircraft measurements sampling rate can be different from the one adopted at ground station, with values bigger than 2 Hz. Moreover, the two subsystem's sampling times could be unsynchronized. According to this condition, it is more realistic to compute the maximum differential error at $t = 2.5$ generated by a fault lasting 3 seconds.

In (ICAO NSP, 2010) it is stated to not consider the airborne processing time (RP box in Figure 81) to derive the monitor performances

5.2 GAST D Integrity Monitoring

This section introduces the monitors present at ground and airborne levels for GAST-D service. Some of them have been already introduced in 2.3.3.3 since they were developed to work also for GAST-C. Monitors developed for GAST-D, or for which a relevant role is expected in the ionosphere anomalies detection, will be described more in details for sake of clarity of the following sections.

5.2.1 GAST D Monitors State-of-Art

5.2.1.1 SQM (Signal Quality monitor)

The Signal Deformation threat has been already introduced in 2.3.3.3.1. In this section a more detailed description of the threat and the monitor will be given.

In (ICAO, 2006) three fault types A, B, C are identified.

- Dead zones; if the correlation function loses its peak, the receiver's discriminator function will include a flat spot or dead zone. If the reference receiver and aircraft receiver settle in different portions of this dead zone, Misleading Information (MI) can result.
- False peaks: If the reference receiver and aircraft receiver lock to different peaks, MI could exist.
- Distortions: If the correlation peak is misshapen, an aircraft that uses a correlator spacing different than the one used by the reference receivers may experience MI.

Signal Quality Monitor (SQM) are designed to protect the users from deformations defined by a threat model, which has three parts that can reproduce the three faults listed above. It is valid for GPS L1 C/A signal:

A. Threat Model A (TMA) consists of the normal C/A code signal except that all the positive chips have a falling edge that leads or lags relative to the correct end-time for that chip. This threat model is associated with a failure in the navigation data unit (NDU), the digital partition of a GPS or GLONASS satellite (ICAO, 2006).

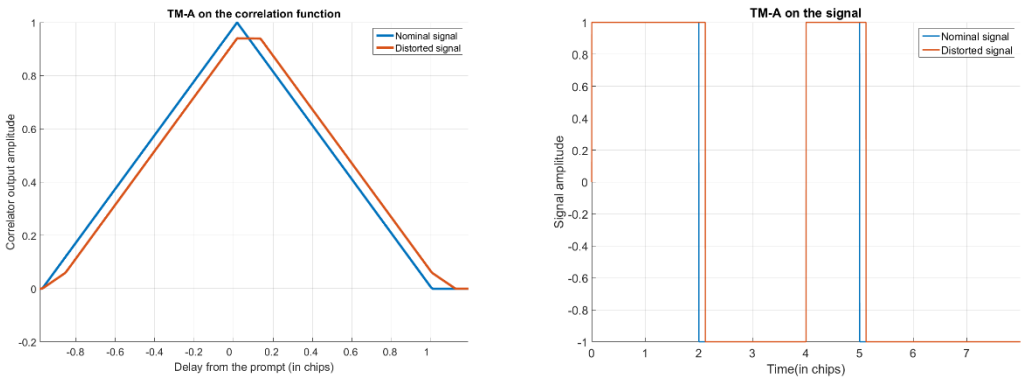

Figure 82 – Threat Model A: Digital failure

Details about the parameters of this threat are shown in (ICAO, 2006)

B. Threat Model B (TMB) introduces amplitude modulation and models degradations in the analog section of the GPS or GLONASS satellite. More specifically, it consists of the output from a second order system when the nominal C/A code baseband signal is the input. Threat Model B assumes that the degraded satellite subsystem can be described as a linear system dominated by a pair of complex conjugate poles. These poles are located at $\sigma \pm j2\pi fd$, where σ is the damping factor in nepers/second and fd is the resonant frequency with units of cycles/second.

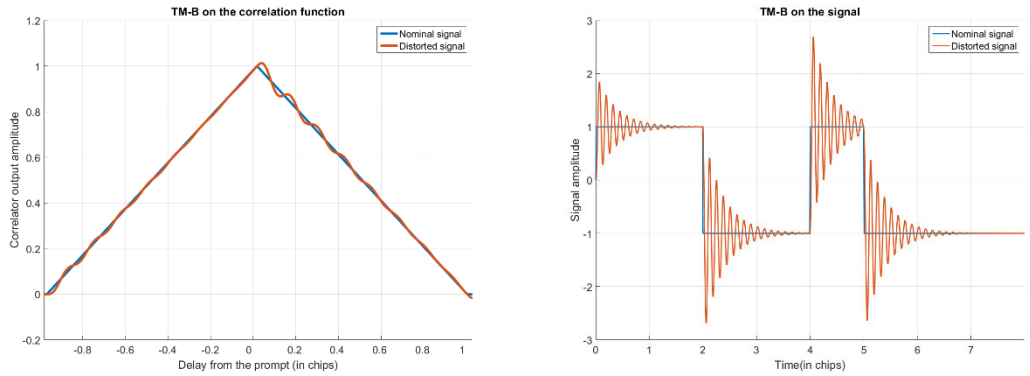

Figure 83 – Threat Model B: Analog failure mode

Details about the parameters of this threat are shown in (ICAO, 2006)

C. Threat Model C introduces both lead/lag and amplitude modulation. Specifically, it consists of outputs from a second order system when the C/A code signal at the input suffers from lead or lag. This waveform is a combination of the two effects described above.

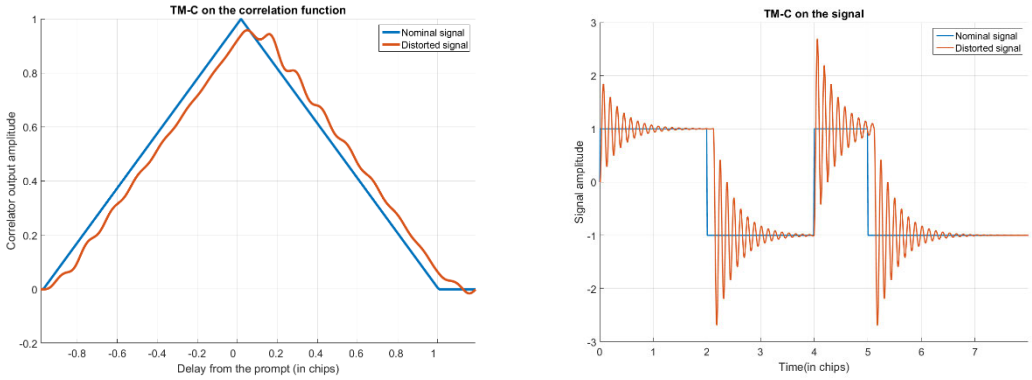

Figure 84 – Threat Model C: Analog and digital failure mode.

Two types of test metrics are formed: early-minus-late metrics (D) that are indicative of tracking errors caused by peak distortion and amplitude ratio metrics (R) that measure slope and are indicative of peak flatness or close-in, multiple peaks. More details about the metrics are given in (Enge, et al., 2000) and (Mitelman, 2004).

The last step is the definition of the thresholds for the two metrics. They are defined as the Minimum Detectable Error (MDE) or Minimum Detectable Ratio (MDR).

$$MDE = (K_{ffd} + K_{md})\sigma_{D,test}$$

$$MDR = (K_{ffd} + K_{md})\sigma_{R,test}$$

Where:

- $K_{ffd} = 5.26$ is a typical fault-free detection multiplier representing a false detection probability of 1.5×10^{-7} per test;
- $K_{md} = 3.09$ is a typical missed detection multiplier representing a missed detection probability of10^{-3}per test;
- $\sigma_{D,test}$ is the standard deviation of measured values of difference test metric D;
- $\sigma_{R,test}$ is the standard deviation of measured values of ratio test metric R.

As for the metrics, further details are given in (Enge, et al., 2000) and (Mitelman, 2004).

A failure is declared when the metrics is bigger than the threshold

$$|D, test - \mu_{D,test}| \geq MDE \quad or \quad |R, test - \mu_{R,test}| \geq MDR$$

Where μ, for both the test metric, is the median value across all visible satellites considered as the nominal value of the metric for an undistorted satellite.

5.2.1.2 Low Signal Level Monitor

As said in 2.3.3.3.2 this kind of threat is covered by the SQM.

5.2.1.3 Code-Carrier Divergence (CCD) Monitor

The code-carrier divergence threat is a fault condition that causes the excessive divergence between the measured carrier phase and the code phase. Possible causes of this divergence could be a payload failure or an ionospheric front. However since payload failure has never been observed, it is mainly attributed to the detection of ionosphere anomalous conditions.

Even if this monitor is present also for GAST-C service, for GAST-D service it has to be present at aircraft level as well.

The threat space, in this case, is 2-dimensional and corresponds to the time of the fault onset relative to initialization of the airborne smoothing filter and the divergence rate. The timing of the fault onset relative to the initialization of the airborne filter defines one axis of the threat space since the filter at

the ground is supposed to be already in the steady state. If both the filters, at airborne and ground side, are in steady state the differential error introduced by any divergence is minimal (Jiang, et al., 2015).

As mentioned in 2.3.3.3.3 the monitor analyzes the rate of change of two consecutive CMC.

$$CMC(t) = \rho(t) - \phi(t) \quad \text{Eq. 5.4}$$

Noting ΔT as the sample interval, it is possible to compute the CMC rate as

$$dCMC(t) = \frac{CMC(t) - CMC(t - \Delta T)}{\Delta T} \quad \text{Eq. 5.5}$$

Thus errors common to code and carrier measurements, such as satellite and receiver clock offsets, troposphere delay error and etc. are eliminated. Constant errors are removed, e.g. the integer ambiguity. The difference between two epochs removes largely the slowly varying biases. The leftover errors appear in the form of rate of change of the ionosphere delay, multipath and noise (Simili, et al., 2006). The errors are then smoothed via two cascaded first order low pass filters f are defined as,

$$F_1(k) = \left(\frac{\tau_{F1} - \Delta T}{\tau_{F1}}\right) F_1(k-1) + \alpha \cdot dCMC(k) \quad \text{Eq. 5.6}$$

$$F_2(k) = \left(\frac{\tau_{F2} - \Delta T}{\tau_{F2}}\right) F_2(k-1) + \alpha \cdot F_1(k) \quad \text{Eq. 5.7}$$

Where:

- τ is the filter constant for the first and the second low pass filter
- F_1 is the first order filter output; F_2 corresponds to the second order filter output
- $\alpha = \frac{\Delta T}{\tau}$ is the filter weight

Shorter time constant results in faster detection of CCD failure, and therefore less susceptible to the build-up of divergence induced filter lag errors, but also in noisier test metric.

The test metric can be expressed in the Laplace domain as in (Hwang, et al., 1999):

$$F_2(s) = \frac{1}{(\tau s + 1)^2}\, dCMC(s) = \frac{s}{(\tau s + 1)^2} CMC(s) \quad \text{Eq. 5.8}$$

The non-centrality parameter of the test metric is the divergence rate d, and the steady state is the same which is independent of the time constant τ,

$$\lim_{s \to 0} sF_2(s) = \frac{s^2}{(\tau s + 1)^2} \frac{d}{s^2} = d \quad \text{Eq. 5.9}$$

Where:

- d is the divergence rate

In the steady state, assuming the input noise follows a first-order Gauss-Markov distribution, the resulting noise attenuation is derived below when the filter weight is small,

$$\sigma_{F2}^2 \cong \frac{\alpha}{4}\sigma_{dCMC}^2 \qquad \text{Eq. 5.10}$$

The next step is to compute the threshold value for the metric,

$$Th_{CCD} = K_{ffd,mon}\,\sigma_{F2} \qquad \text{Eq. 5.11}$$

The value of sigma is related to the smoothing constants employed in the two low pass filters. The value of $K_{ffd,mon}$ is selected in order to meet the probability of fault-free alarm (Simili, et al., 2006). The value of the monitor standard deviation has been derived in (Simili, et al., 2006) and (Jiang, et al., 2015) for the ground monitor using 30 seconds smoothing constant and airborne one using 100 seconds smoothing constant. For the ground station, the monitor standard deviation is 0.00399 m/s and, considering a probability of false alarm at 10^{-9} ($K_{ffd,mon} = 5.83$), the threshold is set at 0.0233 m/s. The airborne monitor standard deviation is 0.0022 m/s, smaller than for the ground station monitor due to the use of 100 seconds as smoothing constant, and the threshold is set at 0.0125 m/s

The metric F_2 is finally compared to the threshold Th_{CCD} to perform a decision test and detect possible faults on the measurements. The performance of the monitor is related to the magnitude of the divergence rate (Simili, et al., 2006).

The detection capabilities of the monitor are, however, not only related to the divergence rate. The time elapsed from the fault onset is at same time important to correctly derive them (Jiang, et al., 2015). In this context only the case where both filters have similar properties (same smoothing constant and in steady state) and they have converged to a new steady state after the divergence fault onset is considered. Under this hypothesis the divergence rate that can be detected with a $P_{md} = 10^{-9}$ can be estimated. This value can be considered as a sort of limit since all values bigger than this will be detected with a $P_{md} < 10^{-9}$.

$$F_{2,limit} = \sigma_{F2}(K_{ffd,mon} + K_{md}) \qquad \text{Eq. 5.12}$$

The value of $K_{ffd,mon} = 5.83$ and $K_{md} = 5.81$ as for the VPL and LPL computation (Simili, et al., 2006).

The limit divergence rates for the ground and airborne monitor are 0.0464 and 0.256 m/s.

5.2.1.4 Excessive Acceleration (EA) Monitor

The Excessive Acceleration (EA) threat is a fault condition in a GNSS satellite that causes the carrier (and code in unison) of the broadcast signal to accelerate excessively. The most probable causes would

be a fault of the operational satellite clock or an undesired acceleration in the satellite position due to an unscheduled manoeuvre. Even if this monitor is already present for GAST-C service, the analysis of the test statistic is useful to introduce the innovations or the analysis done for GAST-F. Moreover an alternative test statistic based on the estimated acceleration and the velocity has been proposed (Stakkeland, et al., 2014).

The range acceleration error is estimated for any satellite measured over any 3-epochs interval, the formula is given in (Brenner, et al., 2010).

$$\ddot{\phi}(k-1) = \frac{\left(\phi(k) - 2\phi(k-1) + \phi(k-2)\right)}{\Delta T^2} \qquad \text{Eq. 5.13}$$

Where:

- $\phi(k)$ is the phase measurement for epoch k
- ΔT is the sampling interval in s, for GBAS ground station this value is 0.5 seconds.

Considering the SiS TTA requirement (5.1.3), the differential error after 2.5 seconds from the first faulty measurement, and caused by 3 seconds acceleration, is given as:

$$E_r\left(t_{fault}\right) = \frac{1}{2}\, a\left(t_{fault}\right)^2 - \frac{1}{2}\, a\left(t_{fault} - t_{gs}\right)^2 - \left(\frac{0.5\, a\left(\left(t_{fault} - t_{gs}\right)^2 - \left(t_{prc} - \Delta T\right)^2\right)}{\Delta T}\right) \cdot t_{az} \qquad \text{Eq. 5.14}$$

Where:

- E_r is the differential error caused by any acceleration, the term in bracket refers to time elapsed from the fault onset
- a represents an acceleration with no limitation in magnitude
- t_{fault} is the time elapsed from the fault onset
- t_{az} is the time between PRC and RRC computation and their application at aircraft side
- $t_{gs} = t_{PRC\ rate} + t_{gnd\ proc}$; $t_{PRC\ rate}$ is the PRC, and RRC, update period in seconds. $t_{gnd\ proc}$ is the time needed at ground station to process measurement, it is assumed to be 1 second.

The first term in Eq. 5.14 is the error induced in the measurement at the aircraft side. The second one, represents the part of acceleration error present in the PRC and compensated when PRCs are applied. The last term is the computation of the RRC based on the difference between two consecutive epochs. RRC are then multiplied by the time elapsed from their computation to the moment when they are used at aircraft side. Developing Eq. 5.14 with a $t_{fault} = 3$; $t_{gs} = 1.5$, $t_{az} = 1.5$ and a $\Delta T = 0.5$ it is possible to derive the impact of an acceleration a on the differential error.

$$E_r\,(3) = 4.5\,a - 1.125\,a - 1.875\,a = 1.5\,a \qquad \text{Eq. 5.15}$$

Eq. 5.15 can be generalized as:

$$E_r\,(3) = a\,\left(t_{gs}\,\left(t_{gs} + 0.5\right)\right)/2 \qquad \text{Eq. 5.16}$$

In Figure 85, it is possible to see the differential error, computed as in Eq. 5.16, at $t = 3.0$ seconds. The fault onset, for this case, is at $t = 0$ just after the measurement done at the same epoch. The first faulty measurement is so recorded at $t = 0.5$ seconds. The maximum differential error, always considering a SiS TTA of 2.5 seconds, is at $t = 3$ s. From this epoch, the PRC and RRC, containing information about the acceleration, permit to decrease the total differential error. It has to be considered that the aircraft may have a different measurement interval than the one used at ground. In this case the differential error after $t = 3$ grows and each 0.5 seconds is reduced by the received PRC and RRC.

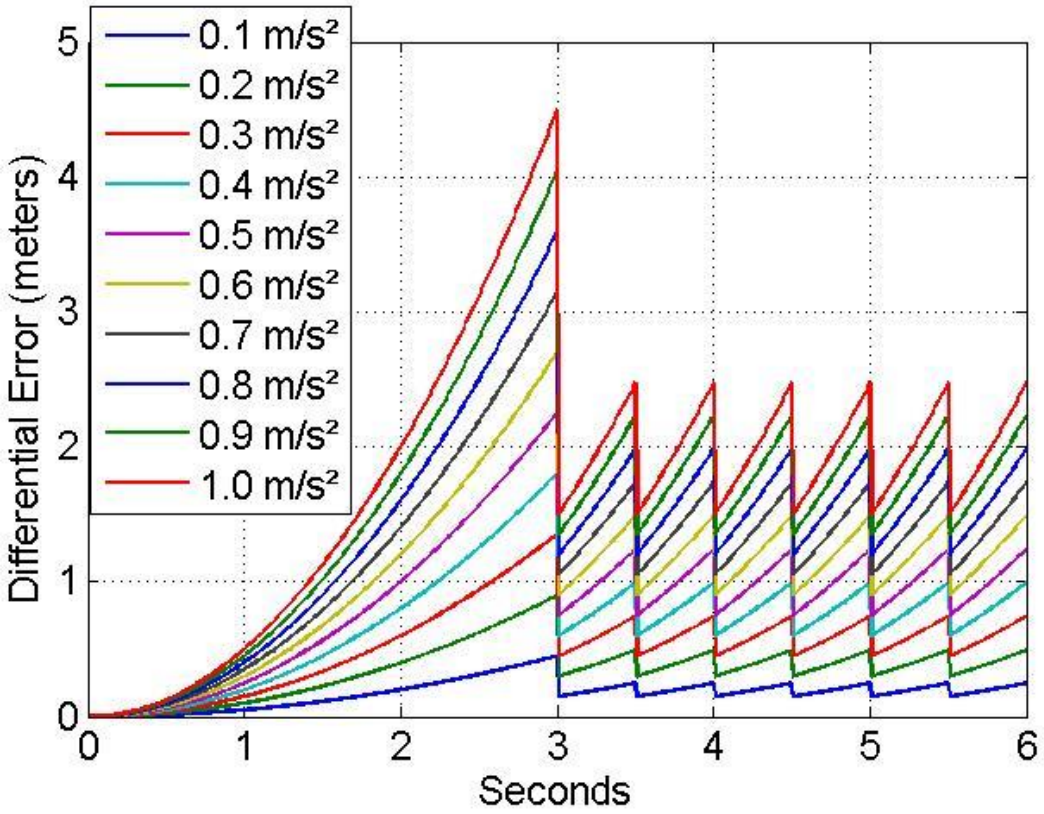

Figure 85 – Acceleration induced differential range error

The shape of the curves, in Figure 85, is caused by the non-synchronization of the measurements between the GS and the aircraft and the possible difference in the measurements interval between the two. Each 0.5 seconds the differential error decreases thank to the reception of a new set of PRC and RRC.

Considering the requirement for the ground monitor presented in 5.1.1, and also taking into account the performances of monitors with respect to the P_{md} curve requirement a maximum differential error of 1.4 meter to detect with a $P_{md} < 1 \cdot 10^{-4}$ is considered (Brenner, et al., 2010).

Knowing that the maximum error after 2.5 seconds from the first faulty measurement is $1.5\,a$, it is possible to derive the maximum acceleration which must be detected by the monitor with the required probability in order to meet the constraint of $E_r < 1.4$ meters.

$$1.5 * a = 1.4 \rightarrow a = \frac{1.4}{1.5} \rightarrow a = 0.933\ m/s^2 \qquad \text{Eq. 5.17}$$

It has to be considered however that the detected acceleration, at first epoch after the fault onset, is the half of the real value (considering the case of a fault onset just after the measurement) or less (considering the case of fault onset in between two ground measurements). Simulating a constant value of the errors on phase measurements ϕ, after the compensation for satellite motion, clock drifts and receiver clock compensation and including an acceleration a lasting 0.5 seconds only on measurement at epoch t, equation Eq. 5.13 becomes:

$$\ddot{\phi}(t - \Delta\mathrm{T}) = \frac{\left(\phi(t) + 0.5a\Delta T^2 - 2\phi(t - \Delta T) + \phi(t - 2\Delta T)\right)}{\Delta T^2} = \frac{0.5a\Delta T^2}{\Delta T^2} = 0.5a \qquad \text{Eq. 5.18}$$

Considering that the detected acceleration in the first epoch is the half of its real value the threshold must be lower than the half of the values computed in Eq. 5.17, so lower than$0.4665\ m/s^2$, to be sure that all undetected values will not cause a differential error bigger than 1.4 meters.

The last step is to analyze the feasibility of the monitor including the noise contribution to the acceleration. According to (Brenner, et al., 2010), the phase noise sigma with only 2 RR and the lowest carrier-to-noise ratio at 32 dB-Hz and PLL tracking loop bandwidth of 10 Hz is $0.25/\sqrt{2}\ cm$. Considering the model of the test as in equation Eq. 5.13, the variance of the test is

$$Var[\ddot{\phi}] = \left(\sigma_\phi^2 + 4\sigma_\phi^2 + \sigma_\phi^2\right)/0.5^4 \qquad \text{Eq. 5.19}$$

Replacing the value of the standard deviation stated before, the standard deviation of the test becomes

$$\sigma_{\ddot{\phi}} = \sqrt{6}\left(\frac{0.25}{\sqrt{2}}\right) / 0.25 = 1.73\ cm/s^2 \qquad \text{Eq. 5.20}$$

Assuming that the threshold is set at 6 sigma in order to take into account the probability of false alarm and another margin of 4 is considered for the probability of missed detection (Brenner, et al., 2010), the value of 10 times sigma represent the limit case and it is $0.173\ m/s^2$ that is well below the acceleration limit of $0.4665\ m/s^2$ (Brenner, et al., 2010). This shows that the monitor is feasible for GAST-D processing scheme with 0.5 seconds update period for PRC and RRC.

5.2.1.5 Ephemeris Error/Failure Monitor

Ephemeris fault has been described in 2.3.3.3.5. According to (ICAO NSP, 2010) several kinds of monitors can be used to monitor ephemeris

- **Long Baseline**. This requires the ground subsystem to use receivers separated by large distances to detect ephemeris errors that are not observable by a single receiver.
- **SBAS**. Using the information provided by the SBAS satellites is possible to monitor the ephemeris data, this technique provides optimum performance improving the detection of small errors.
- **Ephemeris Data Monitoring**. This approaches compare the broadcast ephemeris over consecutive satellite orbits. This monitor assumes that the only possible threat is due to an upload failure from the ground control center.
- **Delta-V**. This monitor covers the cases of uncommented satellite manoeuvres or manoeuvres out of view under unchanged ephemeris.

A last way to monitor the ephemeris state is the computation of the ephemeris error bound. This method is similar to the protection level seen in section 2.3.3.2. The vertical and lateral position bound is computed as:

$$VEB = \max_j \{VEB_j\} \quad \text{Eq. 5.21}$$

$$LEB = \max_j \{LEB_j\} \quad \text{Eq. 5.22}$$

The value is computed for each ranging source, j, used in the position solution computation. For each source the error position bound is:

$$VEB_j = |S_{vert,j}|\, x_{air}\, P_{e,j} + K_{md\,e,j} \sqrt{\sum_{i=1}^{N} S_{vert,i}^2 \times \sigma_i^2} \quad \text{Eq. 5.23}$$

$$LEB_j = |S_{lat,j}|\, x_{air}\, P_{e,j} + K_{md\,e,j} \sqrt{\sum_{i=1}^{N} S_{lat,i}^2 \times \sigma_i^2} \quad \text{Eq. 5.24}$$

Where:

- x_{air} is the slant distance between the LGF and the aircraft
- N is the number of used ranging sources

- $P_{e,j}$ is the ephemeris decorrelation parameter for the j^{th} ranging source in message type 1
- $K_{md\,e,j}$ is the broadcast ephemeris missed detection multiplier from message type 2

As for the protection level, the VEB and LEB do not have to overcome the VAL and LAL limit.

5.2.1.6 Ground Receiver Fault Monitor

In order to detect possible failures of one of the reference receivers used at ground station B values are computed (Shively, 2009). The monitor compares the B-values, computed for each satellite and excluding one station per time to a detection threshold (Shively, 2009). The equation to compute B values is given in Eq. 2.62.

$$B_j^i = PRC^i - \frac{1}{M-1}\sum_{\substack{j=1 \\ j\neq m}}^{M} PRC_j^i$$

Where

- i is related to the i^{th} satellites
- j is related to the j^{th} reference receiver
- PRC^i is the correction computed for satellite i using all RRs

In case of threshold exceeding the related PRC and RRC for a precise satellite-receiver couple are removed from the averaging process shown in 2.3.2.

5.2.1.7 Dual Solution Ionosphere Gradient Monitor Algorithm (DSIGMA)

One of the main threats in GNSS is the ionosphere, and in particular for GBAS, the detection of the ionospheric gradients. This condition generates a different delay between the ground and the airborne that is not fully corrected via the differential process.

In order to mitigate errors induced by ionospheric anomalies, the position solutions is computed relying on two different carrier smoothing time constants (RTCA Inc.; DO253-C, 2008) is used. This dual solution computation has two purposes.

1. The first one is the detection of large ionospheric gradients between ground measurement and airborne measurement observables through both filter outputs. Hence a threshold can be applied to this detection statistic in order to detect a large portion of the ionospheric anomalies.
2. The second application of the dual solutions is to compute a bound for the 30 seconds smoothed position (excluding the impact of ionospheric anomalies). By adding the direct observation of the magnitude of the difference between the 30 seconds smoothed position and the 100 seconds smoothed position to the protection level computation, a new protection level, which is

guaranteed to bound the 30-second position solution with the required 1x10-7/approach is obtained.

At ICAO NSP level, a DSIGMA algorithm has been proposed also in the corrected range domain (ICAO NSP, 2016). The scope of this algorithm is mostly the detection of anomalous ionospheric gradients since information about the position accuracy are not available. The test is performed by analyzing the difference between the corrected pseudoranges smoothed by 2 different time constant, 100 s and 30 s.

$$test = \rho^c_{100} - \rho^c_{30} \qquad \text{Eq. 5.25}$$

Where ρ^c_x are the corrected pseudoranges smoothed with a filter having a time constant x.

Eq. 5.25 can be rewritten considering how the corrected pseudoranges are derived.

$$test = \tilde{\rho}_{air\,100} - PRC_{100} - \tilde{\rho}_{air\,30} + PRC_{30} \qquad \text{Eq. 5.26}$$

Where:

- $\tilde{\rho}_{air\,100}$ is the smoothed pseudorange at airborne side according to the used smoothing constant, 100 seconds for this case
- PRC_{100} are the pseudorange correction for the used smoothing constant.

The test relies on the different response of the filter for 100 and 30 seconds smoothing case in presence of a time-varying ionospheric delay.

In Figure 86, it is possible to see the filter response for the two smoothing constants in presence of a varying ionospheric delay. The delay induced by an ionosphere gradient, impacting an aircraft, is simulated. In this scenario, the aircraft moves faster than the front and the raw delay is decreasing at airborne level (red line on left side figure). The ground station is, instead, impacted at epoch 420 and the delay is growing. In the right side of Figure 86 the filter response for both, aircraft and ground station, is represented for 30 and 100 seconds smoothing constants. It is possible to see that the filter response differs for the two constants.

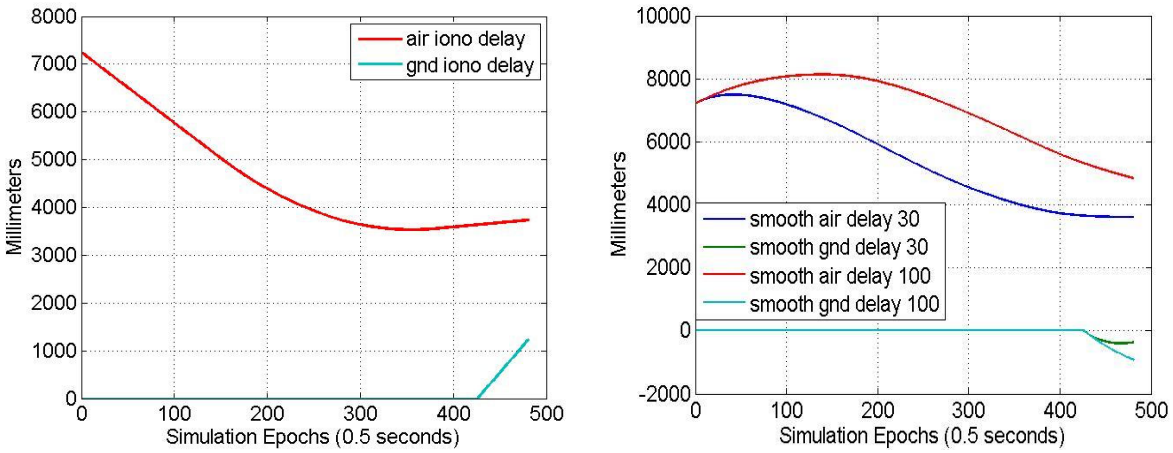

Figure 86 – simulated ionospheric delay (left) and related smoothing time variant filter response

In the case of fault free measurements, the test statistic is assumed to follow a central normal distribution. Results in (ICAO NSP, 2016) show that the standard deviation obtained must be bounded to cover the CDF of the obtained errors. In (ICAO NSP, 2016) the value of the standard deviation of the monitor is determined for all elevations, below 30° elevation angle and above 30° elevation angle.

Table 24 – DISGMA test metric standard deviation (ICAO NSP, 2016)

All Elevations	**< 30°**	**>30°**
0.1740791 m	0.2075552 m	0.1309688 m

Assuming a $P_{fa} = 10^{-8}$ it is possible to compute the P_{md} for each of the test metrics standard deviation.

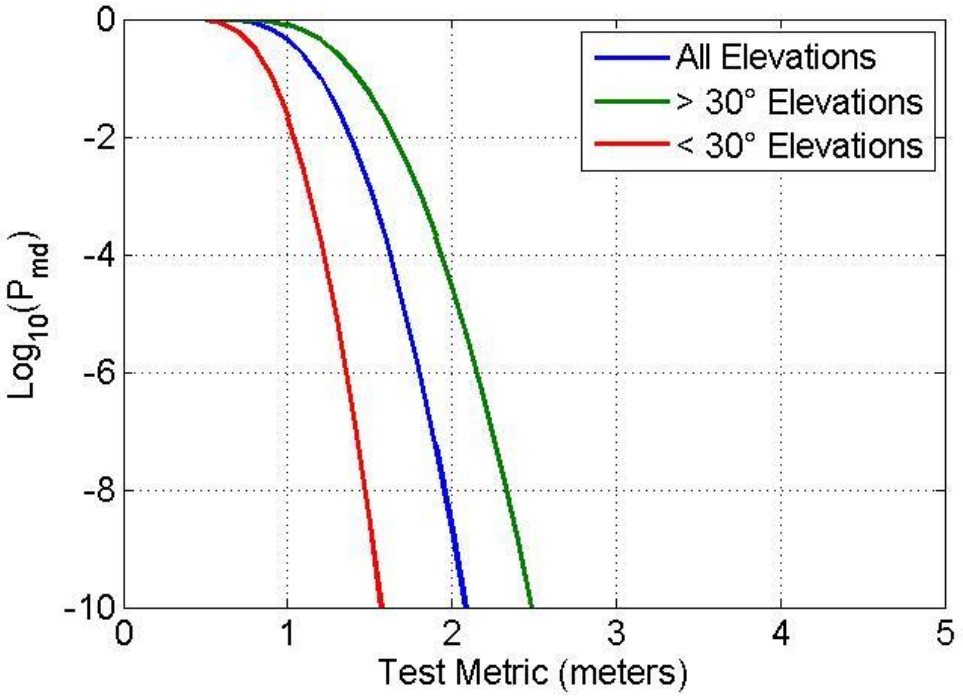

Figure 87 - P_{md} performances for DSIGMA

Figure 87 shows the results for the three test metrics defined in Table 24, it is possible to see that using the all elevations standard deviation, any error bigger than 2 meters can be detected with a $P_{md} < 10^{-9}$.

5.2.1.8 Ionosphere Gradient Monitor (IGM)

In (ICAO NSP, 2010), it is stated that any ground system providing a GAST-D service must monitor "if the probability that there is an undetected spatial ionospheric delay gradient with a magnitude greater than 1.5m/D in the direction of any approach supporting GAST-D is greater than 1×10^{-9}". Where D is the distance between the reference point of the ground subsystem and the threshold typically set at 5 km. The direction of the approach is defined by the runway heading.

To meet previous requirement, an ionosphere gradient monitor algorithm is installed in any ground station providing GAST-D service. The way it works is presented in (Khanafseh, et al., 2010). It uses the phase measurements from different RRs. The principle is based on the phase measurements difference, between at least two RRs, that could exist in presence of an ionospheric gradient. In Figure 88 an example of phase difference due to an ionospheric gradient is shown.

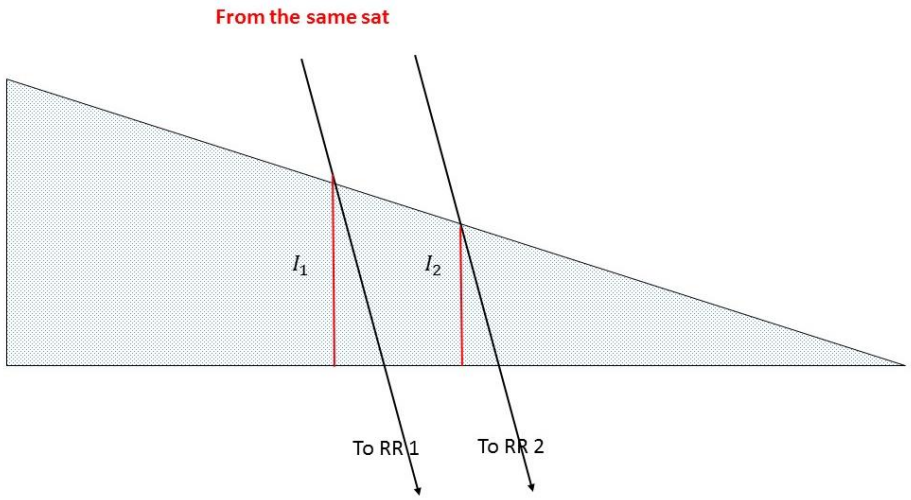

Figure 88 – Ionospheric delay on two different RRs

Under nominal ionospheric conditions, if the baseline length between the 2 RRs is relatively short (less than a kilometre), $I_2 - I_1$ (Figure 88) will be on the order of millimeters and usually can be neglected (Khanafseh, et al., 2010). If an ionospheric front exists, the difference can be detected using the phase measurement from two RRs.

Considering the phase measurement as in Eq. 2.11, the difference between phase measurements from two RRs at the same epoch is (Khanafseh, et al., 2010):

$$\Delta\phi_{RR1/RR2} = e^t\, x_b + \Delta t_{u_{RR1-RR2}} + \lambda\, \Delta \mathrm{N}_{\mathrm{RR1-RR2}} + \Delta \mathrm{I}_{\mathrm{RR1-RR2}} + \eta_{\mathrm{RR1-RR2}} \qquad \text{Eq. 5.27}$$

Where:

- $e^t\, x_b$ is the geometrical term including e, the user-satellite unit line of sight vector, and x_b the baseline vector between the two RR antennas
- $\Delta t_{u_{RR1-RR2}}$ is the receiver clock difference
- λ is the wavelength of the used frequency
- $\Delta \mathrm{N}_{\mathrm{RR1-RR2}}$ is the phase ambiguity difference (only integer values are allowed)
- $\Delta \mathrm{I}_{\mathrm{RR1-RR2}}$ is the ionospheric delay difference
- $\eta_{\mathrm{RR1-RR2}}$ is the phase noise and multipath difference term

Looking at Figure 88, it is possible to rewrite the ionospheric delay difference term as

$$\Delta \mathrm{I}_{\mathrm{RR1-RR2}} = \alpha\, |x_b| \qquad \text{Eq. 5.28}$$

α is the ionospheric gradient given in mm/km. typical values of α are from two to six Table 2.

A problem to solve in Eq. 5.27 is the removal of the receiver clock difference. Assuming that the satellite under analysis is affected by an ionospheric gradient, it is possible to find another one that is assumed to be fault-free (Khanafseh, et al., 2010). To verify this assumption, the other satellite should be spatially separated from the monitored satellite, so that it is not affected by the same ionospheric anomaly. The computation of the double measurement difference with this fault-free satellite removes the receiver clock from Eq. 5.27. The double measurement difference can be written as:

$$\Delta\nabla\phi = \Delta\nabla e^t\, x_b + \lambda\, \Delta\nabla N_{RR1-RR2} + \alpha|x_b| + \Delta\nabla\eta_{RR1-RR2} \qquad \text{Eq. 5.29}$$

All terms now take into account the difference from the two satellites and two receivers (Δ^{∇}), except the ionospheric delay term $\alpha|x_b|$ that is supposed to impacts only the first satellite.

The geometrical term can be removed from Eq. 5.29 knowing the user-satellite vector for any of the two satellites and knowing the baseline vector as well. Eq. 5.29 becomes

$$\Delta\nabla\phi - \Delta\nabla e^t\, x_b = \lambda\, \Delta\nabla N_{RR1-RR2} + \alpha|x_b| + \Delta\nabla\eta_{RR1-RR2} \qquad \text{Eq. 5.30}$$

The test statistic as in Eq. 5.30 is still affected by the phase ambiguity difference term $\Delta\nabla N_{RR1-RR2}$, and so it cannot be used to estimate ionospheric gradients. Knowing that the phase ambiguity is an integer, it is possible to remove it by removing the integer part from Eq. 5.30 (Khanafseh, et al., 2010).

$$s_{IGM} = \Delta\nabla\phi - \Delta\nabla e^t\, x_b - round\left(\Delta\nabla\phi - \Delta\nabla e^t\, x_b\right)\lambda_{L1} = \alpha|x_b| + \Delta\nabla\eta_{RR1-RR2} \qquad \text{Eq. 5.31}$$

The necessary condition for a front detection is that its value is not an integer number of wavelength.

In absence of ionospheric gradients, the test statistic follows a normal distribution with zero mean and standard deviation equal to $\sigma_{test} = 2\sigma_{\phi}$ (Khanafseh, et al., 2010). The threshold for the test statistic is defined as:

$$Th = K_{ffd}\, \sigma_{test} \qquad \text{Eq. 5.32}$$

Considering that an ionospheric front can have all possible direction, at least two non-collinear baselines are needed to have detection for all possible fronts. The advantage of this monitor for the detection of ionosphere fronts, with respect to the CCD monitor, is the non-dependency from the ionospheric delay rate of change.

Details about the monitor performance are given in (Khanafseh, et al., 2010).

5.2.2 GAST D Monitoring Challenges

Despite the implementation of monitors at the airborne side and the development of requirements in the range domain, GAST-D has still some problems related to the integrity that does not allow this service to be validated.

In this section the conditions under which the integrity is not reached will be presented. Finally, after the identification of the threat area to monitor the proposed solution will be presented as well.

5.2.2.1 CCD Inefficiency for Slow-Moving Fronts

As seen in 5.2.1.2, the CCD monitor efficiency is strictly related to the rate of change of the code-carrier divergence. For an ionospheric front, this rate depends on the projection of the speed difference between the satellite-user Ionospheric Pierce Point (IPP) and the front gradient called $slope$ in the following equation.

$$d\left(\frac{m}{s}\right) = \Delta v\left(\frac{km}{s}\right) * slope\left(\frac{m}{Km}\right) \qquad \text{Eq. 5.33}$$

In equation Eq. 5.33 the value of Δv is the difference between the IPP speed and the ionospheric front speed as:

$$\Delta v = \left|v_{sat,proj} - v_{front}\right|$$

Where $v_{sat,proj}$ is the projection of the satellite-user IPP speed in the same direction of the ionospheric front speed.

In case of small values of Δv, a front is undetected by the CCD. In Figure 89, it possible to see a case of stationary front with two satellites impacted by the front. It has to be considered that it is quite unlikely that both satellites have the same value of $v_{sat,proj}$, so just one of them is considered to be totally undetected.

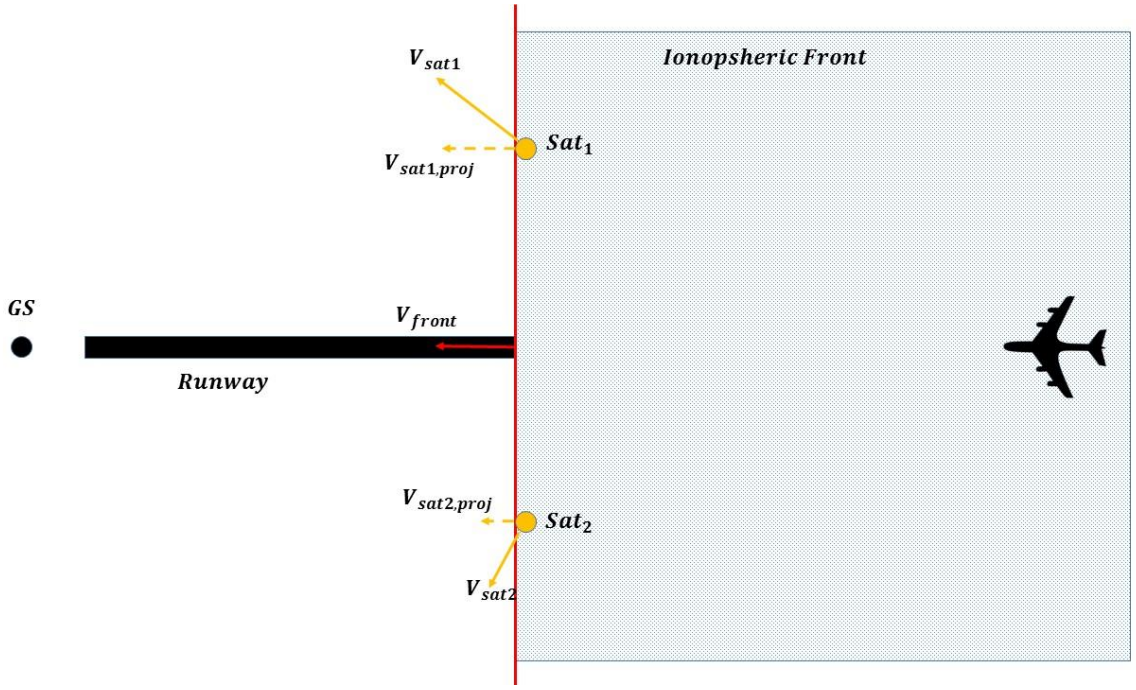

Figure 89 – example of stationary front for possible worst case geometry (Lee, et al., 2011)

Knowing that the detection limit value of d are 0.0464 m/s and 0.0256 m/s, it is possible for defined values of the ionospheric front gradient to compute the limit of Δv according to Eq. 5.33.

Table 25 – Difference speed limit for CCD detection

$\boldsymbol{Iono\ Front\ Gradient\ \left(\frac{m}{Km}\right)}$	$\boldsymbol{\Delta v\ limit\ \left(\frac{km}{s}\right)}$	
	Ground CCD	Airborne CCD
0.1	0.464	0.256
0.2	0.232	0.128
0.3	0.155	0.0853
0.4	0.116	0.0640
0.5	0.0928	0.0512

It is useful to say that the detection performance of the CCD is not related only to the divergence rate. The filter time constant used impacts the time-to-detect (Simili, et al., 2006)as well. The time of the fault onset with respect to the airborne and ground filter initialization impacts the differential error that may occur due to a divergence fault. The analysis has only the scope to derive a series of Δv limits to simulate an undetected ionospheric front.

5.2.2.2 Anomalous Atmospheric Behaviour on IGM

The IGM monitor, as seen in 5.2.1.8, is not dependent from the ionospheric gradient divergence rate, and consequentially from the front/IPP speed. This monitor is supposed to cover all the zones of the ionospheric gradient threat space not covered by the CCD. Unfortunately, Honeywell has observed some malfunctions for an IGM installed at Houston airport (ICAO NSP WGW/WP 16, 2014). In particular, in certain day and more precisely in certain hours, the noise level of the test statistic was increased. In Figure 90, it is possible to see the test statistic for an entire day.

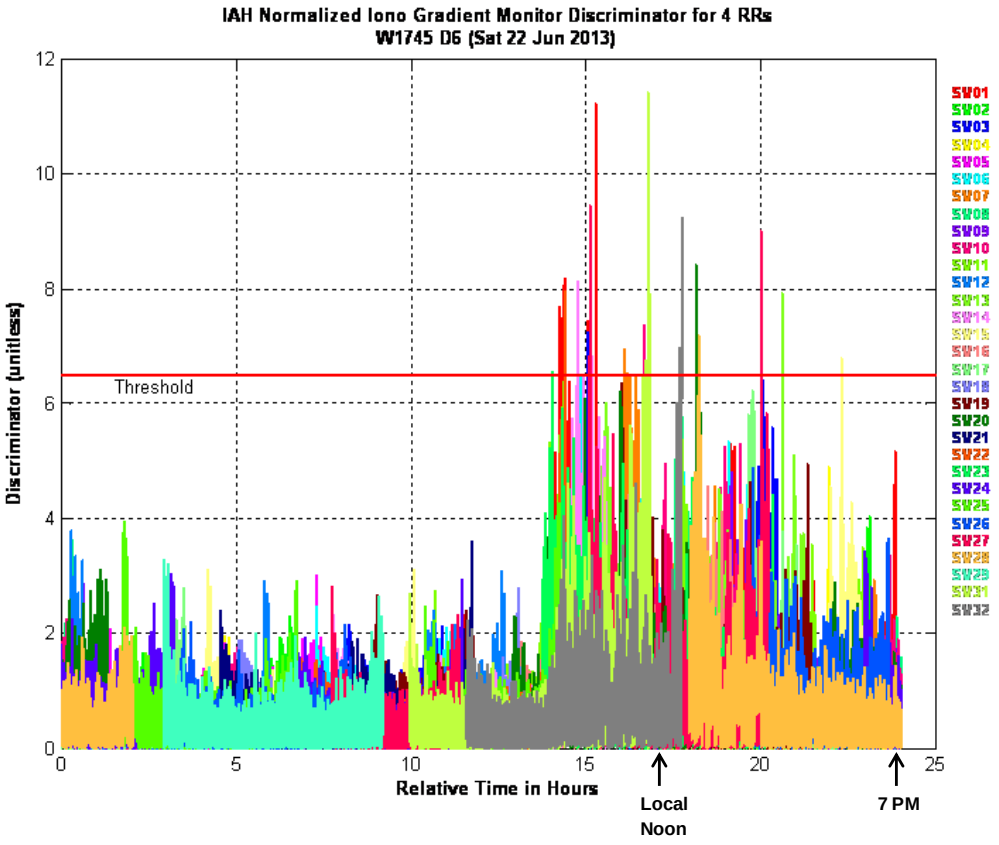

Figure 90 – IGM test statistic for Houston airport (ICAO NSP WGW/WP 16, 2014)

As visible from Figure 90, starting from the local 10:00 and until 19:00, the test statistic is frequently exceeding the detection threshold.

Further investigation of additional days and additional sites revealed these phenomena were present at other locations. General statements about these gradients which could be made based on the observed data include:

1. Observed from approximately 10 AM to 8 PM local time
2. Not observed at night
3. Observed mostly during hotter, mostly clear days
4. Not observed during cold, overcast, or rainy days
5. Observed at all azimuths
6. Observed mostly at lower elevations

This analysis done by Honeywell has led to exclude the ionosphere as a cause of these alarms, since no effects were seen on the other monitors installed in the GS like the CCD or the EA monitor. After further analysis, the possible cause of this anomaly has been identified to be a gradient of the troposphere (or at least the lower region of the troposphere) (ICAO NSP WGW/WP 16, 2014).

This effect can impact the GBAS in two different ways:

- Continuity; A double-difference-based IGM similar to Honeywell's implementation will be impacted by this "tropospheric" activity, which will likely result in false monitor alarms and loss of GAST-D functionality. Based on observed troposphere gradients, the frequency of false monitor trips could lead to unacceptable continuity performance for GAST-D operations.
- Although the range error impact from these hypothesized "tropospheric" gradients is small in comparison to anomalous ionospheric gradients, they could be hazardous when combined with the presence of an anomalous ionosphere gradient. It is possible that these troposphere gradients, although short lived, may blind the Ground Subsystem Monitor used for detection of anomalous ionosphere gradients.

In order to guarantee the integrity level requirement for GAST-D, another monitor has to be found in order to validate it for CAT II/III operations.

5.2.2.3 Residual Ionosphere Threat Model to Monitor

Sections 5.2.2.1 and 5.2.2.2 have shown some particular atmospheric conditions that do not permit to reach the required integrity level for GAST-D service. Before proposing a solution to the presented problems, it is good to identify the area of the ionosphere threat space that is responsible for this issue. It is also important to estimate the maximum ionosphere delay that may impact all the undetected satellites.

Resuming what has been presented in the previous chapter, the critical conditions are assumed to occur under the following circumstances:

- IGM provides insufficient integrity since it is impacted by a tropospheric gradient event. This condition appears in some hours of the day and not all days.
- The front moves with a relatively low speed in order to be undetected by airborne CCD for one or more satellites.
- The ionospheric delay d, given in m/s, has to be limited since it impact the test metric of the DSIGMA. The bigger the induced delay is, the bigger the test metric, and the lower the P_{md} of the test.
- The ionospheric front does not impact the GS since the PRC and RRC may compensate the induced error delay. Moreover the CCD at the ground has different performances than the one at the airborne side, if a front impacts both ground and airborne receivers, the detection performance is improved.

Considering that the critical point for GAST-D is at CAT I decision height (200 ft.), a critical case for an ionospheric front respecting the previous condition is represented in Figure 91.

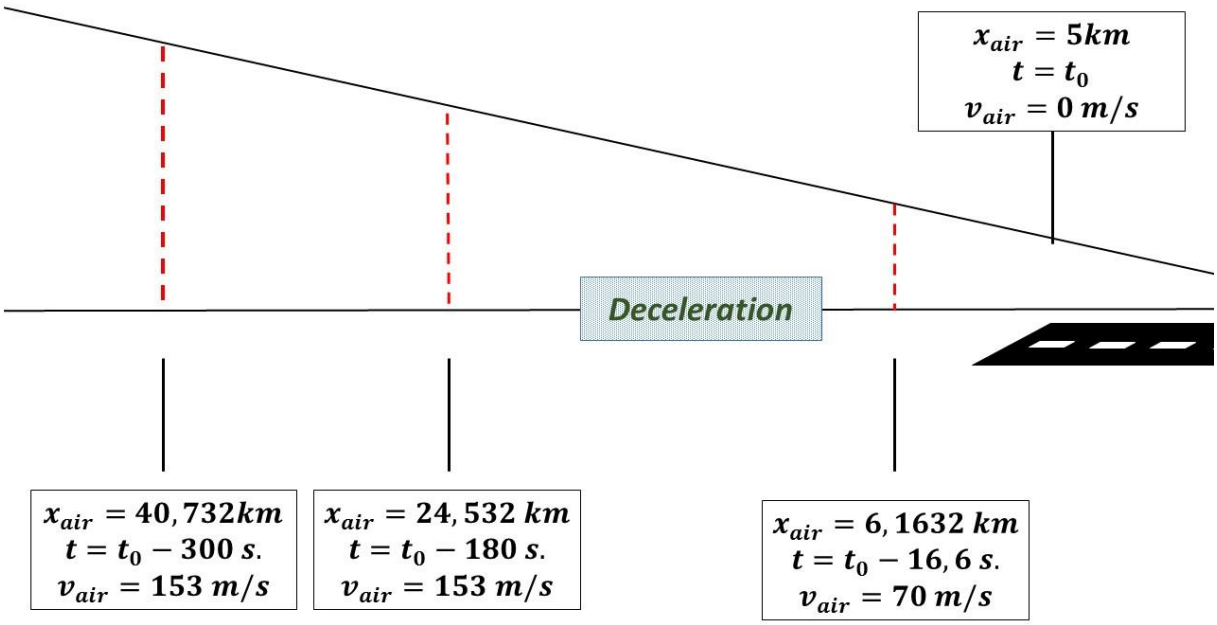

Figure 91 – Simulation of maximum induced delay for an ionospheric front impacting the aircraft but no the GS

The induced range delay for the case depicted in Figure 91 can be computed, taking into account the impact of the smoothing filter and the relative speed between the user IPP and the ionospheric front as:

$$D = slope * \min\left\{(x_{air} + 5) + \left(2 * \tau * \left(v_{IPP} - v_{front}\right)\right); W\right\} \quad \text{Eq. 5.34}$$

Where:

- x_{air} is the horizontal distance between the aircraft and the LTP
- $2 * \tau * \left(v_{IPP} - v_{front}\right)$ is the contribution of the smoothing filter to the range error.
- W is the width of the ionospheric front as depicted in Figure 3

In Eq. 5.34, the smoothing filter contribution term refers to the steady state condition for both 30 and 100 seconds filters. This condition represents the maximum value induced by the smoothing filter. For a 100 seconds smoothing filter, this condition is verified after 360 seconds, during this time the induced range error is smaller than the one in Eq. 5.34.

Considering the biggest slope provided in the threat model, a smoothing time constant of 30 seconds and a relative speed of 0.11 km/s, the value of the delay in equation Eq. 5.34 is 6.38 meters. The value of 6.1632 km is valid only if the front speed is aligned with the aircraft speed. In other cases, the distance

can be even lower. Figure 92 shows an example of an aligned front and one of a misaligned front where the induced range error is lower than the one induced by an aligned front.

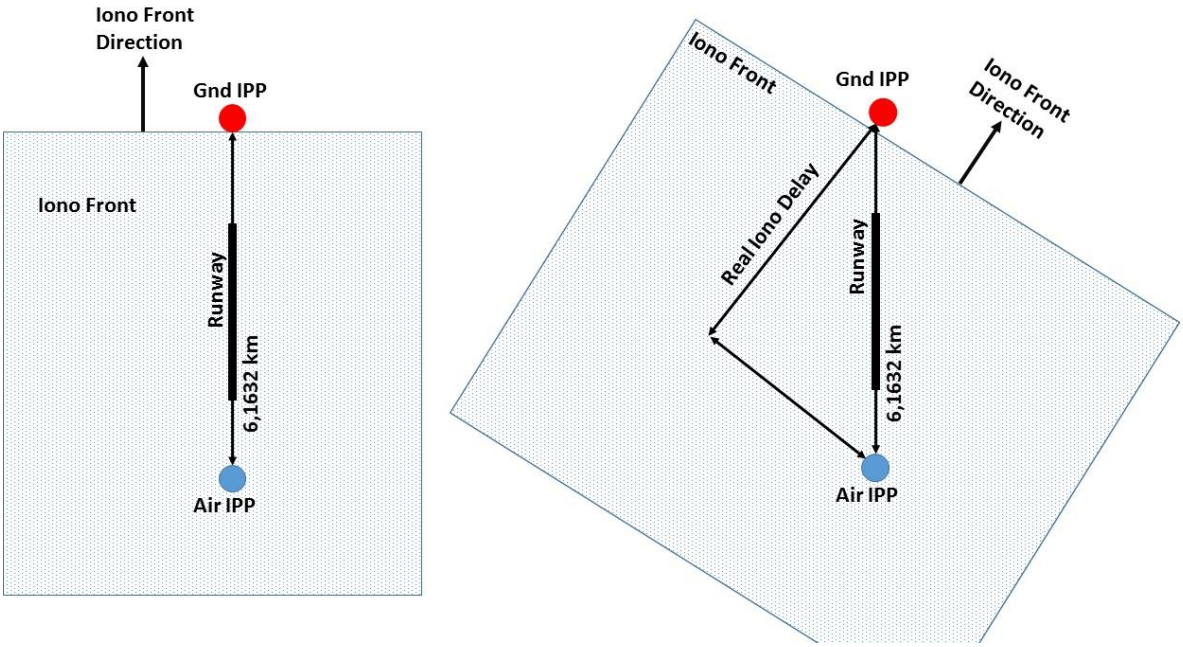

Figure 92 – Ionospheric induced range error for different ionospheric angle

The condition depicted in Figure 91 and Figure 92 describes a possible case on which a faulty satellite may impact the aircraft but not the GS providing the maximum induced range error. When this scenario is considered for all satellites in view, due to their different position in the sky, different interactions with the front are possible. For some of them, both air and ground IPP will be impacted by the front. For other satellites, the differential speed will be different causing either a CCD detection or a lower range error. Satellites present at the opposite azimuth may be not impacted by the front at all.

The scenario presented before can be considered as the worst-case for one satellite, considering an ionospheric front moving in the same direction of the aircraft and impacting only the aircraft IPP but not the ground one.

5.2.2.4 Proposed Solution for GAST-D Ionosphere Monitoring

A possible solution to the integrity issue for this GBAS service is the use of Receiver Autonomous Integrity Monitoring (RAIM) for the monitoring of ionospheric front.

The RAIM technique uses the redundant information to detect possible blunders affecting measurements used to compute the position solution (Brown, et al., 1997) . Considering the need of four measurements to compute the single constellation solution, a minimum of five satellites is necessary to perform a test assuming only one faulty measurement per epoch. In case of dual constellations, the measurement must

be at minimum six as, since a fifth unknown term has to be computed in the solution. In the literature, two main tests have been proposed to detect faults in the snapshot mode: residual-based test and solution separation test. In the following, only the solution separation test will be analyzed and used since it provides marginally better detection performance than the residual test. Details about RAIM residual test can be found in (Liu, et al., 2005).

The solution separation test relies on the comparison between the all-in-view position solution and the one computed using a subset of tracked satellites, where one satellite has been removed (Blanch, et al., 2012). Considering a bias affecting one measurement, this creates a difference between the all-in-view and the subset position solution. Removing the biased satellite, or another critical satellite, in the position computation for subset i, it is possible to obtain the following test statistic.

$$\Delta\hat{x}^{(i)} = \left(\delta\hat{x}^{(i)} - \delta\hat{x}^{(0)}\right) = \left(S^{(i)} - S^{(0)}\right)\Delta y \qquad \text{Eq. 5.35}$$

Where:

- x_0 is the position used to linearize the least square solution.
- $\delta\hat{x}^{(0)}$ is the estimated correction to add to x_0 to obtain the estimate positon computed using all satellites in view
- $\delta\hat{x}^{(i)}$ is the estimated correction to add to x_0 to obtain the estimate positon computed using all satellites except the satellite numerated by i
- $S^{(0)}$ is the S matrix computed as $(G^t W G)^{-1} G^t W$
- $S^{(i)}$ is computed as $\left(G^t W^{(i)} G\right)^{-1} G^t W^{(i)}$ and $W^{(i)}$ is the weight matrix with the i^{th} value on the diagonal is zero.
- G is the observation matrix presented in 2.3.3.2
- Δy is the vector containing the difference between the pseudorange measurements and the range distances computed relying on a point used for the linearization of the position solution

Knowing the relationship between measurements, geometry matrix, user position and error on pseudorange it is possible to write the following equation (Kaplan, et al., 2006):

$$\Delta y = G\ \delta x + \ \varepsilon \qquad \text{Eq. 5.36}$$

Where:

- δx is the solution vector composed by the x, y, and z corrections to apply to the point coordinates used to linearize the position solution and the receiver clock offset

- ε is a vector containing the measurements error.

It is possible to replace the measurement vector in Eq. 5.35 with the relation provided in Eq. 5.36

$$\Delta\hat{x}^{(\mathrm{i})} = \left(S^{(i)} - S^{(0)}\right)(G\ \delta x + \varepsilon) \qquad \text{Eq. 5.37}$$

The development of this product make the following term appear: $\left(S^{(i)} - S^{(0)}\right)G\ \delta x = S^{(i)}\ G\ \delta x - S^{(0)}\ G\ \delta x$.

$$S^{(0)}\ G\ \delta x = (G^t W G)^{-1} G^t W G\ \delta x = \delta x \qquad \text{Eq. 5.38}$$

$$S^{(i)}\ G\ \delta x = \left(G^t W^{(i)} G\right)^{-1} G^t W^{(i)} G\ \delta x = \delta x \qquad \text{Eq. 5.39}$$

Therefore, $\left(S^{(i)} - S^{(0)}\right)G\ \delta x = 0$ and Eq. 5.37 is simplified to:

$$\Delta\hat{x}^{(\mathrm{i})} = \left(S^{(i)} - S^{(0)}\right)\varepsilon \qquad \text{Eq. 5.40}$$

In case of no bias on measurements, the elements of ε are given by a centered normal distribution with a different variance for each satellite according to the used model. Under this condition, the value of $\Delta\hat{x}^{(i)}$ is expected to be under a normal distribution with zero mean and sigma of the test as (Blanch, et al., 2012):

$$\sigma_{ss}^{2\,(i)} = \left(S^{(i)} - S^{(0)}\right)C\left(S^{(i)} - S^{(0)}\right)^T \qquad \text{Eq. 5.41}$$

Where:

- C is the covariance matrix of the measurement errors, $C = W^{-1}$

In case of one faulty measurement the vector ε can be seen as:

$$\varepsilon = \begin{vmatrix}\eta_1\\ \eta_2\\ \vdots\\ \eta_i\end{vmatrix} + \begin{vmatrix}0\\ b\\ \vdots\\ 0\end{vmatrix} = H + B \qquad \text{Eq. 5.42}$$

Where:

- η_i is the noise term of the i^{th} satellite and it follows a centered normal distribution
- b is a bias affecting one or more satellites at the same epoch.
- H and B are the vectors containing respectively η and b

In this case, the value of $\Delta\hat{x}^{(i)}$ follows a normal distribution with standard deviation as in Eq. 5.41 and mean value given by:

$$\mu^{(i)} = \left(S^{(i)} - S^{(0)}\right)B \qquad \text{Eq. 5.43}$$

Where $\mu^{(i)}$ contains the mean value for the three axis, x, y, z and the receiver clock offset.

If the test has to be executed on one of the three axis, x, y or z, or on two of them, for example x and y for the horizontal plane the values of the test standard deviation is

$$\sigma_{ss,q}^{2\,(i)} = \sigma_{ss}^{2\,(i)}(q)$$

Where q could be 1, 2, 3 and it considers the first, the second or the third term on the diagonal of $\sigma_{ss}^{2\,(i)}$

In case of test on two axis, for example x and y the first and the second values have to be used:

$$\sigma_{ss,1-2}^{2\,(i)} = \sigma_{ss}^{2\,(i)}(1) + \sigma_{ss}^{2\,(i)}(2)$$

The same has to be done with the values of μ.

A fault is detected when the solution separation test metric exceeds the threshold which is determined as a multiple of the test statistic noise according to (Blanch, et al., 2012).

$$Th_q = K_{fa}\sigma_{ss,q}^{(\mathrm{i})} \qquad \text{Eq. 5.44}$$

Where:

- $K_{fa}$is the multiplier for the fault-free detection, it is equal to $Q^{-1}\left(\frac{P_{fa}}{2N_{fault\ modes}}\right)$, Q is the quantile of a Gaussian distribution. In case of test of more than one axis, for example the horizontal plane is composed by the x and y axis, the multiplier is computed considering $Q^{-1}\left(\frac{P_{fa}}{4N_{fault\ modes}}\right)$
- P_{fa} is the probability of false alarm
- $N_{fault\ modes}$ is the number of combinations to monitor according to the selected fault mode. One or more faulty satellites can be considered

Therefore for each satellite, it is possible to compute the Minimum Detectable Bias (MDB) according to the required P_{fa} and P_{md}.

$$MDB^{(i)} = (K_{fa} + K_{md}) \cdot \sigma_{ss}^{(i)} \qquad \text{Eq. 5.45}$$

The value of MDB is multiplied by the related S_{vert} and S_{lat} will represent Minimum Detectable Error (MDE) in the vertical and lateral domain.

$$MDE_{vert} = \max_i\left(MDB^{(i)} \cdot S_{vert}^{(i)}\right) \qquad \text{Eq. 5.46}$$

$$MDE_{lat} = \max_i\left(MDB^{(i)} \cdot S_{lat}^{(i)}\right) \qquad \text{Eq. 5.47}$$

The biggest MDE, in vertical and latera domain, is representative of the worst case for the related epoch.

Using RAIM algorithm in GBAS, the value of C in Eq. 5.41 is smaller than using RAIM in stand-alone GNSS thanks to the better accuracy of the corrections. The small values of C directly reflect into σ_{ss} improving the test capability for errors detection. In this context it can be defined as Differential RAIM (DRAIM)

5.2.3 GAST-D RAIM Baseline and Results

5.2.3.1 GAST-D RAIM Simulation Baseline

DRAIM has been tested in 18 airports Table 26 gives the coordinates and the heading of one of the runways for all of them.

Table 26 – Airport latitude, longitude and runway heading for DRAIM simulation

Airports	**Latitude (°)**	**Longitude (°)**	**Main RWY Heading (°)**
Memphis	35.0424	-89.9767	360
Denver	39.8584	-104.667	80
Dallas	32.8964	-97.0376	360
Newark	40.6925	-74.1687	40
Washington	38.9445	-77.4558	10
Los Angeles	33.9425	-118.4081	70
Orlando	28.4289	-81.3160	180
Minneapolis	44.8805	-93.2169	300
Chicago	41.9796	-87.9045	100
Tacoma	47.1377	-122.4765	340
Anchorage	61.2167	-149.90	70
Bremen	53.0429	8.7808	90
Malaga	36.68	4.5124	310
Sydney	-33.9636	151.1859	340
Amsterdam	52.30907	4.763385	360
Rio	-22.8088	-43.2436	100
Peking	40.080109	116.584503	180
Johannesburg	-26.139099	28.246000	30

The heading of the runway will be used to derive a coordinate system with the x-axis aligned with the aircraft longitudinal axis and positive direction in the direction of aircraft speed. The y-axis aligned with

the lateral axis and positive direction pointing toward the left side. The z-axis aligned with the vertical and positive direction on the up direction.

Being a threat affecting GAST-D, the constellation used is GPS. The satellites position and the errors are computed for an entire day with a time resolution of one minute. Two configurations of the GPS constellation has been used:

- GPS Optimal 24 (DoD, Department of Defence USA, 2008)
- GPS 31 satellites constellation as in YUMA almanac (week 862; $T_{oe} = 589824$)

The measurement error model has been defined using the model proposed in 2.3.3.2, with the following parameters:

- Airborne Accuracy Designator (AAD) B
- Airborne Multipath Designator (AMD) B
- Ground Accuracy Designator as derived for L1 band measurement in 2.3.4.1
- $\sigma_{vig} = 6.4$ mm/km as in (Seo, et al., 2012)
- Residual tropospheric and ionospheric errors standard deviation as in (RTCA Inc.; DO253-C, 2008)

The main point analyzed is the CAT I decision height. Because an ionospheric front may be present also before that the airplane reaches this point, and the ionospheric delay being different, performances are computed also for other two points: 3 and 5 minutes before the landing.

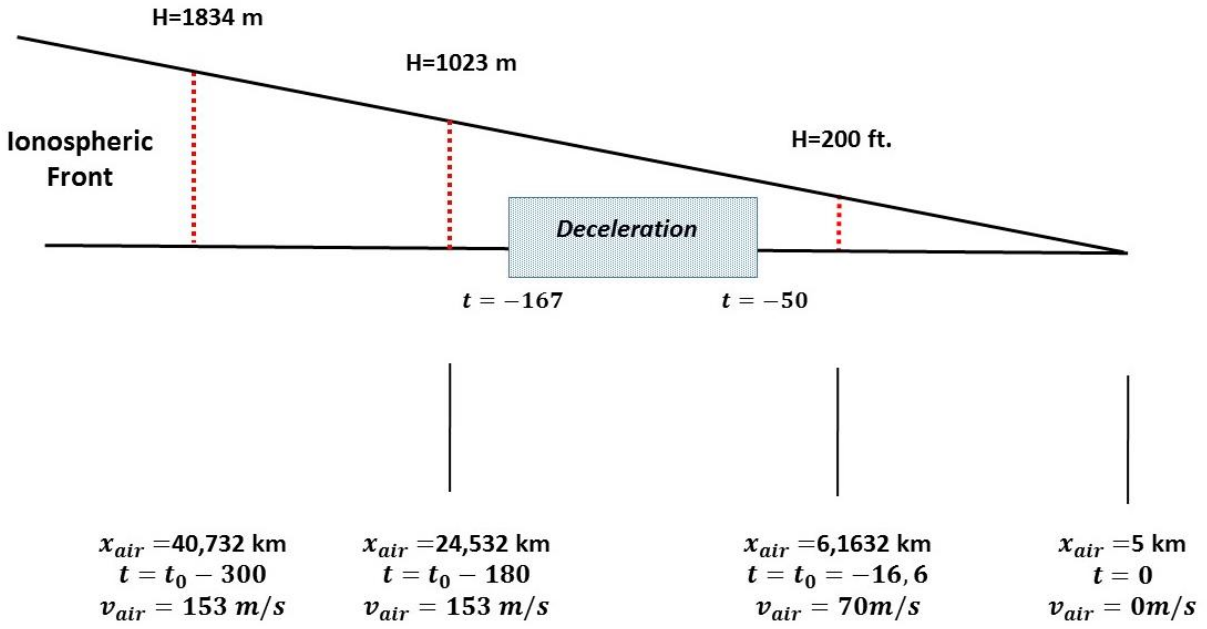

Figure 93 – Point along the approach used to derive DRAIM performances

In Figure 93, jointly with the horizontal distance and the altitude of the points, are shown the aircraft speeds at the different points derived from (ICAO NSP, 2015). The last parameter to define is the maximum range error that may be caused by the ionospheric front. Knowing that the range error caused by a front is given in Eq. 5.34, the parameters of this equation must be defined.

- The value of x_{air} has been already defined according to the three points in along a straight-in trajectory.
- The ionospheric front gradient is assumed to be at his maximum value; 0.5 m/km
- the smoothing time constant $\tau = 30$ seconds
- Δv, considering also the values in Table 25, has been set to 0.07, 0.035 and 0 km/s. Negative values, simulating a front faster than the aircraft will not be considered. The induced range error for this cases, in fact, is smaller than the real one due to the smoothing filter response.

Computing the range error induced by the front for each value of Δv, the following results may be obtained for the three points along the approach. In Table 27, the maximum range error according to the three analyzed velocity are shown. The range error is, however, dependent on the vertical error. In the following of the section the process to compute it is explained.

Table 27 – ionospheric front induced range error (m)

$\Delta v \left(\frac{km}{s}\right)$	x_{air} (km)		
	6.1632	**24.532**	**40.732**
0.07	5.5	16.9	25
0.035	4.2	12.66	19
0	3.1	8.5	12.4

The values of the range error computed for the two points along the approach takes into account the following assumptions:

- The speed of the IPP is considered to be driven by the one of the aircraft at CAT I point. This permits to derive that the front is not moving in the case $\Delta v = 0.07\ km/s$, is moving at almost $0.035\ km/s$ in the second one and $0\ km/s$ for the last one.
- The satellite dynamics is not considered for the derivation IPP speed since it is at an approximated height of 350 km and at this height the aircraft speed is the one having a relevant

impact on it. Moreover considering that an approach and landing procedure last no longer than 5 minutes the satellite may appear as stationary for a ground, or aircraft, user.

The matrix G, the observation matrix, is computed in the same coordinate frame proposed in 2.3.3.2, where the x-axis is aligned with the runway with positive direction in the same direction of the landing. The z-axis is pointing to the up direction and the y-axis is oriented to be orthogonal to the previous two.

The values of S_{vert} and S_{lat} are given in 2.3.3.2

The test standard deviation is computed as in Eq. 5.41, the values of the vector e_q are different for the vertical and lateral cases. In the vertical case it is assumed to be:

$$e_{vert} = \begin{bmatrix} tan(GPA) \\ 0 \\ 1 \\ 0 \end{bmatrix}$$

This because also the longitudinal error, in the runway direction, impact the vertical error.

For the lateral case

$$e_{lat} = \begin{bmatrix} 0 \\ 1 \\ 0 \\ 0 \end{bmatrix}$$

The values in the two cases reflect how the range errors impact the four values of the S matrix to compute the vertical and lateral error.

The test threshold is computed as in Eq. 5.44. The $P_{fa} = 10^{-7}$; the $N_{fault\ modes}$ in this case is equal to the number of satellites used to compute the all-in-view position solution. For the vertical case $K_{fa,vert} = Q^{-1}\left(\frac{P_{fa,vert}}{(2+2\cdot\tan(\mathrm{GPA}))\, N_{fault\ modes}}\right)$, instead for the lateral one $K_{fa,lat} = Q^{-1}\left(\frac{P_{fa,vert}}{2N_{fault\ modes}}\right)$. GPA has been already defined, in this test it is assumed to be 3°.

The scope of simulations is to verify the capability of DRAIM to detect the range error due to ionospheric gradient with a required P_{md}. It is useful to say that in (ICAO NSP, 2010), it is assessed that all errors, in the vertical domain, smaller than 6.4 meters can be undetected. Errors with a bigger magnitude have to be detected with a $P_{md} < 10^{-9}$.

The P_{md} will be computed for all satellites according to the proposed scheme:

- Computation of the range error of each satellite providing a vertical error bigger than $\pm$ 6.44 meter as $\varepsilon_r{}^{(i)} = 6.44/\left|S_{vert}^{(i)}\right|$

- Removal of all satellites having an $|\varepsilon_r|$bigger than the maximum induced error computed in Table 27 because it is out of the residual ionospheric threat model.
- Computation of the P_{md} for all remaining ε_r and selection of the one providing the highest P_{md} as worst case
- Analysis of P_{md} for the points along the trajectory for the same satellites in order to analyze if detection is improved in previous points.
- The induced ionospheric range error for the points along the approach is computed as a linear extrapolation knowing the relationships in Table 27. For example considering the first case, $\Delta v = 0.07\ km/s$ the relation between errors is $5.5:\ 16.9$. the induced range error for this point can be computed as:
    - $x = \frac{16.9 \cdot \varepsilon_r}{5.5}$
- The satellites geometry is computed for 3 and 5 minutes offset with respect to the analyzed epoch. If the satellite is not present in one of the two points the P_{md} for the related case is set to 1 because the system cannot be protected by a detection done in one or both the point along the approach analyzed.
- The same process is used for all other velocities adapting the used maximum range delay.

5.2.3.2 GAST-D RAIM Results

A critical parameter to derive RAIM performances is the number of faulty measurements at the same time. Analysing the condition under which an ionospheric front is undetected by all monitors, for GAST-D service, a single "faulty and not detected" satellite seems to be the most probable case. This condition is not, however, the only one possible. A two "faulty and not detected" satellites scenario is therefore possible.

The results of simulations done considering the baseline presented in 5.2.3.1 are shown here. In Figure 94 the results for a stationary front ($\Delta v = 70\ m/s$) are shown for the optimal 24 GPS constellation.

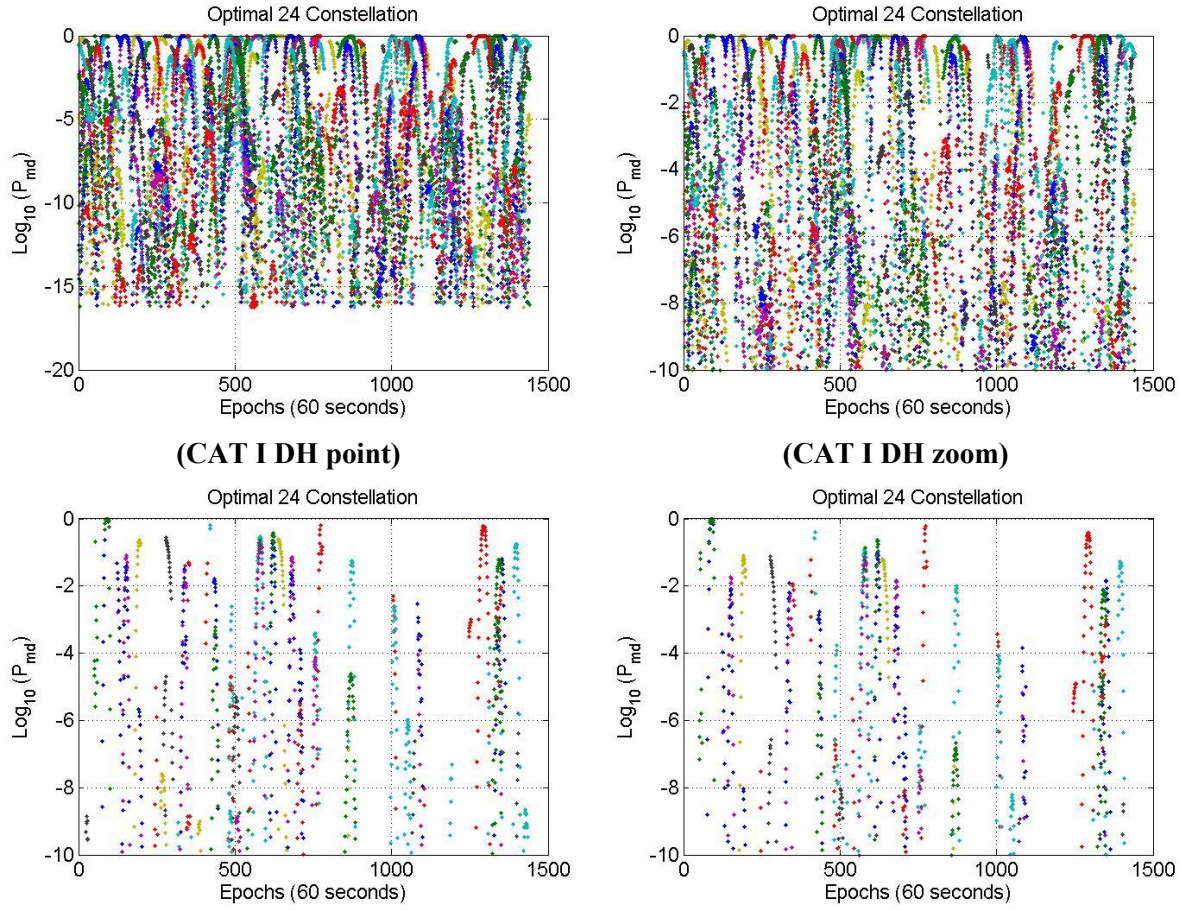

(CAT I DH point) **(CAT I DH zoom)**

(3 minutes before landing) **(5 minutes before landing)**

Figure 94 – DRAIM P_{md} of ionospheric front induced error for GPS Optimal 24 and $\Delta v = 70\ m/s$ for all airports

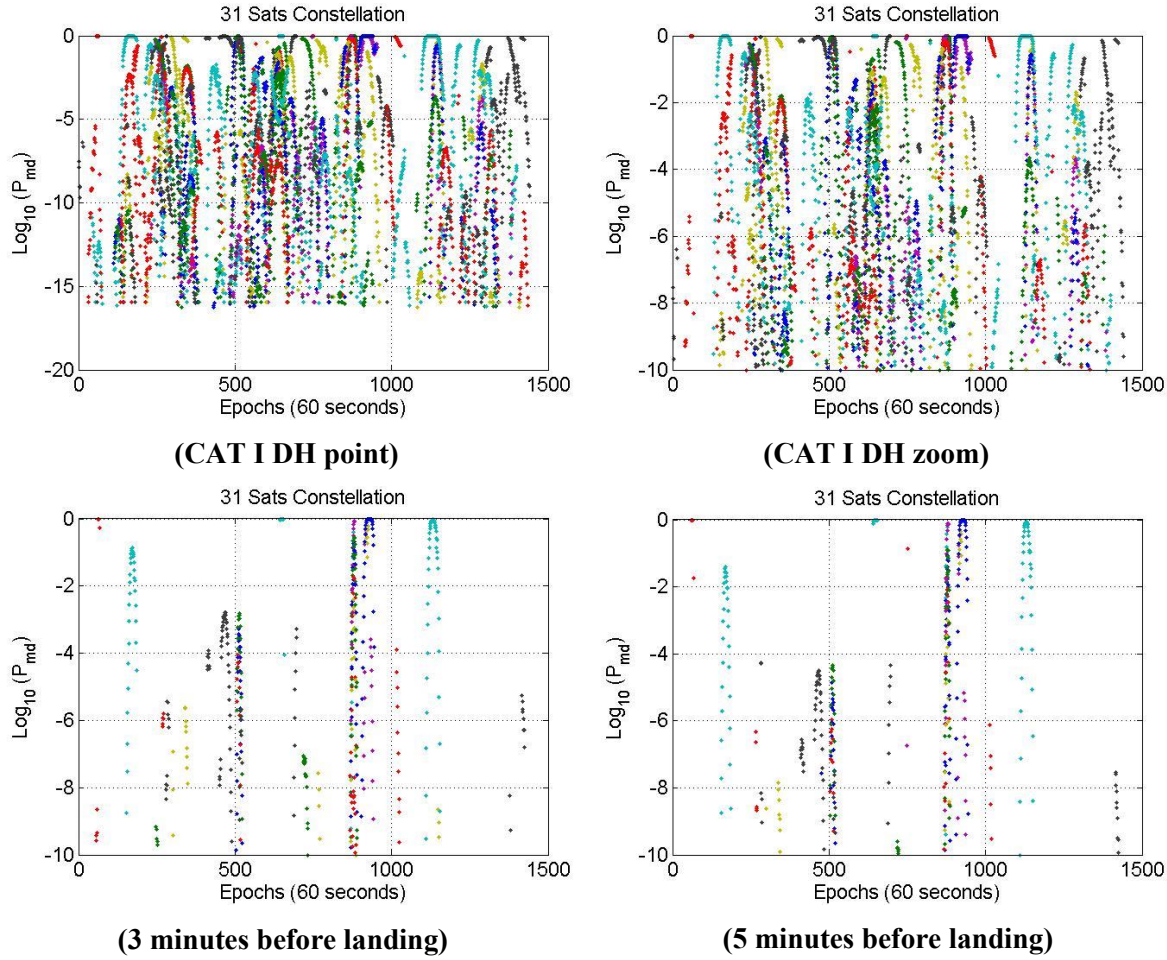

Figure 95 – DRAIM P_{md} for ionospheric front induced error for GPS 31 Satellites and $\Delta v = 70\ m/s$ for all airports

Figure 94 and Figure 95 show the P_{md} for the vertical error bigger than ± 6.44 meters and for which the range error, on one single satellite, does not exceed the 5.5 meters at CAT I DH point.

Knowing that any error bigger than 6.4 meters has to be monitored with a $P_{md} < 10^{-9}$ it is possible to see that DRAIM alone is not able to guarantee the required P_{md} at CAT I decision point. In a lot of cases, the P_{md} is bigger than this limit. If the front is present at the time of the beginning of the approach, the monitor provides better results thanks to the increased magnitude of the induced range error. In some cases also the satellites geometry changes between the points along the approach providing better performances. It has to be considered however that under these conditions the IPP is moving faster than the front, the CCD and the DSIGMA monitor can provide low level of P_{md} once integrated with the one from RAIM leading to the required level. The use of 31 satellites constellation provides better results than the optimal 24, as expected, because the bigger number of visible satellites improves the DRAIM detection capability.

In Figure 96 and Figure 97 the results for the case $\Delta v = 35\ m/s$ are shown. The range error for this case are respectively: 4.2, 12.66 and 19 meters.

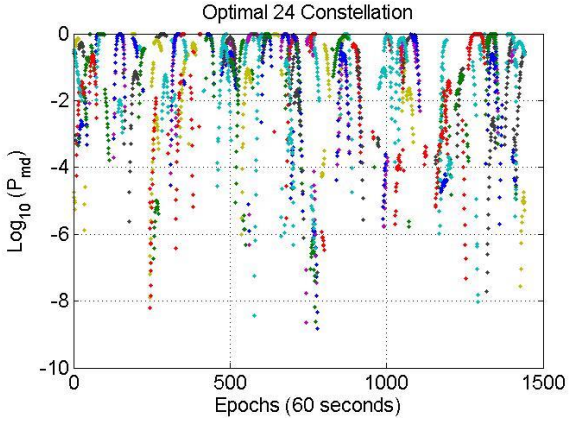

(CAT I DH point)

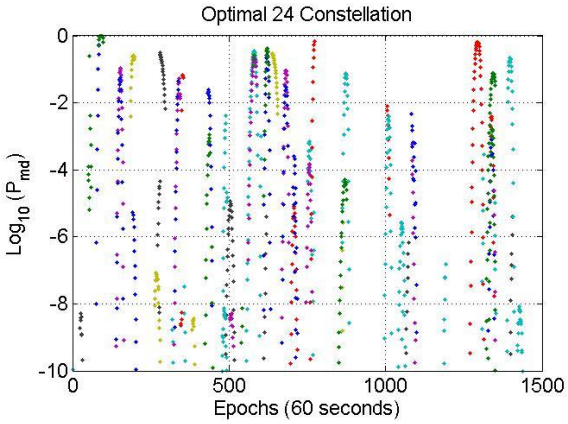

(3 minutes before landing)

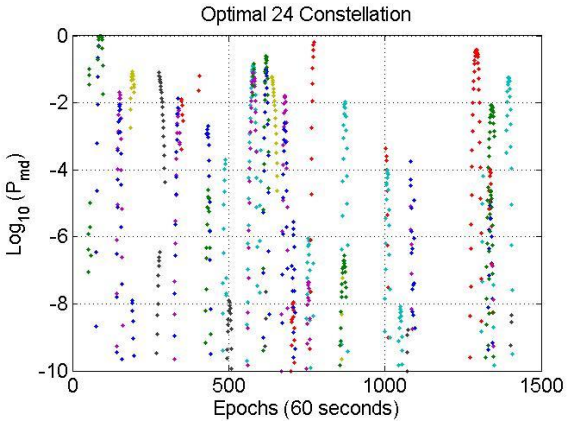

(5 minutes before landing)

Figure 96 – DRAIM P_{md} for ionospheric front induced error for GPS optimal 24 and $\Delta v = 35\ m/s$ for all airports

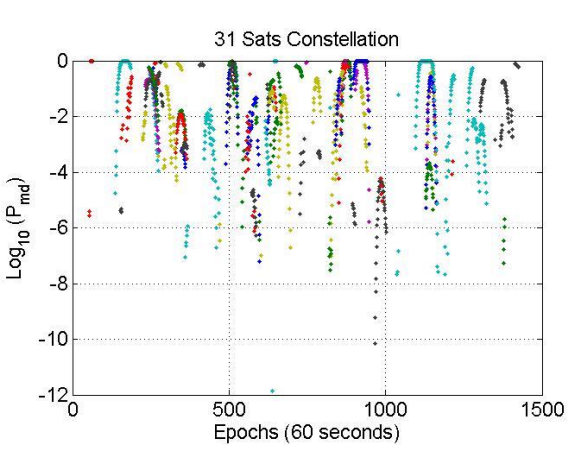

(CAT I DH point)

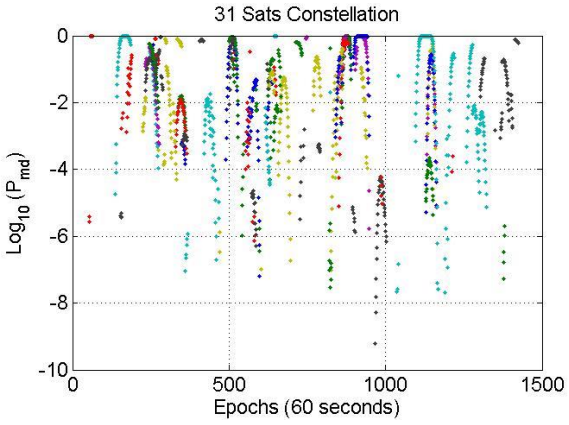

(CAT I DH zoom)

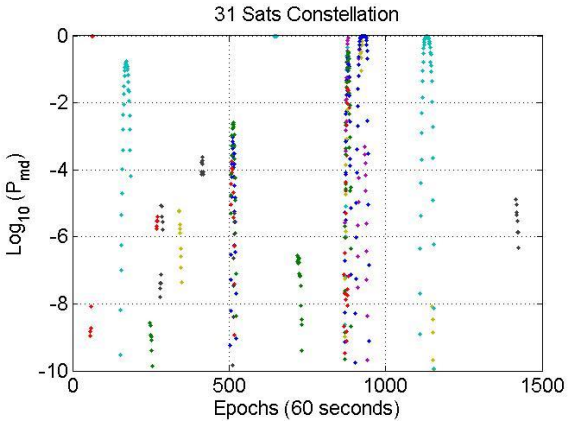

(3 minutes before landing)

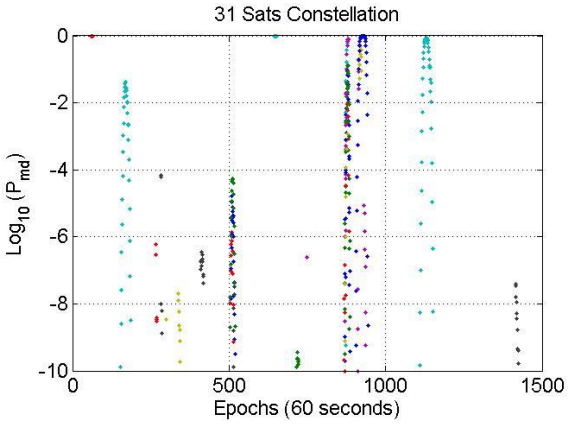

(5 minutes before landing)

Figure 97 – DRAIM P_{md} for ionospheric front induced error for GPS 31 Satellites and $\Delta v = 35\ m/s$ for all airports

Comparing Figure 96 and Figure 97 with Figure 94 and Figure 95, it is possible to see that the number of undetected faults ($P_{md} > 10^{-9}$) is lower because, thanks to the lower range error, the number of epochs where the vertical error overcomes 6.4 meters is reduced thanks also to the presence of the geometry screening monitor that limits the cases of bad geometry. In Figure 96 and Figure 97, it is possible to see that relying on detections done along the approach the performance of DRAIM can improve thanks to the increased range error. In this condition, considering that the Δv is reduced, the detection capabilities of the CCD and DSIGMA are reduced if compared to the previous case where Δv was 70 m/s.

Figure 98 and Figure 99, show the results for the last case analyzed: $\Delta v = 0\ m/s$. In this case thanks to the non-contribution of the smoothing filter to the induced range error the values are: 3.1,8.5 and 12.4 meters respectively.

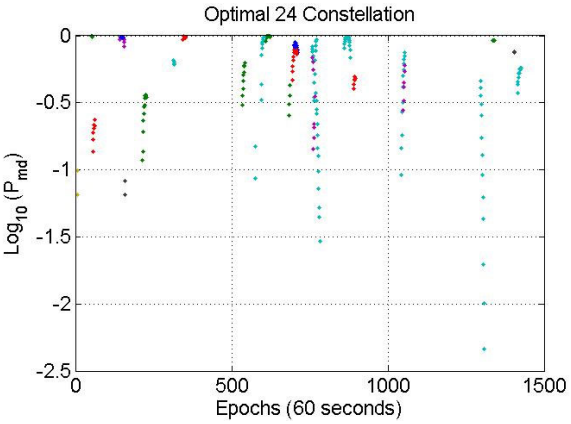

(CAT I DH point)

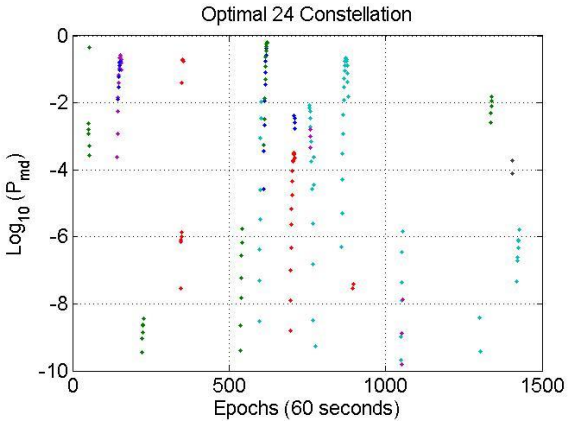

(3 minutes before landing)

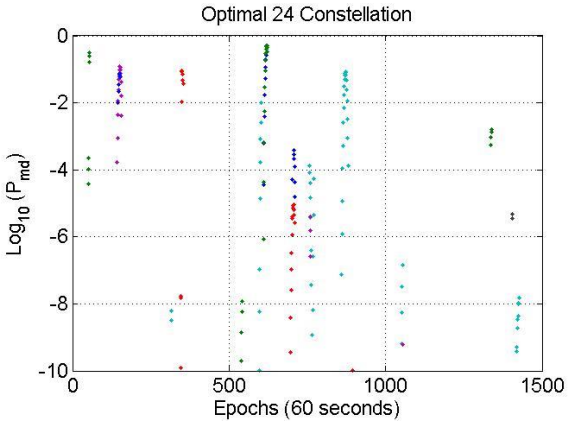

(5 minutes before landing)

Figure 98 – DRAIM P_{md} for ionospheric front induced error for GPS optimal 24 and $\Delta v = 0\ m/s$ for all airports

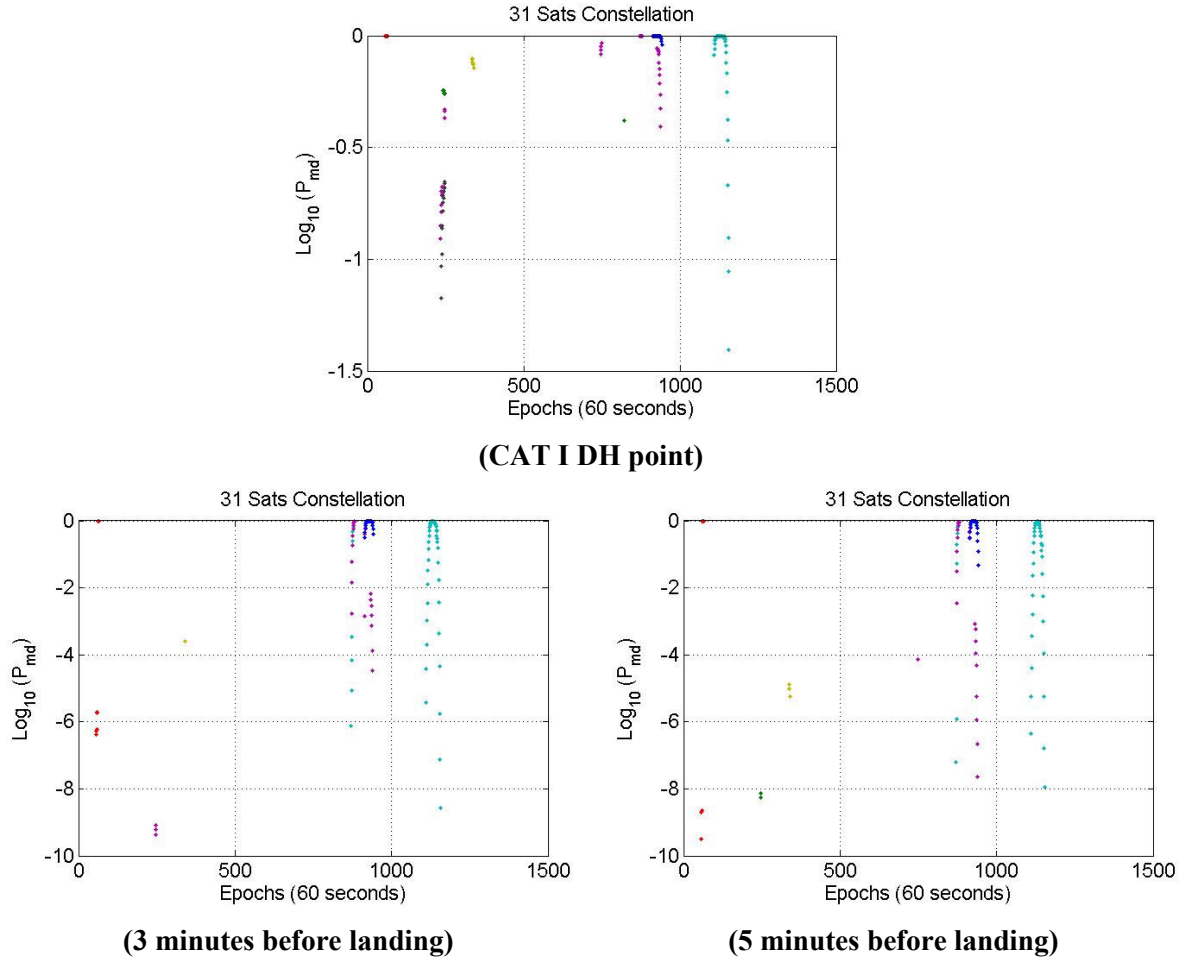

Figure 99 – DRAIM P_{md} for ionospheric front induced error for GPS 31 satellites and $\Delta v = 0\ m/s$ for all airports

The analysis of the last case, Figure 98 and Figure 99, provides the best results among the three analyzed cases. A few cases provide a vertical error bigger than 6.4 and are not detected ($P_{md} > 10^{-9}$) by DRAIM. Under this condition in fact, the range error is only determined by the ionospheric gradient because the smoothing filter does not see any changes of the ionospheric delay. In this condition, however, the detection relying on points along the approach provides the worst results since the front is moving with the plane and the delay is not changing too much. Moreover, it has to be said that the airborne monitors are assumed to have high P_{md} level due to the low differential speed between IPP and ionospheric front. The monitors at ground station can help whenever the ionospheric front impacts the ground station IPP, in this case the differential speed is quite significant.

In order to summarize the results obtained so far, it is useful to evaluate the system availability inside the simulation. This means to see how many epochs have a vertical error that is lower than 6.4 meters (also considering the limitation of the errors in the range domain) and that is not detected with a $P_{md} < 10^{-9}$. In Table 28 the percentage of epochs where the P_{md} is not meeting the 10^{-9} requirement is computed for each analyzed case.

Table 28 – Percentage of epoch with a not sufficient P_{md} for GAST-D

Δv	GPS Constellation used	Unavailability for CAT I DH point ($\lvert E_V \rvert > 6.4$ and $P_{md} > 10^{-9}$)	Unavailability for point along the approach (3, 5 min before)
70 m/s	Optimal 24	29.4 %	3.78 % 2.92 %
	31 Satellites	15.23 %	1.96 % 1.61 %
35 m/s	Optimal 24	11.86 %	3.48 % 2.58 %
	31 Satellites	6.72 %	1.68 % 1.39 %
0 m/s	Optimal 24	1.0 %	0.61 %; 0.56 %
	31 Satellites	0.67 %	0.51 %; 0.52 %

Analyzing the values in Table 28, it is good to remind that the simulation considers already particular atmospheric conditions with a limited occurrence probability. These values are not indicative of the total system availability since the probability that an ionosphere front occur, denoted as P_{priori}, is not considered. To derive the total system availability the P_{md} computed before has to be mulitpalied by the P_{priori} and then the availability can be computed. The value of the P_{priori} for an ionospheric front has not been determined however.

Examining the results for all the cases, it is possible to assess, under the assumption of "one faulty and not detected" satellite that the use of DRAIM with the other monitors may help to reach the required integrity level. DRAIM is, in fact, not dependent on the front speed or the other atmospheric activities.

5.3 GAST-F Integrity Monitoring

The concept to derive the airworthiness for GAST-F is foreseen to be similar to the one adopted for GAST-D. Advantages of the new service will be provided by lower values of the NSE and FTE that will permit to further relax some integrity requirements. Moreover with the use of DF measurements the monitoring of the ionosphere activity will be improved in term of better detection performances or reduction of the induced differential error.

Despite the advantages some challenges rises due to the use of new signals, DF combination, and possible new processing modes.

5.3.1 GAST-F Monitoring Challenges

With the development of a DC/DF GBAS system, a lot of challenges have arisen. Concerning the integrity monitoring these challenges may be divided into three major groups:

- Threats on new signals or DF combinations. Up to now all threats presented in 2.2.3.1 have been defined for GPS L1 C/A signal. It is necessary to analyze the impact of threats on GPS L5, Galileo E1 and E5a and as well on D-free and I-free combinations. In case of significant differences, new threat models have to be derived.
- Integrity issues for new update rate. A possible processing solution to broadcast all corrections and information in case of DF/DC GBAS, is to change the PRC and RRC update interval. Currently, the used value is 0.5 s and integrity performances are derived, for GPS L1 C/A, according to this rate. The integrity considering new values must be re-assessed to verify the feasibility of the monitors.
- Re-assessment of the monitors according to the characteristics of any new signal or DF combination.
- Definition of the monitors to use in case of loss of one constellation or loss of one frequency.

In this thesis the following issues have been analyzed:

- Impact of an extended PRC and RRC update interval on the excessive acceleration monitor
- Use of DRAIM to improve monitoring performances in case of frequency loss

5.3.2 GAST-F Monitors Evaluation

In (Milner, et al., 2015) the impact of using an update interval bigger than the current one, 0.5 seconds, has been analyzed. Results show that a value of 2.5 seconds is feasible in term of system accuracy degradation. In the integrity context, the impact of this proposed update rate on the excessive acceleration monitor has been investigated

5.3.2.1 EA for Extended Latency

With the use of DF combinations new information has to be broadcast in the VDB message to provide a GAST-F service maintaining the inter-operability with the GAST-C/D services. This condition leads to an issue considering the GAST-D message structure, which has a limited free capacity. One possible solution is to decrease the update rate for the PRC and RRC, as proposed in (Milner, et al., 2015) to send corrections for all satellite and all signals or combinations. It has to be clarified that this change does not concern the integrity message for which the structure remains the same as in Figure 81

To cope with this modification, the differential error must be computed at the time when the PRC and RRC are received to also check that a non-detected acceleration does not cause a differential error bigger than 1.4 meters. Figure 100 helps to understand the processing scheme for the new timing diagram. First of all, it can be noted that the two bars representing the time to process and broadcast corrections are now 3.5 seconds long instead of 1.5 s for GAST-D. This is because the time to process measurement at

ground does not change, 1 second, and only the VDB part changes from 0.5 to 2.5 seconds. The yellow triangles represent RRC and PRC which do not contain information about the acceleration threat. The green triangle is the first message where the PRC and RRC take into account for the acceleration. An integrity message is generated each 0.5 seconds and received at airborne side 1.5 seconds later.

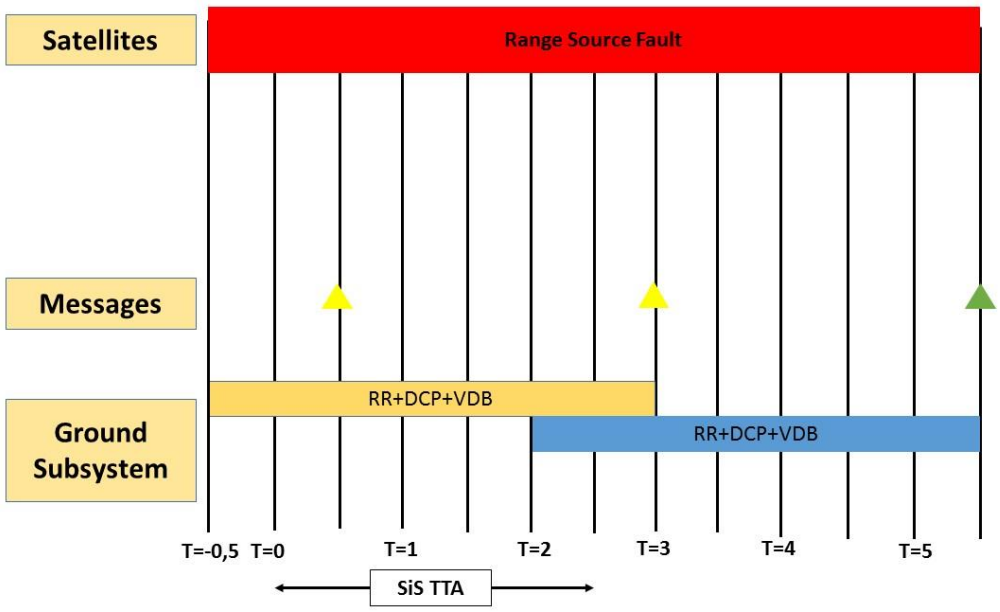

Figure 100 – Timing diagram derivation for below 200 ft. processing with PRC update rate at 2.5 seconds

Knowing that the SiS TTA does not change, it is possible to see that the maximum error, caused by a non-detected acceleration, is obtained at $t = 5.5$. After $t = 5.5$ the PRC and RRC containing information about the acceleration are received and the magnitude of the differential error decreases. Considering that the maximum differential error is caused by an acceleration of 6 seconds the differential error can be computed as:

$$\frac{1}{2}\, a\, (6^2) = 18\, a$$

The acceleration threshold is

$$18\, a = 1.4 \quad a = 0.078 \frac{m}{s^2}$$

Considering the performances of the linear metric for the EA monitor shown in 5.2.1.4 this acceleration cannot be detected with a sufficient P_{md}.

A new monitor to detect accelerations has been presented in (Stakkeland, et al., 2014). The test metric is formed using the rate of the phase measurement across two consecutive epochs and the phase acceleration estimated as in Eq. 5.13.

$$x(k) = \begin{bmatrix} \dot{\phi} \\ \ddot{\phi} \end{bmatrix}$$

The detection metric is the chi-squared distributed quadratic norm:

$$d(k) = x^T \Sigma^{-1} x \qquad \text{Eq. 5.48}$$

Knowing that the variance of the acceleration detector is $6\ \sigma_\phi^2/T^4$ and the one for the velocity estimation is $2\ \sigma_\phi^2/T^2$ ($v = \frac{\phi(k)-\phi(k-1)}{T}$). Considering the correlation between the two as $3\ \sigma_{phi}^2/T^3$ it is possible to compute the covariance matrix for the test as (Brenner, et al., 2010) and (Stakkeland, et al., 2014):

$$\Sigma_x = \frac{\sigma_\phi^2}{T^2} \frac{N}{M(N-1)} \begin{bmatrix} 2 & 3/T \\ 3/T & 6/T^2 \end{bmatrix} = {\sigma_\phi}^2 \frac{N}{M(N-1)} \begin{bmatrix} 8 & 24 \\ 24 & 96 \end{bmatrix}$$

- N is the number of satellites tracked at all ground receivers
- M is the number of ground receivers in operation

When a fault occurs, the detection statistic contains a bias term. The non-centrality parameter is (Stakkeland, et al., 2014):

$$\lambda(k_{fault}) = m(k_{fault})^T \Sigma^{-1} m(k_{fault}) \qquad \text{Eq. 5.49}$$

The value of m is impacted by the value of k_{fault} that represents the epochs elapsed from the acceleration onset

$$m(1) = a \begin{bmatrix} \frac{1}{4} & \frac{1}{2} \end{bmatrix}^T$$

$$m(k>1) = a \begin{bmatrix} \frac{1}{4}(2k-1) & 1 \end{bmatrix}^T$$

Replacing the values of $m(k)$ in Eq. 5.49, it is possible to compute the non-centrality parameter for the detection test.

$$\lambda(1) = \frac{1}{96} \frac{a^2 M(N-1)}{N\ {\sigma_\phi}^2} \qquad \text{Eq. 5.50}$$

$$\lambda(k>1) = \frac{1}{96} \frac{a^2 M(N-1)}{N\ {\sigma_\phi}^2} (12k^2 - 24k + 13) \qquad \text{Eq. 5.51}$$

Setting:

- $P_{fa} = 10^{-9}$
- $\sigma_{\phi} = 0.0025$
- $M = 3$
- $N = 4$

It is possible to compute the P_{md} performance for each acceleration value. The value of k can be at maximum three in order to have time to process and broadcast an integrity message.

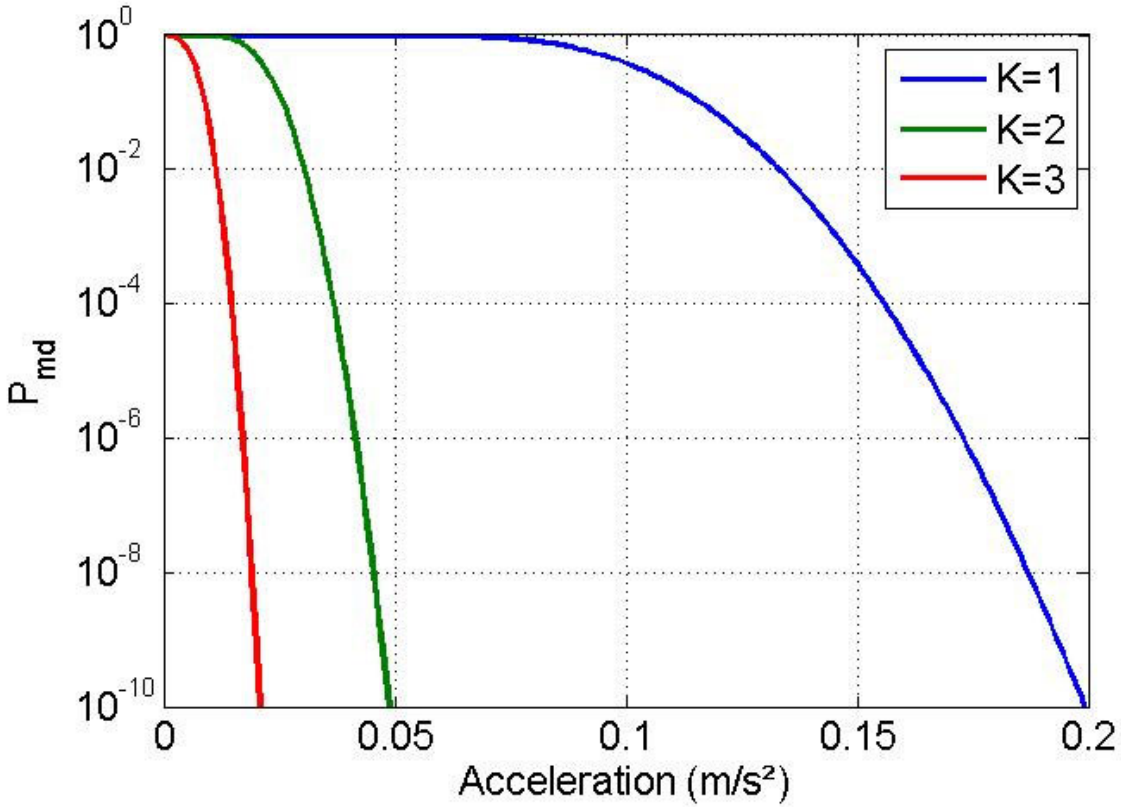

Figure 101 – P_{md} values for different accelerations and K-values for new metric

In Table 29, the values of the acceleration detected with a $P_{md} = 10^{-9}$ are shown.

Table 29 – Acceleration detected with $P_{md} = 10^{-9}$ for different K-values

k_{fault}	$P_{md} = 10^{-9}$
1	$a = 0.193\ m/s^2$
2	$a = 0.047\ m/s^2$
3	$a = 0.020\ m/s^2$

As it is possible to see in Figure 101, the performance of this new metrics improves with the growing of k. However, using $k = 1$ it is not possible to have a differential range error after 6 seconds of acceleration lower than 1.4 meters:

$$E_r(6) = 18 * 0.193 > 1.4\ meters$$

Relying on the detection at $k = 2$ it is possible to have a differential error at $t = 5.5$ lower than 1.4.

$$E_r(6) = 18 * 0.047 < 1.4\ meters$$

This condition will allow only one missed integrity message in the 2.5 seconds of the SiS TTA.

In Figure 102 a possible worst case is considered. The first integrity message (yellow triangle) generated at $t = 0$ and received at $t = 1.5$ could not detect an acceleration lower than 0.193 m/s² with the required P_{md}. The other two integrity messages (red) may be missed at airborne before receiving a new one (green) at $t = 3$. At this time, relying on detection with k_{fault} bigger than 2, any undetected acceleration has a magnitude lower than 0.02 m/s^2. It is possible to see that the worst differential error in this case is at $t = 3$ generated by a 3.5 seconds acceleration.

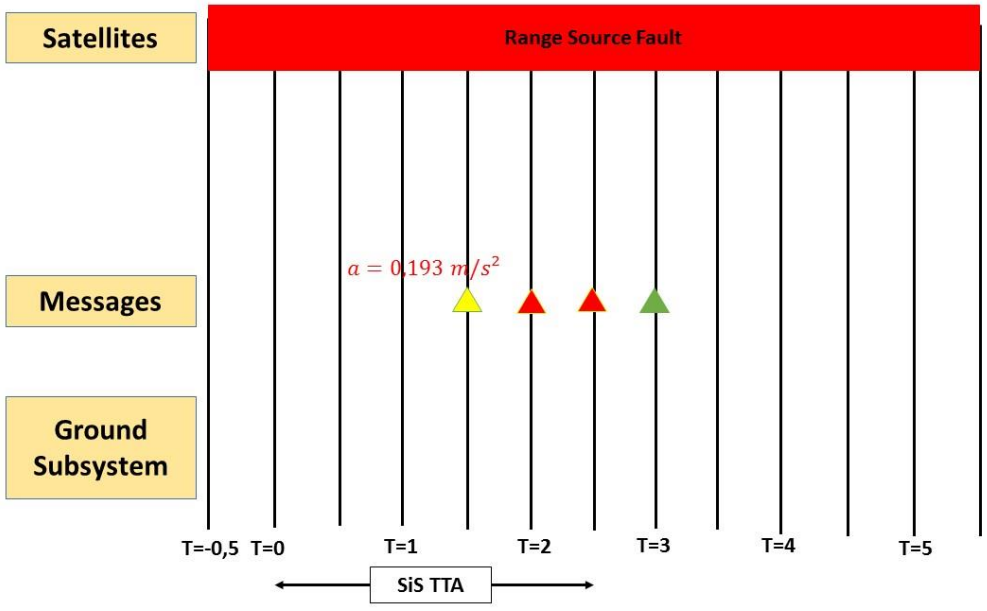

Figure 102 – integrity messages scheme

The differential error at this epoch, $t = 3$, can be generated only by a non-detected acceleration that according to the new metric is not bigger than 0.193 m/s^2. The differential error at this epoch can be computed as:

$$diff\ err\ (3.5) = 6.125\ * 0.193 < 1.4\ meters$$

If the acceleration is not detected, its value is lower than $0.02\ m/s^2$ and the induced range error does not overcome the limit of 1.4 meters until PRC and RRC are received. After the reception of the corrections the error is further reduced.

Using this new metric to monitor the acceleration threats makes possible to extend the PRC and RRC update time up to 2.5 seconds. The maximum undetected differential error does not exceed the 1.4 meters limit in any epoch. It is important to remind that the performances for this metric have been computed considering a more stringent value of the P_{md} than for what done for the linear metric in 5.2.1.4.

5.3.2.2 DRAIM Fallback Mode

As said in 5.3 thanks to the use of DF measurements the monitoring of the ionosphere anomalous activities may be improved or, using I-free combination, ionosphere anomalies no longer present a DF GBAS threat.

Although this condition seems to suggest that integrity could no longer represent a problem for ionospheric anomalies, the case of "fallback" to a SF GBAS service must be taken into account.

In GNSS "history", the Newark airport jamming episode (Grabowski, 2012) is quite famous. The use of personal GPS jammers led to a GBAS unavailability due to the interference. Under this condition, the signals in the jammed band cannot be used, and this require a fall-back situation from DF/DC GBAS to SF/DC GBAS. This condition, due to the presence of measurements on one single frequency, is from a monitor point of view similar to a GAST-D service with a bigger number of satellites. In this case, the integrity level must be provided relying on the same monitors developed so far for GAST-D.

In 5.2.3, the detection capabilities of DRAIM to monitor ionospheric fronts that could not be detected with the required P_{md} by the airborne or the ground monitors have been investigated. Relying on a bigger number of satellites available, this technique can be used also as fall-back monitor for GAST-F service. The following section will study the performances of DRAIM in a SF/DC GBAS case.

5.3.3 GAST-F RAIM Baseline and Results

5.3.3.1 GAST-F RAIM Simulation Baseline

Simulations for GAST-F has been done using some of the parameters presented in 5.2.3.1 for GAST-D. The list of analyzed airports is the same as in of the runways for all of them.

Table 26. Constellations used are GPS and Galileo. In particular for GPS the used almanacs are the same described in 5.2.3.1. For the Galileo case the optimal constellation almanac of 24 satellites has been used (EU-U.S Cooperation on Satellite Navigation, 2016).

The error model used to derive the covariance matrix is the same used for GAST-D and developed for GPS L1 C/A. Simulations considering L5 band measurements error model have not been done because

a model similar to the one developed for GPS L1 does not exists and although in 3.4.7 values of $\sigma_{pr\ gnd}$ have been derived for GPS L5 and GALIELO E5a it has been chosen to not use these values because the issues seen in using the BAE ARL-1900 antenna for L5 ban measurements. Another consideration that justify the analysis using the L1 model is the ionospheric delay on the two frequencies. Relying on the relationship state in Eq. 2.13, in fact, it is possible to see that the ionospheric induced delay on L5 band measurement is bigger than the one on L1 band measurements. Considering that in theory L5 band measurements, both on GPS and Galileo, are expected to have better performance than on L1 band, RAIM results are expected to be better than on L1 band measurements. For this reason analysing RAIM performances on L1 band measurements can be seen as the worst case for the detection of an ionospheric front.

The analysed points along the approach are the same as in 5.2.3.1.

For this simulation, considering the results obtained in 5.2.3.2 for single fault measurement with single constellations, the dual "faulty and undetected" cases will be analyzed. For a dual constellation case the analysis of single fault case provides better performances thanks to the presence of more satellites and an improved geometry. For this reason in this analysis the dual fault case is analyzed without any constraints on the selection of the worst satellite pair. It means that 2 satellites can be faulty, no matter their geometric configuration is. No particular model for the spatial extension of the ionospheric front is assumed, which is a conservative assumption.

The procedure to determine the worst pair of faulty satellites to monitor and the magnitude of the range error on each one is the following for any couple:

- Computation of the vertical error setting the maximum induced range, according to the ionosphere front speed, on both satellites. If the vertical error is not bigger than 6.44 meters the current couple of satellites is not analyzed. For example in the first ionospheric case the maximum range error at CAT I point is 5.5 meters, so the vertical error is:

  $$E_v = 5.5 \cdot (S_{vert}^1 + S_{vert}^2)$$

  Where E_v is the vertical error, S_{vert}^i is the S_{vert} value for the i-the assumed faulty satellites under analysis; S_{vert} has been presented in 2.3.3.2
- In case of vertical error bigger than 6.44 meters the relationship between the range errors on the two satellites providing the worst case to monitor is computed using the methodology described in (ANGUS, 2006) using the eigenvalues and eigenvectors. The range error on each satellite is (ANGUS, 2006):

$$E_r^1 = b \cdot \varepsilon^1$$
$$E_r^2 = b \cdot \varepsilon^2$$ Eq. 5.52

Where E_r^{i} is the range error on the i-thsatellite under analysis, b is the bias to apply to both range sources and is computed at next step, ε^1 and ε^2 are the first and second eigenvalues

- The value of b is computed starting from:

$$E_v = E_r^2 \cdot S_{vert}^1 + E_r^2 \cdot S_{vert}^2$$ Eq. 5.53

Replacing Eq. 5.52 in Eq. 5.53 it is possible to obtain

$$E_v = b \cdot \varepsilon_1 \cdot S_{vert}^1 + b \cdot \varepsilon_2 \cdot S_{vert}^2$$ Eq. 5.54

Setting E_v to 6.44 meters, it is possible to compute b and then to derive the range error for both satellites. If one of the two range errors is bigger than the maximum error than can be induced by an ionospheric front given in Table 27, it is set to the maximum values and the other one is increased to reach a vertical error of 6.44 meters. For example setting the first range error to 5.5 the second one is computed as:

$$E_r^2 = E_v - (5.5 \cdot S_{vert}^1)/S_{vert}^2$$ Eq. 5.55

- The P_{md} is then computed for the couple under analysis.
- If the value of the P_{md} is bigger than the required level of 10^{-9}, the same analysis, if both satellites are visible, is done for the two selected points along the approach. The satellites geometry is computed relying on the constellation status 3 and 5 minutes before the epoch under analysis. If one of the two satellites is not visible the P_{md} for these two points is set to 1 because the system cannot be protected using detections at the analyzed points. The range error for both is computed as done for GAST-D for both satellites.

5.3.3.2 GAST-F RAIM Results

As done for the results of GAST-D RAIM the P_{md} for the analyzed cases will be shown here. Figure 103 and figure YY show the results for the two 24 satellites constellations with a relative front-aircraft speed of 0.07 km/s.

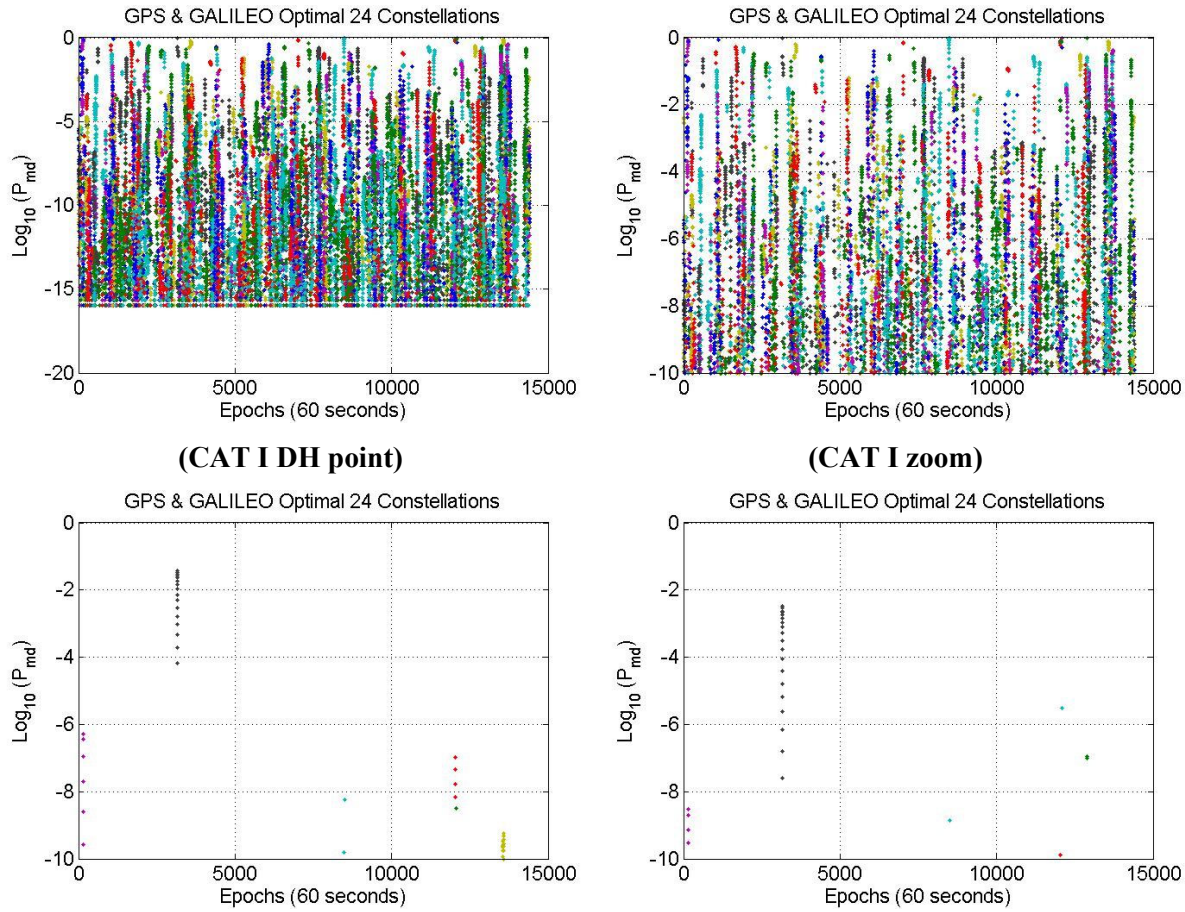

(CAT I DH point) **(CAT I zoom)**

(3 minutes before landing) **(5 minutes before landing)**

Figure 103 – DRAIM P_{md} for an ionospheric front induced error for GPS & Galileo Optimal 24 and $\Delta v = 70\ m/s$ for all airports

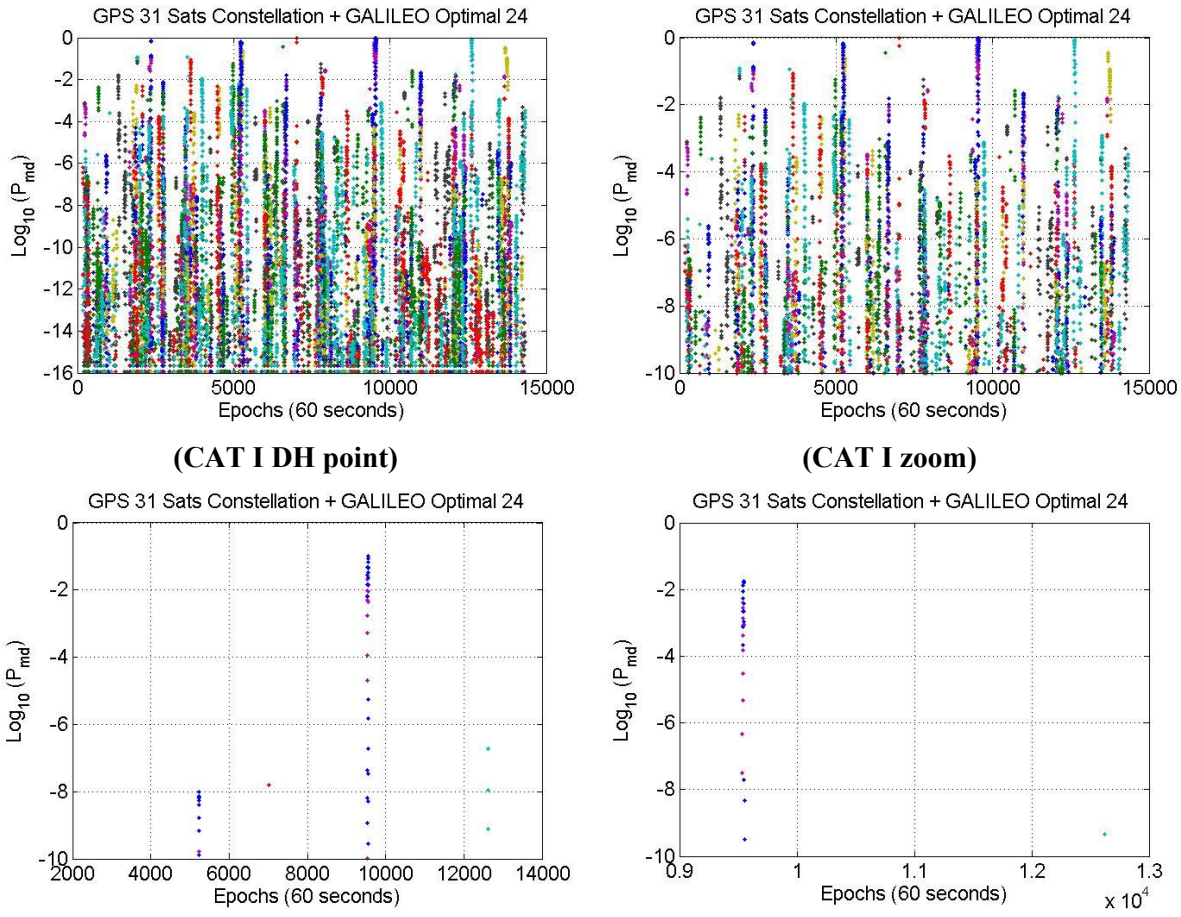

Figure 104 – DRAIM P_{md} for an ionospheric front induced error for GPS 31 satellites and Galileo Optimal 24 and $\Delta v = 70\ m/s$ for all airports

As for the GAST-D case, in Figure 103 and Figure 104, the P_{md} for the CAT I points are shown. In the same figure the results for the two points along the approach, 3 and 5 minutes before landing. It is possible to see that thanks to detection in points along the approach the system, relying only on RAIM detection, is protected for almost all epochs.

Figure 105 and Figure 106 show the results for a front moving with a relative speed of $35\ m/s$.

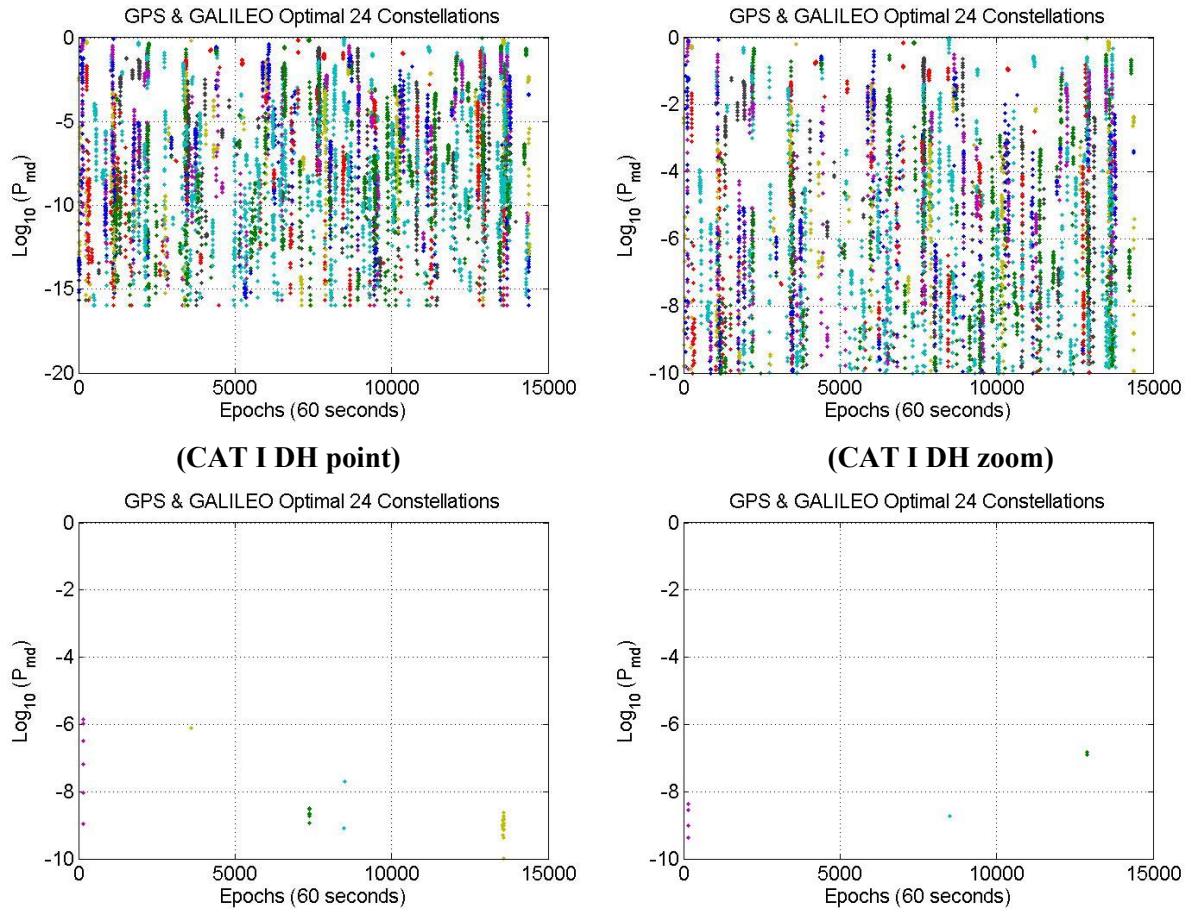

(CAT I DH point) **(CAT I DH zoom)**

(3 minutes before landing) **(5 minutes before landing)**

Figure 105 – DRAIM P_{md} for an ionospheric front induced error for GPS & Galileo Optimal 24 and $\Delta v = 35\ m/s$ for all airports

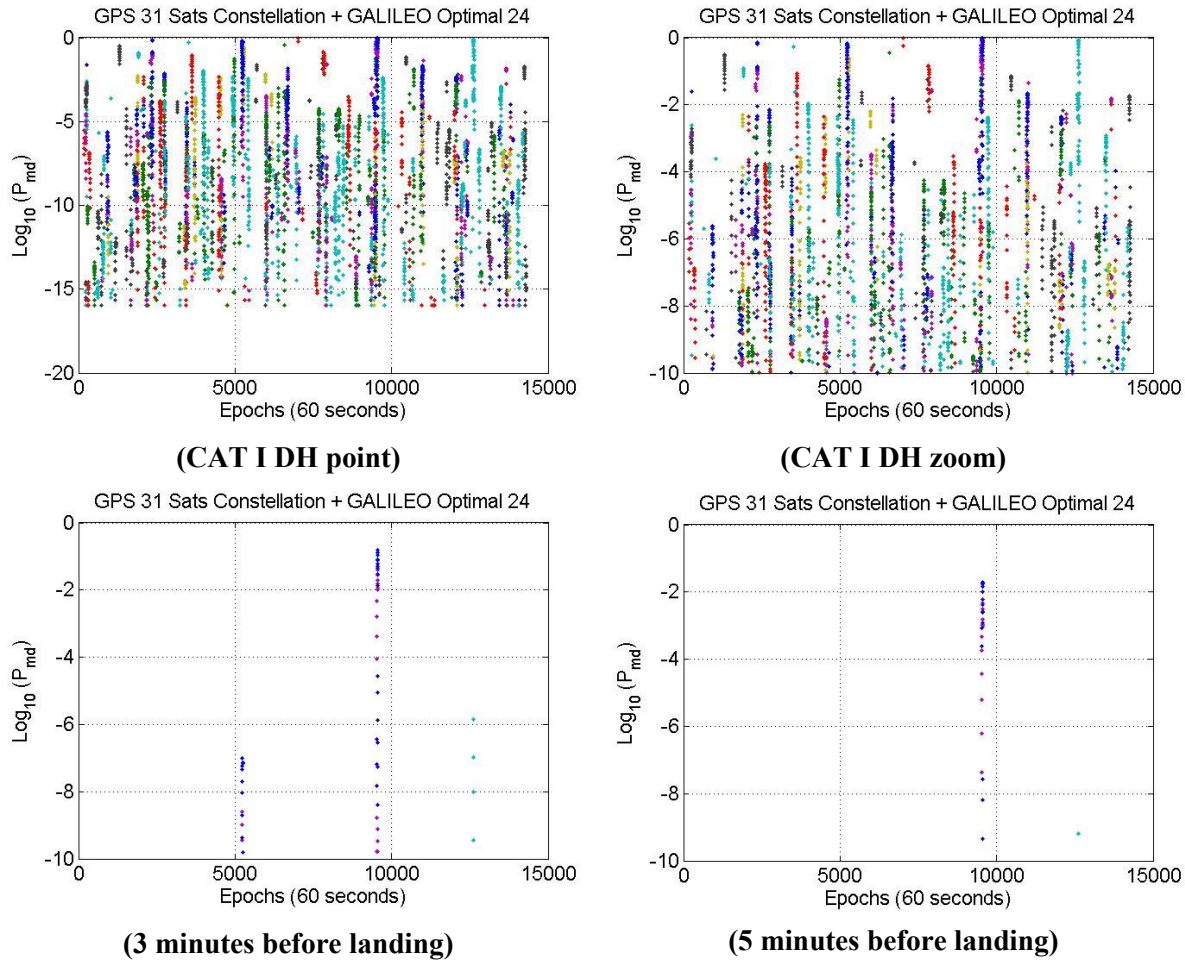

Figure 106 – DRAIM P_{md} for an ionospheric front induced error for GPS 31 satellites and Galileo Optimal 24 and $\Delta v = 35\ m/s$ for all airports

As for the previous case the two figures show the results for the two analyzed cases, GPS optimal 24 and 31 satellites. In both cases thanks to the detection of errors in points along the approach the RAIM detection probability can be strongly improved.

The results for front and IPP front moving at same speed are not shown due to the low number of satellites couples, for all epochs, providing a vertical error bigger than 6.44 meters for a range error of 3.1 meters.

In Table 30 the percentage of epochs where the P_{md} is higher than 10^{-9} is computed.

Table 30– Percentage of epoch with a not sufficient P_{md} for GAST-F

Δv	**GPS Constellation used** + Galileo **Optimal 24**	**Unavailability for CAT I DH point ($\|E_V\| > 6.4$ and $P_{md} > 10^{-9}$)**	**Unavailability for point along the approach (3, 5 min before)**
70 m/s	Optimal 24	3.41 %	<0.1 % <0.1 %
	31 Satellites	1.65 %	<0.1 % <0.1 %
35 m/s	Optimal 24	1.76 %	<0.1 % <0.1 %
	31 Satellites	0.94 %	<0.1 % <0.1 %
0 m/s	Optimal 24	<0.1 %	<0.1 % <0.1 %
	31 Satellites	<0.1 %	<0.1 % <0.1 %

5.4 Conclusions

In this chapter the main challenges concerning the integrity of GBAS GAST-D and GAST-F have been analyzed.

The GAST-D service remains under validation due to the difficulties experienced in monitoring the ionosphere with the current monitor scheme. A first analysis has investigated the use of the RAIM algorithm to improve the monitoring of the ionospheric fronts for GAST-D service. After the analysis of the cases for which the monitors are not able to provide the required P_{md} levels the "residual threat model" has been identified. The analysis of the RAIM performances, according to the derived ionospheric front threat model, has provided the following results. DRAIM alone is not able to provide the integrity monitoring for only one satellite to monitor according to the requirement. Performances can be improved relying on, when possible, detection in different points along the trajectory where the error is expected to be bigger than the ones at CAT I DH point. It has to be considered that P_{md} values are computed only for DRAIM, considering the presence of the DSIGMA and CCD monitors, at airborne level, the joint analysis may improve the performances by decreasing the P_{md} down to 10^{-9} meeting the requirement. The same analysis for a dual "fault and undetected" case has not been done due to the lack of information about the shape of an ionosphere front in the horizontal domain. Despite the good results obtained the integrity issue for GAST-D service cannot be considered as solved. Analysis about the possible presence of more than one satellite "faulty and not detected" have to be done as well as the joint analysis including other monitors performances.

In the following of the chapter, two of the integrity challenges identified for GAST-F service have been analyzed.

The first challenge concerns the possibility to adopt a new PRC and RRC update rate to increase the VDB capacity in order to transmit the additional differential corrections present in a DF/DC GBAS. The impact of this possible new processing modes has been investigated on the EA monitor. Results show that using the test metric as proposed for GAST-D does not permit to have an undetected error lower than 1.4 meters, with a P_{md} lower than 10^{-4}, after the 2.5 seconds imposed by the SiS TTA. Relying on a new metric proposed in (Stakkeland, et al., 2014) it is possible to adopt the proposed PRC and RRC update thanks to the improved detection performances. Adopting the new metrics, the monitoring of the acceleration threat is feasible.

The last analysis has analyzed the case of "frequency loss" for GAST-F. Despite all advantages, especially in the ionosphere monitoring, brought by the use of DF measurements combinations, in case of frequency loss the ionosphere has to be monitored as done for GAST-C or D. Relying on the analysis of RAIM performances done for GAST-D, the same algorithm has been used for a dual-constellation case. In this case, knowing that monitoring one satellite with a DC RAIM provides good results, a dual "faulty and not detected" satellites case has been analyzed. Due to the absence of an ionosphere front model in the horizontal plane, no limits to the selection of the worst satellites couple to monitor have been imposed. This condition has a conservative impact in some cases because, even if it is not possible to derive a unique model for an ionosphere front in the horizontal domain, it is almost impossible that a unique front impacts two satellites at the opposite of the user skyplot. Results for this analysis are better than the one derived for GAST-D thanks to the presence of a second constellation. The worst case remains the one where the IPP is faster than the front with some cases where the P_{md} is not meeting the requirement. Relying on detection along different points on the approach trajectory improve performances consequently thanks to the increased magnitude of the range error on one side and the change in the satellites geometry on the other. Also, in this case P_{md} values are computed considering only RAIM detection, the analysis of joint performances between RAIIM, CCD and DSIGMA may provide even better results. RAIM can help the detection of ionosphere front also in this case, furthermore, if the worst couple of satellites to monitor could be limited by any ionosphere front model results are expected to be better in some cases. As for the GAST-D case at this stage RAIM cannot be considered as a definitive solution for the monitoring of ionospheric fronts in SF cases.

6 Conclusions and Future Works

This section presents the conclusions from the results obtained from the analysis of the results obtained in the previous chapters. Perspectives for future works are also presented.

6.1 Conclusions

The development of a DC/DF GBAS service, known as GAST-F, brings a series of benefits with respect to GAST-D that is intended to provide the same level of service: up to CAT III precision approach and landing guidance. The system, in fact, relying on two constellations is more robust against a constellation failure. Moreover, with the use of new signals, GPS L5, Galileo E1 and E5a better level of accuracy may be reached. The availability of two frequencies permits also to improve the monitoring of the ionosphere anomalies, and it has to be reminded that GAST-D is still under validation cause of lack of integrity. Dual frequency combinations permit also to further mitigate the residual errors increasing consequentially the total system availability. If on one side this new concept brings a lot of benefits it has to be said that the use of a new constellation, Galileo, and new signals rise a series of challenges that have to be solved to have a full benefit of the advantages of this new concept

In this thesis some of the issues related to the development of a DC/DF GBAS system have been investigated. The aim of the work was to provide analysis and results for some of the challenges that have risen in the initial development of the GAST-F concept

To select the optimal processing mode for GAST-F, especially considering the possibility to adopt DF combinations, the accuracy of the new signals and combinations has to be derived. On this topic, the impact of errors at ground level has been derived analysing the impact of noise and multipath on the PRC. Data used to perform the analysis were recorded at Pattonville airport and at Toulouse Blagnac airport. The antenna used was, for both data collection, the BAE ARL-1900 (Lopez, 2008) which was designed to have good multipath rejection properties for GPA L1 C/A signals and to be used particularly in a GBAS ground station.

The first outcome of the analysis is the need to calibrate the antenna for GPS L5 and Galileo E5a measurements because they are affected by an elevation dependent bias similar for all satellites, constellations, and for both locations. After that calibration is applied, results show that GPS L1 and Galileo E1, for smoothed case, have a lower noise and multipath error standard deviation than GPS L5 and Galileo E5a. This results, considering the used modulation (BPSK(10)) on both GPS L5 and Galileo E5a, is surprising because the opposite of was expected from theory or another analysis done, e.g. (Circiu, et al., 2015). A possible cause of this results is the antenna characteristics that were optimized

for GPS L1 C/A signal. The computation of $\sigma_{pr\ gnd}$ values, for Toulouse data, and comparison with GAD curves shows that the antenna is not able to provide the required accuracy for GPS L5 and Galileo E5a signal. Their values of $\sigma_{pr\ gnd}$ are, in fact, bigger than the lowest GAD curves denoted as C. Values are provided also for I-free combination even if they are affected by the L5 band performances and no accuracy model is provided for this combination. the $\sigma_{pr\ gnd}$ computed for GPS L1 C/A and Galileo E1 signals show that the values are lower than the most accurate GAD curve. If results, at least on L1 band, are confirmed analysing data from other airports a new class of GAD curves may be defined for this kind of antenna.

The implementation of a MC/MF GBAS directly leads to a problem related to the increased number of satellites and the use of a second frequency. The big number of satellites, in particular, raises the problem of broadcasting a big number of PRCs and RRCs on the VDB link, which has a limited capacity. This problem is also related to the limitation, especially at the airborne side, of the number of tracking channels of the MC/MF receivers.

To cope with this issue a possible solution is to implement a satellite selection algorithm. Results show that relying on a 15-satellites subset, values of VDOP < 2 and HDOP < 1.15, indicator of a good geometry, are provided in more than 99.9% of the simulated cases. The protection level is lower than 10 meters for 100% of cases, and the parameters S_{vert} and S_{vert2} do not exceed the related limits. The same analysis for a 12 satellites subset, despite providing similar results for DOP values, leads to some availability problems. Protection levels, S_{vert} or S_{vert2} values exceed the related limits, in 0.2% of cases, when the all-in-view solution has the 100% of the availability across all simulations. The results do not consider the impact of smoothing and integrity process on the performances. The fast satellite selection (Zhang, et al., 2008) method is the one providing the best combination of good availability, low DOP values and low computational burden.

The last analysis has concerned the integrity monitoring. Because GAST-D service, due to a lack of integrity performances in monitoring ionosphere anomalous conditions, is still under the validation process, a first analysis has regarded the state-of-art of the monitors for this service. The aim was to understand under which circumstances the integrity requirement is not met. The analysis has permitted to derive a "residual" ionospheric threat model under which not all satellites are monitored with the required P_{md}. In particular ionosphere fronts moving with a relative low speed, and considering all possible slope values, are representative of this residual threat.

To improve monitoring performances, the use of RAIM algorithm has been proposed. Results show that for one "faulty and not detected" satellite, considering that the maximum range error is limited by the ionospheric front, RAIM provides good results. Moreover relying on detection on several points along the approach, 3 and 5 minutes before the landing, P_{md} values are further reduced, this because the value of the induced range error, according to the simulated scenarios, is bigger than in the first analysed case; the CAT I Decision Height (DH) point. It has also to be considered that the performances of the other monitors are not taken into account. This lead to the consideration that in some epochs where the P_{md} is below the requirement ($P_{md} < 10^{-5}$), including the performances of CCD and DSIGMA a global value lower than 10^{-9} may be obtained.

The analysis of a "dual faulty and not detected" case is also needed since this case cannot be excluded a priori. However it has to be considered that the choice of the worst couple of satellites to monitor has to be done considering an ionosphere front horizontal shape. This information is necessary to exclude cases where the two satellites are separated by a distance that exceeds the ionosphere front dimensions. Unfortunately a model for the ionosphere front, in the horizontal domain, does not exist. For this reason, and to avoid to compute performances under a quite pessimistic case, the simulation for the dual fault case has not been done. For the moment, due to the absence of simulations considering more than one faulty satellite, RAIM cannot be considered as a solution to the monitoring issue for GAST-D.

In the following of the integrity monitoring study, the challenges that have risen with the implication of a new constellation and new signals or new processing mode in GAST-F are presented.

Considering analysis done in (Milner, et al., 2015), where the impact of a lower PRC and RRC update rate is analyzed in term of accuracy loss, the impact of a lower update rate (2.5 s update interval instead of 0.5 s) is analyzed on the excessive acceleration monitor. Results show that the current monitor test metric, as used for GAST-D, is not able to meet the requirements (to monitor all faults that cause a differential error bigger than 1.6 meters) when an update period of 2.5 seconds is used. Relying on a new test metric proposed in (Stakkeland, et al., 2014), the requirement can be met thanks to the improved detection performances.

Another integrity issue regarding GAST-F is the possibility to lose a frequency, for example due to the presence of interferences in one of the frequency bands, as experienced at the Newark airport in 2009 (Grabowski, 2012). In this case, the expected integrity monitoring conditions are similar to the ones of GAST-D, except that a second constellation is present. To guarantee the integrity under this condition, the GAST-D monitor scheme is not sufficient to meet the integrity requirement. Relying on the proposal done for GAST-D, the performance analysis of adding RAIM to other monitors has been done for a SF/DC GBAS system. For this simulation, a "dual faulty and not detected" case has been analysed. No constraints have been imposed to the selection of the worst satellites couple, i.e. no geometric constraint

on the spatial extent of the ionospheric front, so that a pessimistic scenario is taken into account. Results are better than the ones obtained for GAST-D, and relying on detection on several points along the approach, the integrity can be provided by RAIM in almost 100% of the analyzed epochs. The impact of 3 "faulty and not detected" satellites has not been analysed due to the lack of information about ionospheric front in the horizontal domain. As for GAST-D, due to the lack of information about all possible fault monitors, RAIM cannot be considered as the definitive solution based only on this study.

6.2 Perspectives for Future Works

The $\sigma_{pr\ gnd}$ computed for GPS L1 C/A signals using Toulouse Blagnac data is well below the most accurate GAD curve. The same analysis has not been done for Pattonville data due to the absence of several RRs. However the comparison between the standard deviation shows that the accuracy is similar to the one obtained in Toulouse. Analysing data collected in more airports will permit to define a new GAD curve for GPS L1 C/A. Curves for L5/E5a signals and I-free combination may be established as well by applying the presented methodology, but require solving the calibration issue (elevation-dependent pseudorange bias) of the antenna. Some of the analysis done in this context may be applied to aircraft data to derive performances of ne signals and combinations.

Satellite selection is one of the proposals done to overcome the problem of the increased number of available signals to track and the number of corrections to broadcast. If this solution is selected, more analysis have to be done to determine the rate of change of the best subset. Due to the smoothing process and the presence of monitors in the range domain, too frequent changes in the satellites subset are not possible. Considering that a convergence time (360 seconds for 100 seconds smoothing filter) is needed from the first tracking of a satellite, such frequent changes in the satellites subset may impact the system availability and in some case the integrity performances. A new solution taking into account this parameter should be derived.

On the integrity aspect, more simulations have to be done when more information about ionosphere fronts will be available. The dual fault case must be analyzed for GAST-D case and for GAST-F considerations about three faulty and not detected satellites have to be derived. The aim is to determine if RAIM can solve the integrity issue present for SF GBAS to provide CAT II/III services. Simulations with considerations about the time of onset of the ionospheric fault, jointly with the other information about aircraft position and impacted satellites and the transient state of the carrier-smoothed tracking, have to be done in order to derive also performances for the airborne CCD and the DSIMGA monitor in the range domain, thus obtaining a global analysis of the integrity monitoring performances for GAST-D and GAST-F in presence of the identified residual ionospheric threats.

Lire
la fin de la thèse